MASTER THESIS

Suitability of a newly developed fluidized bed reactor for the activation of alternative bed materials

performed for the purpose of obtaining the academic degree of master of science
under the supervision of

Univ.Prof. Dipl.-Ing. Dr.techn. Hermann HOFBAUER

and the co-supervision of
Dipl.-Ing. Katharina FÜRSATZ

submitted to the Vienna University of Technology

Institute for Process Engineering, Environmental Technology and Technical Biosciences

by

Markus LANGER
Matr. No.: 0626211
Ufergasse 1
3474 Altenwörth

Vienna, August 2020 ....

Markus Langer

This master thesis was written in cooperation with

BEST
Bioenergy and
Sustainable Technologies

Affidavit

I, Markus Langer, declare in lieu of oath, that I wrote this thesis independently and performed the associated research myself, using only literature cited in this volume. I have not used sources other than those specified. If text passages from sources are used literally, they are marked as such.

Signature: ....

Markus Langer

Acknowledgement

By writing this thesis and the completion of my studies, I would like to take this opportunity to thank all those who accompanied me in the creation of this thesis and supported me during my studies.

Special thanks to my supervisor Univ.Prof. Dipl.-Ing. Dr.techn. Hermann Hofbauer for giving me the opportunity to do this thesis at the Institute for Process Engineering, Environmental Technology and Technical Biosciences at the Vienna University of Technology.

Many thanks to Dipl.-Ing. Katharina Fürsatz for the very good supervision and support during the development of this thesis. Both during the practical implementation of the experiments, the analysis of the bed material samples, as well as for the constructive criticism which has led to a continuous improvement of this thesis.

A big thank you to my two colleagues Christoph Hammerl and Juraj Priscak for the active support in the technical center during the practical work on the bench scale fluidized bed pilot plant.

In addition, I would also like to thank Dipl.-Ing. Dr. Matthias Kuba and the entire BEST team for their nice support and informative discussions.

Thanks to my colleague Thomas Karel, who actively accompanied me during my studies and helped me with many hurdles during my studies.

A big thank you to my partner Julia, who never gave up on me and who gave me strength and perseverance through her years of support and good encouragement to complete my apprenticeship.

Extra thanks go to my family, especially my father, who supported me in my education and enabled me to complete my studies at the Vienna University of Technology.

I could not have done it without you.

Many thanks to all of you!

Markus Langer

Kurzfassung

Der stetig steigende Energiebedarf unserer heutigen Gesellschaft fordert die Errichtung neuer Anlagen um diese enorme Nachfrage decken zu können. Die Herausforderung besteht darin, den Wechsel von fossilen Rohstoffen hin zu erneuerbaren Energieträgern zu vollziehen, um die anthropogene Belastung für Umwelt und Lebewesen zu minimieren und die den Klimawandel fördernden Treibhausgasemissionen möglichst rasch zu unterbinden.
Die Wirbelschichttechnik ist eine sehr vielversprechende Technologie, mit der es möglich ist aus Biomasse bzw. biogenen Reststoffen Energie CO_2-neutral und klimafreundlich zu gewinnen. Wirbelschichtanlagen sind in der Lage die im Brennstoff gespeicherte chemische Energie in eine für uns benötigte Form der Energie wie Wärme, Strom oder Produktgase überzuführen. Die dadurch erlangten Energieformen sind sehr gut geeignet, um in bestehende Infrastrukturen eingegliedert zu werden.
Ein essenzieller Bestandteil von Wirbelschichtanlagen ist das Bettmaterial. Einerseits dient das wirbelnde Bettmaterial als Wärmespeicher bzw. Wärmeübertrager und sorgt damit für eine möglichst homogene Temperaturverteilung im Brennraum des Reaktors, andererseits kann das Bettmaterial auch katalytische Eigenschaften besitzen, welche besonders für die bei der Vergasung ablaufenden Reaktionen einen wichtigen Aspekt darstellen. Durch den intensiven Kontakt mit dem Brennstoff und dem Fluidisierungsmedium interagieren die einzelnen Partikel des Bettmaterials mit dem Brennstoff und der bei der Verbrennung entstehenden Asche womit es zu Schichtbildungen an den Oberflächen der Partikeln kommt.

Um die katalytischen Effekte verschiedener Bettmaterialien besser verstehen und untersuchen zu können, wurde eine Versuchsanlage im Labormaßstab gebaut, mit dem Ziel eine möglichst hohe Brennstoff- als auch Bettmaterialflexibilität zu erreichen. Um eine qualitative Aussage über die zeitliche Abhängigkeit des Schichtaufbaus geben zu können, wurden mehrere Versuche mit unterschiedlichen Bettmaterialien durchgeführt. In regelmäßigen Abständen wurden Bettmaterialproben entnommen, welche anschließend mit Hilfe eines separaten Festbettreaktors auf deren katalytische Aktivität untersucht wurden. Wie sich dadurch herausstellte, ist die bestehende Wirbelschichtanlage für die ursprüngliche Aufgabe und Fragestellung, der Anreicherung und Aktivierung des Bettmaterials, im derzeitigen Zustand nur bedingt geeignet. Begründet ist dies vor allem in der konstruktiven Ausführung und der daraus resultierenden geometrischen Abmessungen des Brennraums der Anlage. Insbesondere die Art der Fluidisierung und die damit verbundene Mindestmenge an erforderlichen Bettmaterial, um die Anlage über längere Dauer konstant betreiben zu können, stellt sich als problematisch für die Anreicherung dar. Um diese Aussage zu bekräftigen, wurden einige Proben zusätzlich mit einem Rasterelektronenmikroskop untersucht, wodurch die elementare Zusammensetzung an der Partikeloberfläche ermittelt wurde.
Es hat sich gezeigt, dass sich die Versuchsanlage, nicht zuletzt wegen den vielen vorgenomme-

nen Detailverbesserungen, basierend auf den Beobachtungen und Erkenntnissen der durchgeführten Versuche, sehr gut für die Verbrennung biogener Festbrennstoffe sowie für den Einsatz verschiedener Bettmaterialien eignet. Die umfangreichen Erkenntnisse und das daraus gewonnene Wissen wird in dieser Arbeit zusammengefasst.
Mit dem Ziel der besseren Veranschaulichung sowie der Vervollständigung der Dokumentation wurde die Versuchsanlage in einem 3D CAD Programm modelliert, um das daraus gewonnen Wissen auch visuell für eventuell spätere Umbauten oder weitere Versuchsanlagen gleichen Typs heranziehen zu können.

Abstract

The increasing energy demand of our society demands the construction of new power plants to be able to meet this enormous demand. The challenge is to switch from fossil fuels to renewable energy sources as quickly as possible, in order to minimize the anthropogenic impact on the environment and living beings and to prevent greenhouse gas emissions that promote climate change.

Fluidized bed technology is a very promising technology, which allows generation of energy in a CO_2-neutral and climate-friendly manner from biomass or biogenic residues. Fluidized bed systems are able to convert the chemical energy, stored in biomass, into various forms of energy required for our society such as heat, electricity or product gases. The resulting forms of energy are very well suited for integration into existing infrastructures.

The bed material is an essential component of fluidized bed systems. On the one hand, the swirling bed material serves as a heat accumulator or heat exchanger and thus ensures that the temperature distribution in the combustion chamber of the reactor is as homogeneous as possible. On the other hand, the bed material can also have catalytic properties, which is an important aspect, especially for reactions taking place during gasification. Due to the intensive contact with the fuel and the fluidization medium, the individual particles of the bed material interact with the fuel and the ash during combustion. This leads to layer formation on the surfaces of the particles.

In order to better understand and investigate the catalytic effects of different bed materials, a testing plant was built on a laboratory scale, with the aim of achieving the highest possible fuel and bed material flexibility. In order to be able to give a qualitative statement about the temporal dependence of layer formation, several experiments were carried out with different bed materials. Bed material samples were taken at regular intervals, which were then examined for their catalytic activity, using a separate fixed bed reactor. As it turned out, in its current state the existing fluidized bed system is of limited suitability for the original task, the enrichment and activation of the bed material. This is mainly due to the design and the geometric dimensions of the combustion chamber of the testing plant. In particular the type of fluidization and the associated minimum amount of bed material, in order to be able to operate the system constantly over a long period of time, is problematic in order to sufficiently enrich the bed material. To confirm this statement, some samples were examined in a scanning electron microscope, whereby the elemental composition on the particle surface was determined.

Because of many detailed improvements that have been made, based on the observations and findings of the experiments, it turned out that the testing plant is very suitable for the combustion of biogenic solid fuels and for the use of various bed materials. The extensive insights and the knowledge gained from the experiments are summarized in this thesis.

With the aim of better illustration and to complete the documentation, the testing plant was modeled in a 3D CAD program in order to be able to use the knowledge gained visually for possible later modifications or for other testing plants of the same type.

Contents

Chapter 1

Introduction

The increasing energy demand of our current society necessitates the construction of new facilities and power plants to meet this enormous demand. The current challenge is to move away from fossil fuels and switch to renewable energy sources in order to minimize the anthropogenic burden on the environment and other living beings. It is also very important to prevent as many greenhouse gas (GHG) emissions as possible that promote climate change. Moreover, even from a geopolitical point of view, it is reasonable to reduce purchased fossil fuels and change to the use of locally occurring biogenic raw materials or biogenic residues.

The problem of anthropogenic emissions and the resulting greenhouse effect will challenge present and future generations. This is a global challenge that can only be mastered together, as global warming affects all life on this planet.

Only the future will tell whether this challenge can be overcome and whether the switch to renewable and sustainable generation of energy to reduce GHG emissions will succeed.

1.1 Historical energy transitions

History has shown that global primary energy use has risen steadily in the past [1, p. 13]. Technical achievements and the rising standards of living in our society are leading to an ever increasing energy consumption. With the beginning of industrialization in the second half of the 18th century, energy and generation of energy became a central challenge.

As shown in Figure 1.1, the world energy supply of pre-industrial societies was largely based on renewable energy sources. The most important primary energy sources were wood, manure, hydropower and wind energy. From 1900 onwards, coal was the largest contributor to energy consumption. Around 1950, oil and natural gas have taken the lead.

Since 1950, there was a rapid increase in demand for primary energy sources. Global energy use increased from approximately 100 EJ/yr to approximately 450 EJ/yr over the following fifty years. This rapid increase was due to the increasing need for wealth and higher standards of living. Figure 1.1 also illustrates that todays primary energy demand is mainly covered by fossil fuels such as coal, gas and oil. However, for some years now, there has been a slight increase in renewable energies and biomass.

The global consumption of primary energy sources is currently estimated at around 583.9 EJ/yr for 2019 [2, p. 9]. The slightly decrease in energy demand in Austria and elsewhere in Europe since 2005 can not be seen in Figure 1.1, as there is considerable economic growth in other parts of the world [1, p. 33].

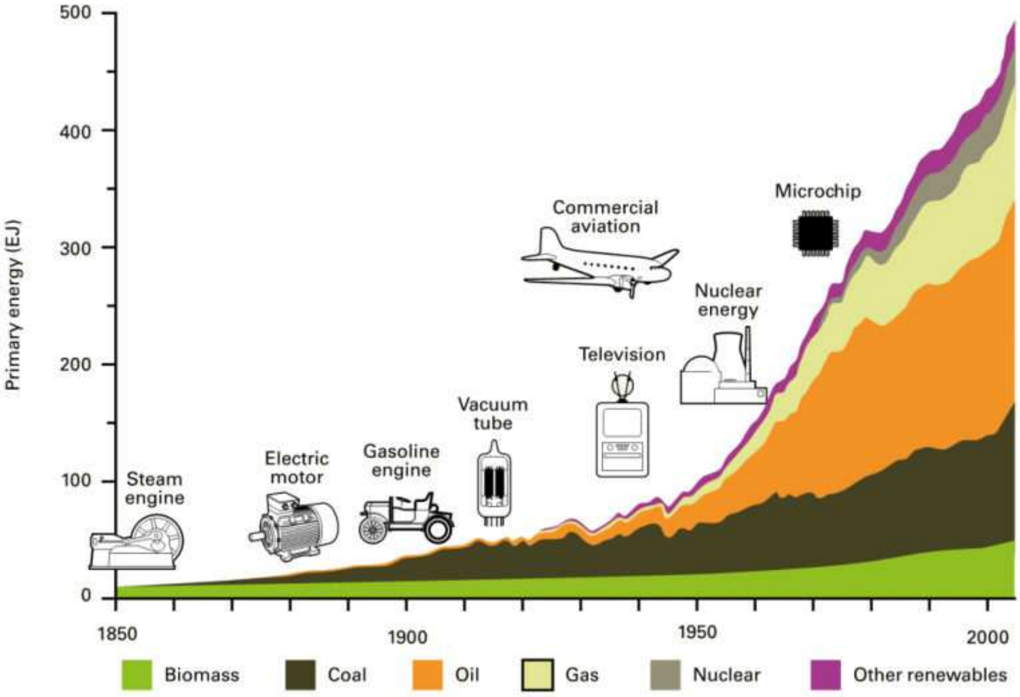

Figure 1.1: *Quantitative representation of the six most important energy sources worldwide, since 1850 to 2005 (adapted from [3]).*

1.1.1 Rethinking

The premise for the future can only be in the saving and the departure from fossil energies. This is the only way a long-term reduction or suppression of greenhouse gases can be achieved. For some years a rethinking has taken place in many parts of Europe. In recent years, in Austria and Germany, it has been observed that especially the younger generations of the population have increasingly dealt with this topic.
In many cities demonstrations and public events take place [4], which point out the problems and the importance of environmental protection. Politicians in particular are criticized for not doing enough for environmental protection in the past [5].

1.2 Energy supply

Providing sustainable energy is one of the biggest challenges of the coming decades. Probably the most important approach to sustainable generation of energy is the reduction of CO_2 emissions that are released during the conventional use of fossil fuels. In the search for suitable alternatives, biomass as a carbon neutral carbon source is increasingly becoming the focus of technical applications [6]. With the help of biomass, a great contribution can be made to achieve political as well as economic goals.
The challenge is to make the most efficient use of the potential of biomass with the help of efficient process plants. In addition, the use should also be on an economically justifiable level. The following is a brief overview of the current energy supply worldwide.

1.2.1 Worldwide energy demand

As illustrated in Figure 1.1, global energy demand has increased significantly in the last century. Technical achievements, rising prosperity, the increasing interconnectedness of the world and the growing population do not show any end to the demand for energy. As mentioned in Section 1.1, the primary energy demand worldwide is currently around 583.9 EJ/yr [2, p. 9].

The most important energy sources today are crude oil, followed by coal and natural gas [1, p. 34]. All of these conventional energy sources come from fossil sources. The rapid increase of these predominant energy sources can be seen in Figure 1.1. The thermochemical conversion of oil, coal and natural gas is associated with massive environmental burden. Oil, coal and natural gas are followed by larger distances by nuclear energy and other forms of renewable energy [1, p. 34].

1.2.2 Renewable energy

A relatively small part of the primary energy demand is currently covered by renewable energy sources. Figure 1.2a shows the primary energy input for 2015, broken down by energy source. The dominance of fossil fuels is clearly visible. The share of the fossil fuels oil, coal and natural gas is 85.5%. The share of renewable energies is comparatively low at about 10% of the annual global energy demand.

Figure 1.2b shows a study by the International Energy Agency (IEA) and the Intergovernmental Panel on Climate Change (IPCC), which represents the share of biomass in renewable energy sources. This study was published in 2007 [7, p. 6] and already indicated the great potential of biomass. About 50 EJ/yr [7, p. 6] of primary energy is provided by biomass worldwide.

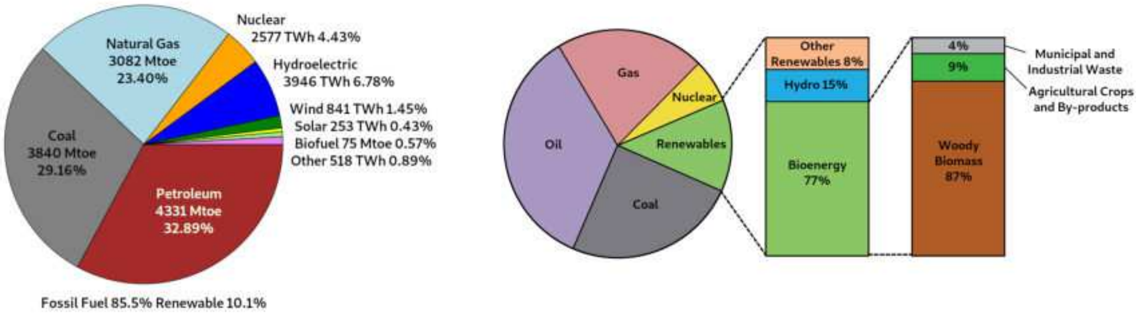

(a) *Global primary energy consumption by type of fuel for 2015 [8].*

(b) *Share of biomass in renewable energy sources in the world primary energy mix (adapted from [7, p. 6]).*

Figure 1.2: *Shares of renewable energies, as well as the contribution of biomass to global primary energy consumption.*

1.2.3 Outlook

In the past, energy was provided by large, centralized power plants. Many of these power plants use fossil fuels. In order to be able to cover the energy demand in the future and at the same time to accomplish a shift away from fossil fuels, new approaches and visions are needed.

From the current point of view, generation of energy has to change. Unlike before, the provision of energy will be much more networked and decentralized [9]. A trend away from individual, large-scale power plants and towards comparatively small and distributed power plants can already be observed occasionally [10, p. 4].
The type of generation of energy has to change fundamentally. The extraction of energy will be divided into many different processes and techniques. Only by combining systems that use a variety of forms of energy such as wind, water, tides, sun, geothermal energy and biomass, does the project to meet the energy demand appear promising [10].

Chapter 2

Fundamentals

This chapter is intended to give an overview of the fundamentals necessary for this thesis. First, an overview of biomass is given in Section 2.1. Then, Section 2.2 explains basics of fuel conversion. The individual phases of the thermochemical conversion are discussed in more detail in Section 2.3. Section 2.4 gives an overview of the substances from thermochemical conversion. The fluidized bed technology and its classification are dealt with in detail in Section 2.5. Right afterwards, the characteristics of fluidized beds are discussed in Section 2.6. Layer formation and agglomeration of bed materials is explained in Section 2.7. Finally, some fields of application of fluidized bed technology are given in Section 2.8.

2.1 Biomass

The use of biomass as a CO_2-neutral carbon source gains interest in the search for alternative energy sources. In addition to electrical energy and heat, biomass offers the possibility of being transformed into other important forms of energy [11, p. 18]. By means of suitable processes, biofuels can be produced out of biomass, for example via the Fischer-Tropsch synthesis [11, p. 250]. Furthermore, it is possible to obtain many other high-quality products via thermochemical conversion of biomass. Important phases of the thermochemical conversion are explained in more detail in section 2.3.

2.1.1 Stored solar energy

According to the law of thermodynamics, energy is a conserved quantity. Therefore, energy can neither be generated nor destroyed. However, it is possible to convert energy to other forms of energy [12, p. 6].

There are different types of energy resources on Earth. For example, energy is stored in the form of chemical energy in fossil fuels such as coal, oil or natural gas. There are also renewable energy flows that can be used. These can be divided into three different primary energy sources [13, p. 2]:

- **Tidal energy** results from planetary gravity and planetary motion.
- **Geothermal energy** has been stored as geothermal energy in the interior of the Earth since the formation of the planet.
- Through the sun, energy is continuously delivered to the surface of the Earth in the form of **solar radiation**.

The energy radiated by the sun is by far the largest source [13, p. 1] of regenerative energy supply.

For process applications, energy is divided into *primary energy* and *secondary energy.*

Primary energy is the form of energy that is directly available as a usable form of energy or source of energy without conversion processes. These include, for example, wind energy, oil and coal [11, p. 6]. If primary energy passes one or more transformation processes before the energy can be used, the resulting energy is called secondary energy. Examples of secondary energy are pellets, electricity and petroleum products such as gasoline, diesel or kerosene [11, p. 6].

Tidal energy, geothermal energy and solar radiation cause a series of very different energy flows through different natural transformations within the atmosphere of the Earth. Due to the incoming solar energy, the air in the atmosphere is heated differently, resulting in winds. Solar radiation also causes the evaporation of water and cloud formation, which causes rain showers in other places. Wind energy, water power as well as ocean currents and biomass are converted forms of solar energy [13, p. 2].

In the formation of biomass, solar radiation is converted into organic matter through the process of photosynthesis. Biomass thus represents stored solar energy [11, p. 7]. Compared to other direct and indirect methods of solar energy use such as solar thermal use or wind power, biomass use is therefore not subject to the fluctuating supply of solar radiation. Biomass thus has the property of providing energy when it is needed.

This decoupled form of stored solar energy eliminates some complicated and technically demanding storage systems, which are needed for the technical utilization of other renewable energy sources. Also in terms of security of supply, biomass has great potential to deliver a stable energy supply [13, p. 1].

2.1.2 Definition of biomass

The term *biomass* is understood to mean all substances of organic origin, i.e. carbonaceous matter. The definition of biomass is defined in ÖNORM M 7101 [14, p. 7] as an organic matter of biogenic, non-fossil type. The standard distinguishes biomass into solid, liquid and gaseous biomass.

Biomass is realized through the process of photosynthesis. In order for this bio-chemical process to proceed, light, water and CO_2 are needed [13, p. 83]. These components then form oxygen and carbohydrate [13, p. 95].

The opposite process to photosynthesis is respiration. By respiration, the carbon bound in the high-energy organic compounds is converted back into its oxidizing form, i.e. into CO_2. This provides the cells with the necessary metabolic energy in the form of adenosine triphosphate (ATP) [13, p. 95]. Such respiration occurs in all aerobic living organisms such as bacteria, fungi or animals. However, respiration also occurs in *non-green* plant organs such as roots, flowers or channels. This results in a *closed* carbon cycle in which the totality of the biomass and the carbon content of the atmosphere remain constant. Figure 2.1 shows the composition of photosynthesis products and their degradation by respiration.

During evolution, this cycle was responsible for storing large amounts of CO_2 bound in the atmosphere into biomass. By fossilizing this biomass, the CO_2 was stored in coal, gas and oil [13, p. 96]. This removed the CO_2 from the atmosphere. In the course of evolution, a dynamic equilibrium was established between CO_2 binding and CO_2 release, which was largely constant over a long period of time.

Today, however, the intensive anthropogenic use of fossil fuels such as coal, oil and gas again

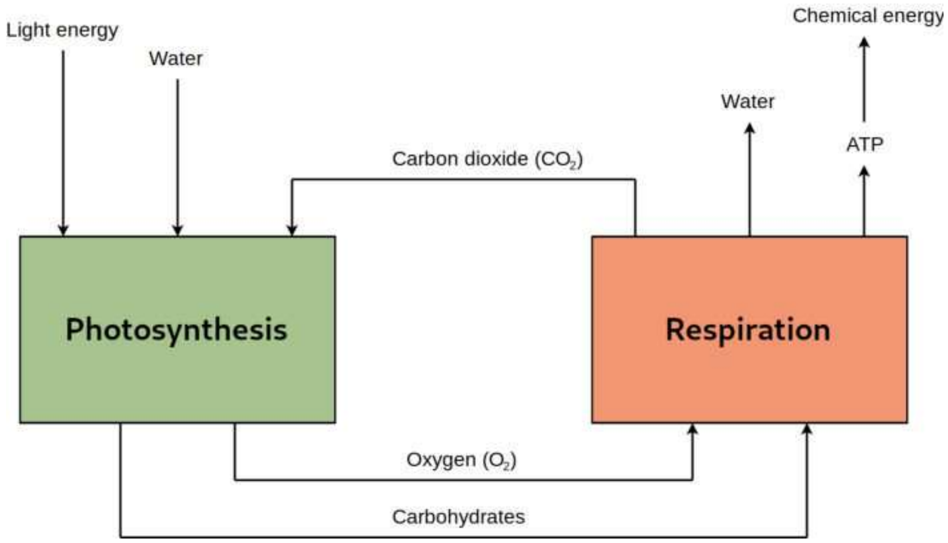

Figure 2.1: *Composition of photosynthesis products and their degradation by respiration (adenosine triphosphate, ATP) (adapted from [13, p. 96]).*

leads to a shift in equilibrium. From a geological point of view, this happens in a very short period of time. The basic process of plant growth, photosynthesis, can be described by equation 2.1 [13, p. 96].

$$6CO_2 + 12H_2O \rightarrow C_6H_{12}O_6 + 6O_2 + 6H_2O \tag{2.1}$$

The, in equation 2.1, quoted spelling has become established, because it is intended to illustrate that the oxygen origins from water and not from CO_2.
This reaction requires an energy input of 2816 kJ per mole of glucose, which is provided by incoming sunlight [13, p. 96].

2.1.3 Classification of biomass

For energy use, biomass can be divided into different classes. However, the classification of biomass is not uniform and therefore there are several classifications in the literature.
A common classification is the classification into forest-produced lignocellulose plants, agriculturally produced lignocellulose plants, oil plants as well as sugar and starch plants [13, p. 167]. Another suitable classification of biomass is the classification by its use into the following subgroups [11, p. 18]:

- **Renewable resources:** Cereals, sugar beet, forest wood,...
- **Residues:** Straw, manure, residues,...
- **Waste:** Sewage sludge, waste wood, household waste,...

For the energetic use, above all, the elemental composition, i.e. the chemical-material properties, as well as the fuel-technical and physico-mechanical properties are significant [13, p. 580]. The classification of biomass, much like the differentiation of biomass from fossil fuels, is not clearly defined. Often, peat is considered as the boundary between biomass and fossil fuels [11, p. 18]. Peat is an organic sediment consisting of an accumulation of incompletely decomposed plant substances. Peat represents the first stage of coalification and thus the first step in the natural process of coal production. Peat is thus a fossil secondary product and therefore no longer belongs to biomass. However, in some countries, such as Sweden or Finland, peat is still classified as biomass [11, p. 19].

Elemental composition

The plant dry matter consists of about 90wt% of the elements C, O and about 6wt% of the element H [13, p. 88]. All organic compounds contain these three elements. Therefore, these are also called *main elements* [11, p. 95].

Furthermore, plants contain elements that are classified into *macronutrients* and *micronutrients*. The most important macronutrients are N, K and Ca. Elements such as P, Mg and S are also among the macronutrients [13, p. 89].

Micronutrients or trace elements, which may be present in the plant in a concentration of 0.001% to 0.03% of dry matter. These include B, Mn, Cu, Zn, Mo, Co, Cl and Na [13, p. 89]. The element Fe can be assigned to both macroutrients and micronutrients. Si is another element that acts as a nutrient and can be a growth-influencing factor when the plant incorporates silicate into its cell walls [13, p. 89]. All nutrients can limit the growth of plants if they are present in insufficient quantities. Table 2.1 lists the most important components and their effects on energy use in thermal utilization.

2.1.4 Fuel properties of biomass

For biomass, there are a variety of properties that are important for the use of energy. Some of these properties, such as fuel moisture, can be optimized by suitable treatment and storage of the fuel. Other properties, such as ash content, are fuel specific properties that can not be influenced. However, it is possible to influence the ash melting behaviour by appropriate process control and addition of suitable components.

In this subsection, some of the most important properties of biomass will be explained in more detail.

Lower heating value H_i The lower heating value H_i (LHV) is understood to mean the maximum amount of heat that can be used in the event of complete oxidation of the used fuel. The LHV is related to the amount of used fuel, in which there is no condensation of the water vapor contained in the exhaust gas [13, p. 607].

The LHV is therefore the measure of the specific usable amount of heat without consideration of the condensation enthalpy of the water vapor. The water should be present in the determination of the calorific value in the vapor state and at a temperature of 25 °C. The procedure for determining the calorific value of biogenic solid fuels is defined in detail in the standard ÖNORM EN ISO 18125 [15].

The LHV is thus a variable that has been adapted for technical applications. In many applications, such as heating systems or motors, water vapor escapes before it can condense, which means that the condensation enthalpy can not be used.

The index i stands for English or Latin word *inferior* (lower). Frequently, the literature also includes the terms *net calorific value (NCV)* or *lower calorific value (LCV)*.

If it would be possible to utilize the heat of vaporization of water vapor by condensation, the

Table 2.1: *The most important and quality-relevant properties of biogenic solid fuels with their effects on thermal utilization (adapted from [13, p. 90]).*

Components	Effects on energy use in thermal utilization
Main elements	
Carbon (C)	Lower heating value, higher heating value, air requirement, particulate emissions;
Oxygen (O)	Lower heating value, higher heating value, air requirement;
Hydrogen (H)	Lower heating value, higher heating value, air requirement;
Macronutrients and micronutrients	
Nitrogen (N)	Ash utilization, NO_x-emissions and N_2O-emissions;
Potassium (K)	Ash softening behaviour, ash utilization, high temperature corrosion, particulate emissions;
Calcium (Ca)	Ash softening behaviour, ash incorporation of pollutants, ash utilization, particulate emissions;
Phosphorus (P)	Ash incorporation of pollutants, ash utilization, particulate emissions;
Magnesium (Mg)	Ash softening behaviour, ash incorporation of pollutants, ash utilization, particulate emissions;
Sulfur (S)	SO_x-emissions, high temperature corrosion, particulate emissions;
Trace elements	
Chlorine (Cl)	Emissions of HCl and organohalogen compounds (PCDD/F), high temperature chlorine corrosion, particulate emissions;
Silicon (Si)	Ash softening, ash utilization, particulate emissions;
Sodium (Na)	Ash softening behaviour, ash incorporation of pollutants, particulate emissions;
Heavy metals	Ash utilization, heavy metal emissions, catalytic effect (PCDD/F-formation), particulate emissions;

amount of heat emitted would be slightly higher [13, p. 607].

The LHV of dry biogenic solid fuels is mainly determined by the content of oxidizing elements primarily C and H [11, p. 113]. The LHV of biogenic solid fuels influenced much greater by the water content than by the type of biomass [11, p. 111]. For this reason, calorific values of different fuel types should always be compared in terms of the absolutely dry biomass. Frequently, the water and ash free value LHV_{waf} is given.

For wood, the LHV is between 18 MJ/kg and 19 MJ/kg [11, p. 111].

Higher heating value H_s In contrast to the LHV, the higher heating value H_s (HHV) takes into account the energy required to heat the combustion air and the exhaust gases and also the enthalpy of condensation of the liquids condensing on cooling [13, p. 607]. In particular, the water formed in the combustion of hydrogen-containing fuels is taken into account in condensed form.

To determine the calorific value, the exhaust gases must be cooled so that the water vapor can condense. As a reference temperature, the standard provides a temperature of 25 °C [13, p. 607].

The index s stands for English or Latin word *superior* (higher). The literature also includes the terms *upper heating value*, *gross calorific value (GCV)* or *higher calorific value (HCV)*. The HHV of biogenic solid fuels on average is about 6% for bark, 7% for wood and 7.5% for stalk above the LHV [11, p. 111]. However, this only applies to solid fuels in the absolutely dry state, i.e. based on dry matter [13, p. 607]. With moist biomass, this relative distance increases, so that the energy gain that can be achieved by recondensation of the resulting water vapor increases. Therefore, the heat released by condensation contributes to the energy yield. The HHV therefore always exceeds the LHV. Table 2.2 shows characteristic values for the LVH and the HHV for some typical biomass solid fuels compared to bituminous coal and lignite.

Water content The water content of biomass depends on many factors such as biomass type or the time of year [11, p. 110].
The content of water which can be removed from the fuel under defined conditions is referred to as water content w. The water content describes the ratio between the mass of water m_w and the mass of the total biomass m_b. The water content is related to the fresh mass, i.e. to the wet basis [13, p. 613].

$$w = \frac{m_w}{m_b + m_w} = \frac{u}{1+u} \tag{2.2}$$

Fuel moisture In the field of forestry, the term fuel moisture u or *wood moisture* is often used instead of the term water content [13, p. 614].
Unlike the water content w, the moisture is related to the dry matter. The fuel moisture u describes the ratio between the mass of water m_w and the mass of the dry matter of the biomass m_b.

$$u = \frac{m_w}{m_b} = \frac{w}{1-w} \tag{2.3}$$

In the case of energetic biomass use, the indication of the water content has largely become established internationally. Fuel moisture is a characteristic, that is used more in traditional forestry.
The water content as well as fuel moisture can be subject to considerable fluctuations in the period between making available and the energetic use [13, p. 614]. As shown in Figure 2.2, a water content of 50% corresponds to a fuel moisture of 100%. With information on humidity, values of greater than 100% are possible.
The LHV or the HHV are significantly influenced by the fuel moisture content and the water content. Through suitable storage conditions or drying of the biomass, the water content and the fuel moisture can be kept low [11, p. 111].

Ash content Ashes are those inorganic residues that remain after the combustion of a biogenic solid fuel. This residue can come directly from the fuel [13, p. 616]. However, the residue can also come from impurities added throughout the supply of the fuel. These can get into the fuel during harvesting, processing, transport or storage.
The lowest ash content, usually less than 1% of dry matter, is found in wood fuels. For debarked wood, the ash content is usually even less than 0.5% [13, p. 616].

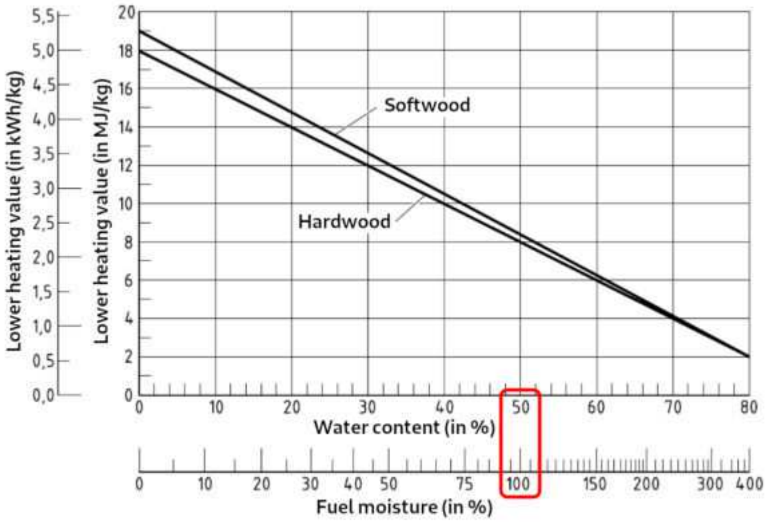

Figure 2.2: *Lower heating value of hardwood and softwood as a function of the water content and the fuel moisture (adapted from [16, p. 6]).*

In ashes many of the elements mentioned in Subsection 2.1.3 can be found. The ash mainly consists of Ca, Mg, K, P and Na [13, p. 617]. For example, the average composition of the coarse ash of wood is about 42wt% CaO, about 6wt% K_2O, about 6wt% MgO, about 3wt% P_2O_5 and about 1wt% Na_2O and smaller amounts of Fe and Mn. For straw and cereal whole ash, the shares of K_2O and P_2O_5 are higher [13, p. 617].
The ash content of a fuel primarily has an impact on pollutant emissions in the form of particulate matter. However, the expected ash content also significantly influences the technical design of a firing plant. A higher ash content of the fuel causes a higher effort in the cleaning and deashing of the system. For example, heat transfer surfaces and filter devices are particularly susceptible to ash packaging. A high ash content is therefore often associated with higher costs for recovery or disposal of the resulting combustion residues [13, p. 617]. Table 2.2 shows the ash content for some typical biomass solid fuels compared to bituminous coal and lignite.

Ash melting behaviour An important factor in thermal biomass utilization is the ash melting behaviour. As a result of the heat-induced processes that take place during thermochemical conversion, physical changes in the ash can occur in the ember bed [13, p. 617]. Depending on the prevailing temperature and the ash melting behaviour of the fuel, the ash particles may melt. Particularly undesirable is a sticking (sintering), which can lead to agglomerations of the ash. This can be associated with considerable technical disadvantages in the conversion plant. The ash melting behaviour must therefore be taken into account in the technical realization of the combustion process [13, p. 617].
The melting behaviour of biomass ashes depends on the composition of the ashes and thus, above all, on the fuel and its composition. The presence of certain impurities also influences the melting behaviour. Measured variables are four specific characteristic temperatures at which certain observations on the ash are noticed. These characteristic temperatures are shown in Figure 2.3 and describe the onset of *shrinkage starting temperature* (SST), *deformation temperature* (DT), *hemisphere temperature* (HT) and *flow temperature* (FT) of the

starting sample [13, p. 618]. Table 2.2 shows characteristic ash melting temperatures for some typical biomass solid fuels compared to bituminous coal and lignite.

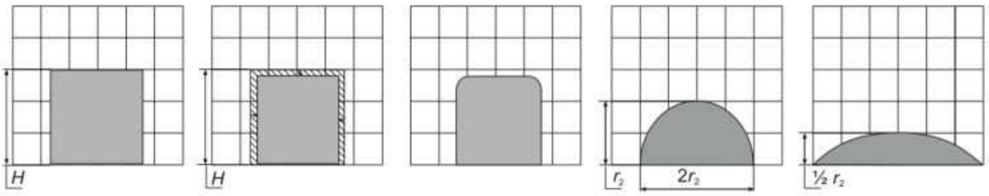

Starting sample **Deformation** **Softening** **Hemisphere** **Flow**

Figure 2.3: *Characteristic phases during the melting process of the cylindrical ash specimen according to standard test method (adapted from [13, p. 618]).*

The procedure for determining the melting behaviour is precisely defined and specified in the standard ÖNORM CEN/TS 15370-1 [17].

For fuels with low ash melting temperatures, there is a high risk of caking, agglomeration and sedimentation in the conversion plant. Particular of risk are the combustion chamber, the grate and heat transfer surfaces [11, p. 118]. This cakings can often lead to interruptions of the operation. It can also lead to cross sectional changes within the system, whereby, for example, the combustion air supply can be impaired. Furthermore, the problem of high-temperature corrosion [13, p. 619] is favoured, whereby costly and expensive cleaning and maintenance work is necessary.

The ash melting temperature depends on the presence of certain elements. For example, the elements Ca and Mg generally increase the ash melting temperature while the content of Si in combination with K results in a melting point depression [11, p. 118].

Wood and bark ash have a melting temperature of about 1300 °C to 1400 °C [13, p. 619]. From a technical point of view, these relatively high temperatures do not result in restrictions for most applications. As can be seen from Table 2.2, the melting temperature of pulp-like fuels is almost always at a temperature below 1200 °C. For many applications, these low melting temperatures can already be problematic and lead to the described complications.

For example, the melting point of triticale straw is often between 900 °C and 950 °C. Particularly critical are rye grains, where even FT can be below 900 °C [13, p. 619]. In the literature, the term *ash softening behaviour* is often used instead of the term ash melting behaviour.

Volatile constituents Volatile constituents of biogenic solid fuels are volatile products which arise in the phase of pyrolytic decomposition of the dry organic substance. The content of volatile constituents thus characterizes the property of the biogenic solid fuel to decompose under the action of heat into combustible gaseous constituents and coke [13, p. 613].

The content of volatiles makes it possible to draw conclusions about the formation of flames during combustion or gas formation during gasification in the gas atmosphere. The content of volatile constituents is therefore a fuel characteristic which is determining for the construction of a furnace or a gasifier.

The proportion of volatile matter in the total fuel is usually 74% to 83% [11, p. 115] of the dry matter in lignocellulosic fuels. Wood fuels have the highest percentage of volatile constituents with an average share of 82% [13, p. 613]. As Table 2.2 shows, cereal straw like wheat straw at 77% and triticale straw at 75% [13, p. 613] have a lower level of volatile components.

The procedure for determining the volatile constituents of biogenic solid fuels is described in detail in ÖNORM EN ISO 18123 [18].

Table 2.2: *Typical characteristics of biomass solid fuels compared to bituminous coal and lignite (Typical w: Bituminous coal 5%; Lignite 50%) (adapted from [13, p. 609]).*

Fuel/biomass type	LHV	HHV	Ash content	Volatile constituents	Ash melting		
	in MJ/kg	in MJ/kg	in %	in %	DT in °C	HT in °C	FT in °C
Bituminous coal	29.7	n/a	8.3	34.7	1,250	n/a	n/a
Lignite	20.5	n/a	5.1	52.1	1,050	n/a	n/a
Spruce	18.9	20.2	0.9	82.9	1,320	1,340	1,350
Beech	18.1	19.5	1.2	84.0	1,350	1,410	1,430
Bark (pinophyta)	19.2	20.4	3.8	77.2	1,440	1,460	1,490
Wheat straw	17.2	18.5	5.7	77.0	998	1,246	1,302
Triticale straw	17.1	18.3	5.9	75.2	911	1,125	1,167
Wheat grain	17.0	18.4	2.7	80.0	687	887	933
Rye grains	17.1	18.4	2.0	80.9	710	n/a	810
Streetgrass clippings	14.1	15.2	23.1	61.7	1,200	1,270	1,286

2.2 Fuel conversion

Biomass can be processed in many different ways throughout a supply chain. This processing makes it possible to convert the energy, stored in chemical form in the biomass, into the respectively desired final energy or useful energy. An example is the comparatively simple thermochemical conversion by combustion. After the biomass has been mechanically processed, it can be burned in an oven or in a power plant [13, p. 5].

Other applications of biomass processing are, for example, liquid or gaseous secondary energy carriers. These carriers of energy can be used in car engines or truck engines for power supply or in gas turbines for power generation.

For the conversion of biomass into useful energy, often it is necessary that various processing processes as well as refining processes are carried out. The aim is to upgrade the carriers of energy with regard to one or more of the following properties: Energy density, handling, storage and transport properties, environmental compatibility, potential for the substitution of fossil fuels, recoverability of by-products and/or residues [13, p. 6].

2.2.1 Thermochemical conversion

In thermochemical refining processes, solid bioenergy carriers are primarily transformed under the influence of heat into solid, liquid and/or gaseous secondary energy carriers. The primary aim of this conversion is to provide energy carriers with clearly defined fuel properties. Another objective of this conversion is to provide well-transportable secondary energy carriers with a high energy density [13, p. 6].

As this master thesis mainly deals with the thermochemical conversion of biomass in a fluidized bed combustion, this transformation is discussed in more detail in Section 2.3. For the sake of completeness, it should be mentioned that in addition to thermochemical conversion, there are also *physicochemical conversion* as well as *biochemical conversion* as other biomass conversion possibilities.

2.2.2 Physicochemical conversion

Physicochemical conversion deals with the provision of vegetable oil-based energy carriers. The starting material are oil-containing biomasses such as oilseed rape, sunflowers or the fruits of the oil palm [13, p. 7]. During physicochemical conversion, the oil phase must first be separated from the remaining biomass. This can be, for example, realized by a mechanical extrusion process. The remaining residue is called *press cake*. The press cake still contains an oil content. This oil content can be removed with a solvent [13, p. 8]. The oil and solvent as well as the remaining biomass and solvent are separated by distillation. The solvent is then recycled. The recovered vegetable oil is energetically usable in its pure form in vegetable oil suitable diesel engines and in certain cogeneration plants as fuel [13, p. 8].

2.2.3 Biochemical conversion

In biochemical processing the biomass is converted by microorganisms and thus by biological processes. Sugary, starchy and cellulosic biomass can be converted into C_2H_5OH (ethanol) by alcoholic fermentation [13, p. 8], for example with the aid of yeast. The ethanol is then separated by distillation or rectification from the mash. Subsequently, this can be obtained by dehydration in pure form. Ethanol can then be used as fuel in gasoline engines or in incineration plants for final energy supply or for useful energy provision [13, p. 8].

2.3 Phases of thermochemical conversion

The fundamental aim of thermochemical and thus heat-induced conversion processes is to convert the chemical energy, stored in biogenic solid fuels in the form of heat, as efficient as possible. In order for the conversion to be as efficient as possible, the biomass undergoes transformation processes. At the end of thermochemical conversion, usually all combustible and oxidizable components of the fuel are completely oxidized [13, p. 646]. The chemical energy stored in solid biomass is released in the form of thermal energy (heat). The resulting flue gas consists mainly of the oxidation products CO_2 and H_2O [13, p. 646]. The mineral components of the biomass are called *ash* [13, p. 646] and remain in oxidized form.

Thermochemical conversion can be *direct* or *indirect*. During direct thermochemical conversion, the heat is released by complete oxidation [13, p. 646] of the products. Indirect thermochemical conversion produces secondary energy carriers [13, p. 646]. These secondary energy carriers are incompletely oxidized products. Secondary energy carriers can be used in one or more subsequent conversion processes to provide useful energy. The advantage of secondary energy carriers is, that they are available at a decoupled time, as well as spatially decoupled [13, p. 647].

The best known and most important example of a direct (complete) thermochemical conversion is the combustion of biogenic solid fuels, like wood chips, with air in a commercial firing plant. A typical example of indirect (incomplete) thermochemical conversion is gasification [13, p. 647]. The biogenic solid fuel is heated and reacts with an oxidizing agent. The oxidizing agent converts the biogenic solid fuel into a combustible gas. The result is a product gas, that contains among other components, CO, H_2 and CH_4 [13, p. 647].

In complete thermochemical conversion, various conversion phases proceed in succession. As the fuel passes these phases, the fuel is successively oxidized. The process of thermochemical conversion in air atmosphere is divided into four sub-processes [13, p. 648].

These four sub-processes are:

- Heating
- Pyrolytic decomposition
- Gasification
- Oxidation

The four sub-processes of a thermochemical conversion in air atmosphere are shown in Figure 2.4. The temperature limits between the individual phases are not strict limits.

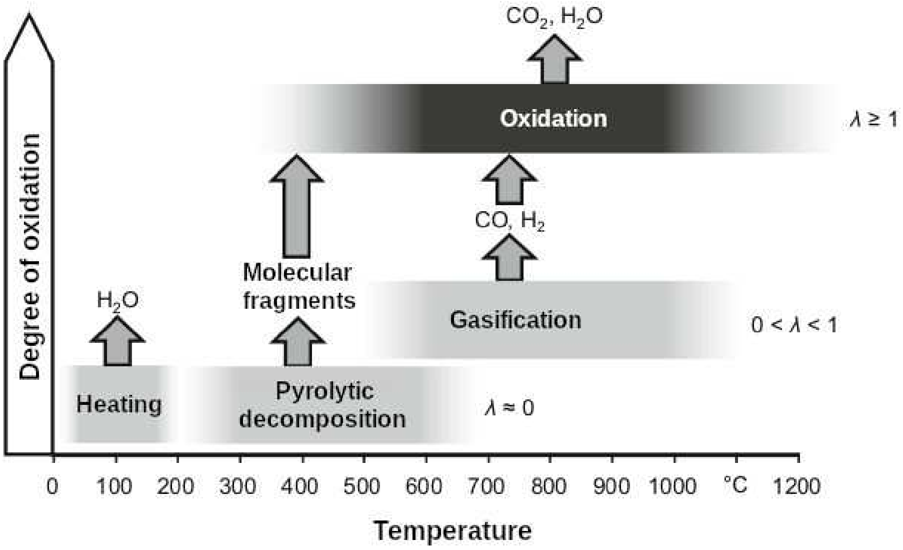

Figure 2.4: *Sequences of the four sub-processes of a thermochemical conversion in air atmosphere (adapted from [13, p. 648]).*

As shown in Figure 2.4, the processes of thermochemical conversion can be characterized by the air-fuel equivalence ratio λ. The air–fuel equivalence ratio is a dimensionless index, whose definition is shown in equation 2.4. The air–fuel equivalence ratio gives the mass ratio of the actual air available m_{AIR-av} to the minimum required air mass theoretically required m_{AIR-st} for stoichiometrically complete combustion [13, p. 651].

$$\lambda = \frac{m_{AIR-av}}{m_{AIR-st}} \tag{2.4}$$

Depending on the numerical value of λ the following areas are distinguished:

- $\lambda = 1$**:** For the stoichiometric combustion air ratio, $m_{AIR-av} = m_{AIR-st}$:
  In this case, all fuel molecules could completely react with the oxygen in the air, without any excess of oxygen or unburned fuel left over. This means *complete combustion.*
- $\lambda < 1$**:** Means *deficient air*:
  There is less oxygen available in the combustion air than would be required for a complete oxidation of the fuel.

- **$\lambda > 1$:** Means *air excess*:
  There is enough air available and more oxygen is involved in the combustion than would be necessary for a stoichiometric reaction.

Figure 2.5 shows a biomass particle that goes through the four sub-processes of thermochemical conversion. The indicated temperatures are not hard limits, but only intended to give approximate ranges.

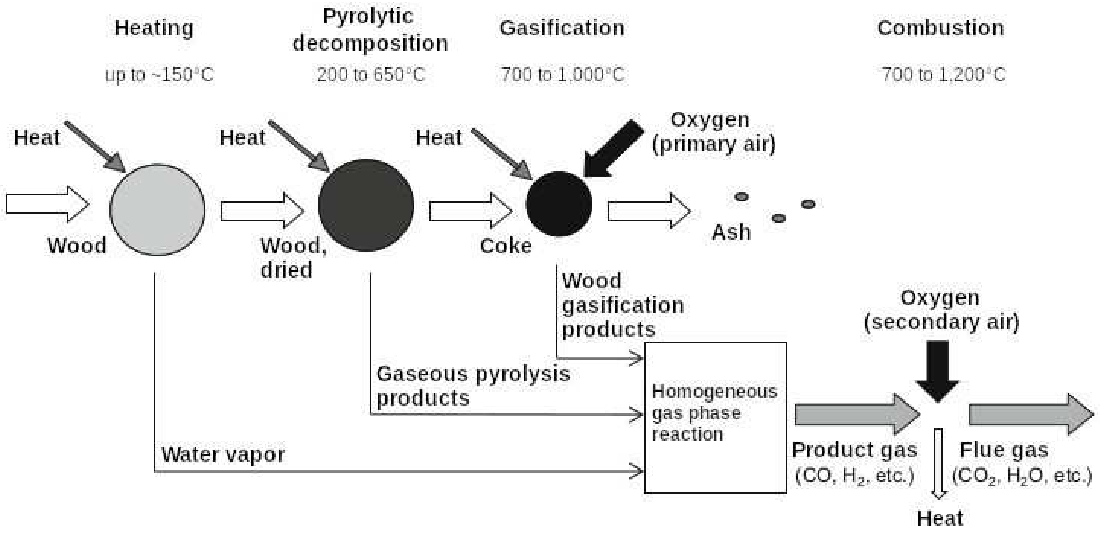

Figure 2.5: *A biomass particle that goes through the four sub-processes of thermochemical conversion (adapted from [13, p. 682].*

2.3.1 Heating

The first sub-process of thermochemical conversion is heating. In the heating phase, the biogenic solid fuel is heated. At first, the free water and then the water bound in the biomass cells escapes. At temperatures between 98 °C and 103 °C [13, p. 653], the hygroscopic bond of the water is broken up and drying begins. The organic matter remains largely intact.
If, on the other hand, the water bound in the actual biomass is evaporated, this leads to a shrinkage of the organic material. This evaporation process is endothermic [13, p. 653], which means that energy must be supplied in the form of heat for this process to proceed. As a result, a completely dried fuel remains. Due to the high enthalpy of evaporation of water, the temperature increase in the solid biofuel is thereby greatly slowed down until complete drying.
As the temperature increases, the chemical structure of the organic matter decomposes. There is a heat-induced disruption of the macromolecules from which the biomass is built up. However, this decomposition runs very slowly between 100 °C and 200 °C [13, p. 654]. Therefore the boundary between the heating phase and the pyrolytic decomposition is usually placed in this temperature range [13, p. 654].

2.3.2 Pyrolytic decomposition

The second intermediate step for complete oxidation of biogenic solid fuels is pyrolytic decomposition. The pyrolytic decomposition is basically thermolysis [13, p. 657]. Thermolysis is a chemical reaction, in which basic material is decomposed it into several products by heating. This macromolecules are thermally induced so that it comes to the dissociation of the bonds. These macromolecules are, for example, lignin, cellulose and hemicellulose, from which the biomass is composed. In this process, individual chemical bonds within the macromolecules are broken up and irreversibly destroyed [13, p. 657]. This creates smaller molecular fragments from the macromolecules of the biomass. By heating, these molecular fragments change their state of aggregation. Compared to the original state, this is associated with an increase in volume. Due to lack of space, the molecular fragments must leave the fuel particles in the form of gases and vapors [13, p. 657].

As with the heat-up phase, this thermochemical conversion step is an endothermic decomposition process that requires energy. This decomposition process requires heat energy and starts at temperatures of approximately 150 °C to 220 °C [13, p. 657]. At temperatures of about 500 °C [13, p. 657], the pyrolytic decomposition is largely completed. There remains a solid residue, the so-called *pyrolysis coke*. The pyrolysis coke mainly consists of carbon and ash. The pyrolytic decomposition almost always takes place in the absence of (additional) externally supplied oxygen. During pyrolysis, typically more than 70% [13, p. 658] of the volatiles present in biogenic solid fuels are released.

Reaction kinetics in pyrolytic decomposition

Reaction kinetics provide information about how fast certain chemical reactions take place [13, p. 664]. For the description of pyrolytic decomposition, there are various reaction kinetic models. Figure 2.6 shows a simplified kinetic scheme for the heat-induced decomposition of biomass.

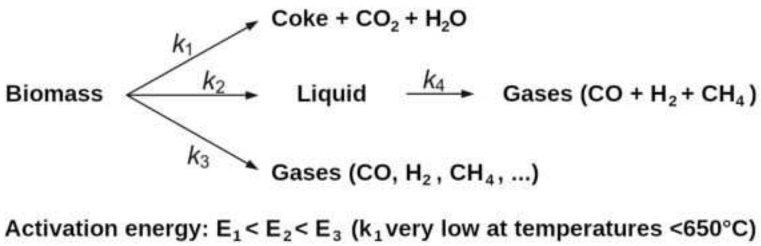

Figure 2.6: *Simplified kinetic scheme of pyrolytic decomposition of biomass (adapted from [13, p. 664]).*

According to the simplified kinetic scheme of Figure 2.6, three reactions take place in parallel. These three reactions are characterized by different rate constants k_1, k_2 and k_3. The activation energy denotes the energy that is required for the respective reaction to take place. The respective activation energies increase from E_1 to E_3. The amount of the primary products are thus significantly influenced by the temperature at which the decomposition takes place:

- The reaction 1 with the rate constant k_1 dominates at low temperatures. This corresponds to the slow pyrolysis. Coke is the main product [13, p. 664]. However, also CO_2 and H_2O are released.

- At higher temperatures and fast heating rates, reaction 2 dominates. Reaction 2 has the rate constant k_2. This reaction mainly leads to the formation of liquid products. This is the area of fast pyrolysis. Fast pyrolysis is the preferred reaction for the production of liquid fuels and chemical raw materials [13, p. 664]. Liquid products are mainly made up of decomposition products of cellulose and hemicellulose. The lignin degradation also causes coke and gases to appear here.
- At even higher temperatures, reaction 3 mainly takes place with the rate constant k_3. In this reaction, the organic matter is predominantly converted to gases [13, p. 664].

Depending on the desired ratio of gases, liquids and coke, different process conditions are selected for the pyrolytic decomposition.

At high temperatures and sufficient residence time, more extensive, secondary reactions of the products occur. These reactions can take place inside the particle, in the gas phase or on the surface of the coke particles. For example, liquid products are cracked to CO, H_2 and CH_4 [13, p. 665]. However, it can also lead to the formation of secondary coke. These secondary reactions are shown in Figure 2.6 and are characterised by the rate constant k_4.

2.3.3 Gasification

The gasification phase, like the pyrolytic decomposition phase, represents an intermediate step towards complete oxidation of biogenic solid fuels. During thermochemical conversion phase of gasification, solid fuels are converted into gaseous fuels by supplying thermal energy. Suitable oxidizing agents besides pure oxygen are mixtures of substances as well as chemical compounds which contain oxygen.

During pyrolytic decomposition, some residual carbon remains. In gasification, as complete as possible conversion of this residual carbon is achieved to combustible gases. For this conversion to take place, it is necessary to use an oxygen-containing gasification agent that is as oxygen-containing as possible. Thereby, the solid carbon can be converted with the oxygen of the gasification agent. Oxygen-containing gasification agents are, for example, air, O_2, H_2O (water vapor) or CO_2 [13, p. 647]. It should be noted that in special cases, H_2 [13, p. 668] can be used as a gasification agent.

If air and therefore oxygen is used as a gasification agent, the gasification can be characterized by the air-fuel equivalence ratio λ, as described in equation 2.4. Gasification takes place in the range between 0 and 1 ($0 < \lambda < 1$). Therefore, gasification is also referred to as *partial combustion* [13, p. 668].

During gasification of biomass, various physico-chemical processes take place, which can be found to a greater or lesser extent in almost all gasification processes. However, the temporal and spatial assignment of the reactions depend on the design of the reactor, the process control and the presence of catalysts. When considering a biomass particle, gasification can be divided into the stages of *heating and drying*, *pyrolytic decomposition*, *oxidation* and *reduction* [11, p. 136]. Figure 2.5 shows the individual stages of gasification. The first three sub-stages are considered for gasification. The last sub-stage is the complete oxidation, which is not part of gasification. The aim of gasification is to obtain a product gas that is available as a secondary energy carriers [11, p. 129].

During gasification, a large number of chemical reactions take place simultaneously. These ongoing reactions can basically be divided into *heterogeneous gas-solid reactions* and *homogeneous gas-phase reactions.*

Heterogeneous solid reactions

Heterogeneous reactions of solid carbon at substoichiometric conditions include both, oxidation reactions and reduction reactions [13, p. 669]. Table 2.3 lists some important reactions that occur during gasification and also shows their reaction enthalpies ΔH_R.

Table 2.3: *Oxidation reactions and reduction reactions, as well as their reaction enthalpies at temperatures of 25 °C and 850 °C (adapted from [13, p. 669].*

Number	Reaction	$\Delta H_{R,25\,°C}$ in kJ/mol	$\Delta H_{R,850\,°C}$ in kJ/mol
(1)	$C + O_2 \rightarrow CO_2$	-393.4	-394.9
(2)	$C + \frac{1}{2}O_2 \rightarrow CO$	-110.5	-87.6
(3)	$C + H_2O \rightarrow CO + H_2$	+131.3	+135.7
(4)	$C + CO_2 \rightarrow 2CO$	+172.4	+169.4
(5)	$C + 2H_2 \rightarrow CH_4$	-74.9	-89.8
(6)	$CO + H_2O \leftrightarrow CO_2 + H_2$	-41.2	-33.6
(7)	$CH_4 + H_2O \leftrightarrow CO + 3H_2$	+206.2	+226.8
(8)	$C_mH_n + mH_2O \rightarrow mCO + (m + \frac{1}{2}n)H_2$		

By oxidation reactions, the carbon stored in the biomass gets converted with oxygen. The carbon can be partially or completely oxidized. An example of a complete reaction is shown as equation (1) in Table 2.3. Equation (2) shows a partial oxidation of the carbon to CO. These reactions occur when enough O_2 is present. The negative sign of the reaction enthalpy indicates that energy is released in the form of heat in these reactions [13, p. 669]. These are *exothermic* reactions.

However, most of the combustible gases produced during gasification are formed by reduction reactions [13, p. 669]. Reduction reactions are *endothermic*, in which energy must be supplied in the form of heat for them to occur. Table 2.3 lists the two most important reduction reactions, the heterogeneous water-gas shift reaction (WGSR) (3) and the Boudouard reaction (4). As mentioned previously, C can also be gasified with H_2, as shown in equation (5) in Table 2.3.

Homogeneous gas-phase reactions

The gaseous products of heating, pyrolytic decomposition and coke gasification products continue to react in homogeneous gas phase reactions [13, p. 670]. Important reactions are shown in Table 2.3 as equations (6) to (8). In the case of gasification with steam, for example, the homogeneous WGSR (6), the steam reforming of CH_4 (7) and the steam reforming of hydrocarbons (8) are of importance.

Homogeneous gas phase reactions can be both exothermic and endothermic. Overall, the energy balance of the gasification reactions is endothermic [13, p. 670]. This means that heat is needed to gasify biogenic solid fuels. The required heat can be supplied to the system in various ways. Depending on the type of heat input, a distinction is therefore made between *autothermal* and *allothermal* gasification [13, p. 670]. In autothermal gasification, the heat is provided directly by partial combustion of the biogenic solid fuel during gasification. In the allothermal gasification, the heat is supplied indirectly. This can be done for example via a heat exchanger or by a circulating bed material, as in circulating fluidized beds (CFB).

Gasification medium

Gasification can be realized in different gas atmospheres. Mainly air, steam and oxygen are of technical importance as gasification medium [13, p. 674]. The gasification medium significantly influences the properties of the resulting product gas. In the gasification medium air, as well as in the gasification medium oxygen, exothermic oxidation reactions occur. This provides the heat required for the endothermic gasification reactions. Gasification by air and oxygen are autothermal processes and represented by the equations (1) and (2) in Table 2.3. Partial oxidation with air, causes the gaseous, liquid and solid products of the pyrolytic decomposition to react with oxygen by the action of further heat. This raises the temperature to over 700 °C [13, p. 674]. The coke is transferred into the gas phase. The main advantage of oxygen, compared to air as a gasification medium, is that the product gas is not diluted by N_2 [13, p. 675].

In contrast to gasification with air or oxygen, no free oxygen is supplied during steam gasification. The gasification agent is H_2O. As shown in equation (3) in Table 2.3, this is converted with the solid carbon to CO and H_2. In addition, the Boudouard reaction proceeds according to equation (4) and the homogeneous WGSR according to equation (6). Since there is no partial combustion of the feedstock during steam gasification, the reaction enthalpy must be supplied from the outside [13, p. 675].

Reaction kinetics

The residual carbon (pyrolysis coke) after the pyrolytic decomposition is in solid form. During its gasification, heterogeneous reactions take place. The most important steps in solid gasification can be summarized as follows [13, p. 677]:

- Mass transport of the gaseous reactants into the reaction zone of the particle.
- Diffusion through the gas boundary layer to the surface of the particle.
- Diffusion into the pores of the particle.
- Reaction of the gasification agent with the solid.
- Diffusion of vaporizable gaseous (volatile) gasification products from the pores of the particle.
- Diffusion of the volatile products through the boundary layer to the outside and mass transport of gasification products from the reaction zone.

The slowest sub-step determines the speed of the entire solid gasification. Which of the respective sub-steps determines the speed of gasification, depends on the corresponding mass transfer and the reaction conditions [13, p. 677].

2.3.4 Oxidation

Oxidation describes the last step in thermochemical conversion of biomass. During oxidation, the products formed by the partial steps of the pyrolytic decomposition and the gasification are completely oxidized with O_2 [13, p. 681]. When oxidized with oxygen, energy is released in the form of heat. In contrast to gasification, the oxidation phase is a highly exothermic

process. The final reaction products in the event of complete combustion are mainly CO_2 and H_2O (water vapor) [13, p. 681]. Figure 2.5 shows the combustion, i.e. the oxidation phase, as the last of the four sub-processes of thermochemical conversion on a biomass particle. Combustion provides the thermal energy needed for the three previous phases of *heating*, *pyrolytic decomposition* and *gasification* [13, p. 687].
Sufficient oxygen must be available for this complete oxidation to take place. This ensures that the fuel can be fully oxidized. For this reason, the air–fuel equivalence ratio λ must be greater than 1 ($\lambda > 1$). In this context, the *3-T criterion* [11, p. 157] is of great importance for combustion, which can be described as follows:

- **Temperature:** The temperature must be high enough for the oxidation reagents to proceed completely.
- **Turbulence:** To ensure that complete oxidation occurs, the combustion gases must be well mixed with the combustion air or with the oxidizer.
- **Time:** There must be enough time for the complete course of the oxidation reactions.

Combustion reactions

Oxidation reactions, that occur when burning solid fuels, can be both heterogeneous and homogeneous [13, p. 681]. Table 2.4 lists the most important oxidation reactions and associated reaction enthalpies at temperatures of 25 °C and at 850 °C in incinerators.

Table 2.4: *Some of the most important oxidation reactions and their reaction enthalpies at 25 °C and at 850 °C in incinerators (adapted from [13, p. 681]).*

Number	Reaction	$\Delta H_{R,25\,°C}$ in kJ/mol	$\Delta H_{R,850\,°C}$ in kJ/mol
(9)	$C + O_2 \rightarrow CO_2$	-393.4	-394.9
(10)	$C + \frac{1}{2}O_2 \rightarrow CO$	-110.5	-87.6
(11)	$CO + \frac{1}{2}O_2 \rightarrow CO_2$	-282.9	-366.8
(12)	$H_2 + \frac{1}{2}O_2 \rightarrow H_2O$	-241.8	-224.1
(13)	$CH_4 + 2O_2 \leftrightarrow CO_2 + 2H_2O$	-808.2	-801.0
(14)	$C_mH_n + (m + \frac{n}{4})O_2 \rightarrow mCO_2 + \frac{1}{2}nH_2O$		

Heterogeneous oxidation reactions occur in the firing bed of the furnace. Solid carbon is oxidised to CO_2 (9) or to CO (10). Both reactions are the same as they occur during gasification, listed in Table 2.3. The subsequent oxidation in the gas phase proceeds as a homogeneous process, as shown in equations (11) to (14) [13, p. 681].

Reaction kinetics

The oxidation reactions are very fast reactions. As with gasification, the most important steps in solid matter combustion can be summarized as follows [13, p. 682]:

- Mass transport of the gaseous reactants in the reaction zone.
- Gaseous oxygen migrates through the boundary layer to the surface of the fuel particle.

- Diffusion of oxygen through the pores into the interior of the particle.
- Reaction of the oxidizing agent with the fuel.
- Release of heat and gaseous (volatile) products.
- The volatile products diffuse out of the pores through the boundary layer to the outside.
- Reaction of the volatile products with oxygen in the reaction zone.
- Formation of CO_2, which escapes from the reaction zone.

2.4 Substances from thermochemical conversion

If biogenic solid fuels pass through the four sub-processes of thermochemical conversion, described in Section 2.3, the two gaseous combustion products H_2O as well as CO_2 are produced with the release of heat [13, p. 697]. In addition to these two products, ash and dust particles also form from the unburned fuel constituents. Depending on the nature of thermochemical reaction, it may also lead to the formation of further gaseous, liquid and solid substances. These substances can be discharged via the flue gas path and/or in solid or suspended form in a wastewater stream out of the conversion plant. The subdivision substances can be made into the following categories [13, p. 698]:

- **Substances from complete oxidation of the main fuel constituents:**
  The main fuel constituents are C, H and O. This group includes CO_2 and H_2O (water vapor).
- **Substances from incomplete oxidation of the main fuel constituents:**
  These include the combustible portion of dust emissions as well as particulate emissions and the proportion in the ash. Also further oxidizable gases such as CO and hydrocarbons (tars, black carbon, polycyclic aromatic hydrocarbons) may be mentioned here.
- **Substances from trace elements or impurities contained in the fuel:**
  These include gaseous nitrogen compounds (NO, NO_2, HCN, NH_3, N_2O), sulfur compounds, chlorine compounds and potassium compounds as well as dioxins and furans. The residual mineral ash is also assigned to this category.

The residues from the furnace, the flue-gas-side surfaces as well as from any existing secondary dust-collecting devices, which remain when burning biogenic solid fuels, are called ashes. Important characteristics of the ashes have already been discussed in more detail in Subsection 2.1.4. The ashes of thermochemical conversion plants can basically be divided into four different fractions [13, p. 701]:

- The **coarse ash** or **grate ash** is understood to mean the predominantly mineral residue of the biomass in the combustion part of the furnace.
- At the flue gas side surfaces of the reactor, **solid and liquid flue gas components** collect, since these heat exchanger surfaces are cooler than the flue gas. These unwanted

residues must be removed regularly mechanically or by rinsing. Particularly in the case of condensing heat exchangers, wastewater added with these residues leaves the conversion plant.

- **Cyclone ash** is the solid, predominantly inorganic fuel constituents entrained as particles in the flue gas. These are often collected by downstream centrifugal separators. Typically, the particles collected here have a size of over 1 µm [13, p. 701].
- **Flue ash** consists of ash and fuel particles as well as deposits in the exhaust duct, which are released under certain conditions and are entrained by the flue gas volume flow. Their particle size is usually in the size range below 10 µm [13, p. 701]. These very small particles are problematic and require secondary filtering such as fabric filters or electrostatic precipitators.

In addition to the physical and mechanical properties of ash, the nutrient contents of the ash are an important factor. The nutrient contents of ashes from fluidized bed firing can sometimes differ significantly from those of fixed bed firing systems. The mixing of the ash with the bed material, which is mostly quartz sand, results in high silica (SiO_2) contents in ashes from fluidized bed combustions. A dilution effect occurs, which reduces the concentrations of all other elements accordingly.
The ash fractions produced, for example during wood combustion, contain a significant amount of nutrients. It seems expedient to use these ashes on agricultural and forestry land as fertilizer. The only missing essential nutrient is nitrogen. Nitrogen almost completely passes into the gas phase during combustion, as a result it is introduced into the atmosphere together with the flue gas. This happens on the one hand in the form of pure nitrogen, as well as in the form of nitrogen oxides (NO_x) [11, p. 117]. The essential component of wood ash is Ca. Calcium can contribute to soil irrigation by its basic action, as it increases the pH value. The main constituent of straw ash, however, contains Si, which is a neutral element for soils and plants. Other important elements in the ash are Mg, K and P [11, p. 117].
A special attention has to be paid to P. Phosphorus is a non-renewable limited resource [19]. P is an important component that is indispensable for the growth of organisms and can not be replaced by other elements [19]. The demand for the recovery of P must therefore be given increased importance. For the recovery of P from the biomass ash, there are already very promising approaches.
In summary, there are three promising criteria that can be considered of particular importance in phosphorus recovery [19]:

- The solubilization of phosphatic minerals by **bio-leaching technology** is an important way to bio-fertilization.
- The **supercritical extraction** technology is a good pretreatment method for a better release of phosphate in the biomass ash.
- **Chemical extraction** is a promising method for separating elements from biomass ash.

As shown in Table 2.1, thermochemical conversion of biomass also results in the formation of ash, which may also contain heavy metals. Also organic pollutants and levels of organic carbon are contained in the ash. However, these components are not discussed in more detail here. It should be noted that the resulting ash in many cases can be problematic and reintroduction into the ecosystem is limited. As a result of the heavy metal input, ashes from wood from old wood firing can not be spread out without prior treatment on agricultural or forestry land [13, p. 789].

2.5 Fluidized bed technology

Fluidized bed technology has its origins in the field of thermal and mechanical process engineering. Fluidized bed technology is one of many ways of converting the chemically stored solar energy of biomass into a usable form of energy for humans. Therefore, fluidized bed technology is often used in thermochemical conversion processes. Typical applications of fluidized beds are, for example, the drying of solid and granulated materials, the combustion, gasification or pyrolysis of fossil or biogenic fuels or the thermal utilization of residues such as sewage sludge. Fluidized beds are also suitable for fluid catalytic cracking processes (FCC) [20, p. 3] for the production of fuels.

However, fluidized bed technology is not limited to thermochemical conversion of biomass and other fuels. In Section 2.8 some fields of applications of fluidized bed technology are given. This section aims to provide an overview of fluidized bed technology and to deal with technically important aspects in the design and implementation of fluidized bed systems.

2.5.1 Historical beginnings

As early as 1922, the first fluidized bed gasification plant was developed by the German chemist Fritz Winkler. Fritz Winkler worked for the chemical company BASF (Badische Anilin- & Soda-Fabrik) [21]. The great need for low cost synthesis gas for ammonia synthesis was the starting point for optimizing the Haber-Bosch process [21] for recovering this synthesis gas. The result was the first reactor, which operated on the principle of fluidized bed gasification and named after its inventor *Winkler-generator*. With the help of the Winkler-generator, it was possible to extract the gases H_2 and CO from fine-grained brown coal via autothermal gasification. The H_2 thus obtained could be converted into the synthesis gas NH_3 (ammonia gas) at the end of the process with N_2. With the help of H_2 and CO, the production of CH_4O (methanol) was also possible [21]. In 1926, the first large-scale plant was put into operation.

Figure 2.7 shows a schematic representation of how the Winkler-generator works.

2.5.2 Structure of a fluidized bed

There are different fields of application of fluidized beds, which are explained in more detail in Section 2.8. Based on the respective requirements, there are different versions of fluidized bed systems, which mainly differ in their complexity.

A fluidized bed is a bed of solid particles which is brought into a fluidized state by an upward flow of a fluid. Due to the fluidization from below the solid particles, the so-called *bed material*, are getting suspended. In this swirling bed material various fuels, as well as other components, can be added. Figure 2.8 shows the schematic arrangement of a possible fluidized bed apparatus.

The simplest fluidized bed apparatus consists of a container (1), the bed material (2), a blower for fluidization (3) and a gas distributor (4). Depending on the application, additional

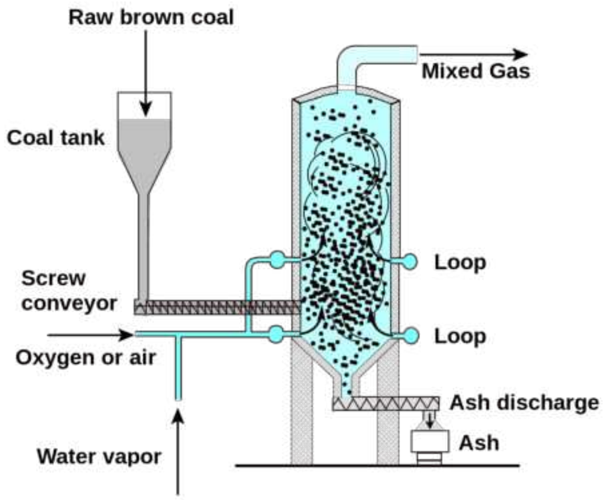

Figure 2.7: *Schematic representation of the Winkler-generator (adapted from [22]).*

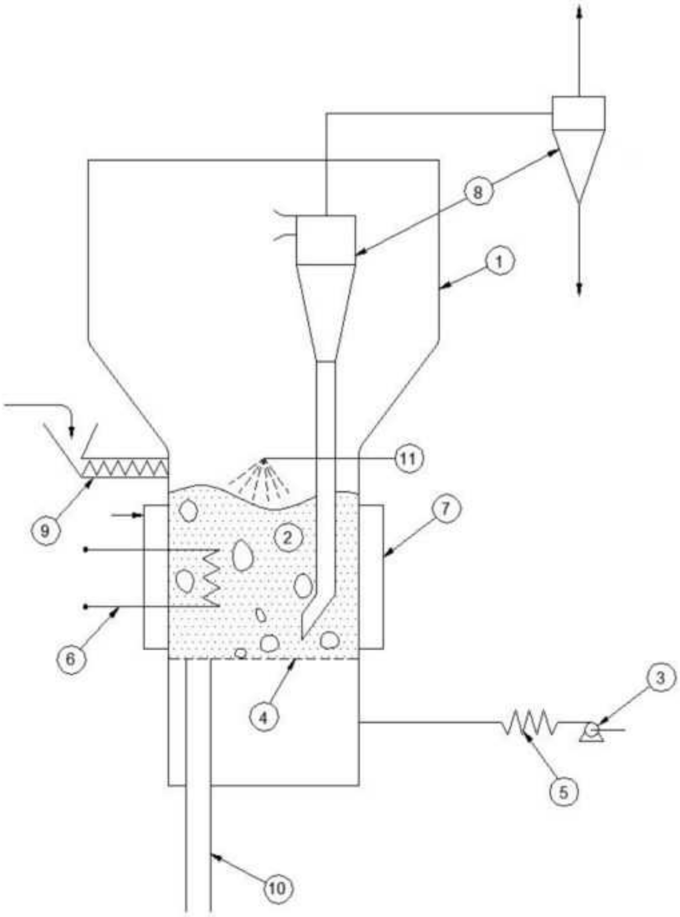

Figure 2.8: *Scheme of a fluidized bed: Container (1), bed material (2), blower for fluidization (3), gas distributor (4), gas preheater (5), internal heating or cooling surfaces (6), external heating or cooling surfaces (7), particle separator (8), solid fuel conveyor (9), solid discharge (10), spray feed (11); (adapted from [23, p. 6])*

components will be used. For example a fluidizing gas preheater (5), internal heating or cooling surfaces (6), external heating or cooling surfaces (7), a particle separator (8), a solid fuel conveyor (9), a solid discharge (10) or a spray feed (11) can be used [23, p. 6].
The different types of fluidized beds are discussed in more detail in Subsection 2.5.3.

2.5.3 Classification of fluidized beds

There are various ways in which fluidized beds can be characterized. In the following, fluidized beds are characterized according to the fluidization rate. This results in different fluidization states. Depending on the different conditions of fluidization, the hovering speed of a single particle is exceeded, causing the bed material to whirl. Another possibility of division was made by Derek Geldart [23, p. 27]. These are discussed in more detail in Subsection 2.5.4.
Fluidized beds are characterized by the fact that they are maintained over a wide range of fluidization rate. Therefore, it is obvious that fluidized beds can be characterized by their fluidization. The requirement for a fluidized bed is that the density of the below supplied fluid ρ_g is less than the density of the solid particles ρ_s. Otherwise the particles would float on top of the surface. Possible operating states of fluidized beds, based on fluidization velocities are characterized in Figure 2.9.

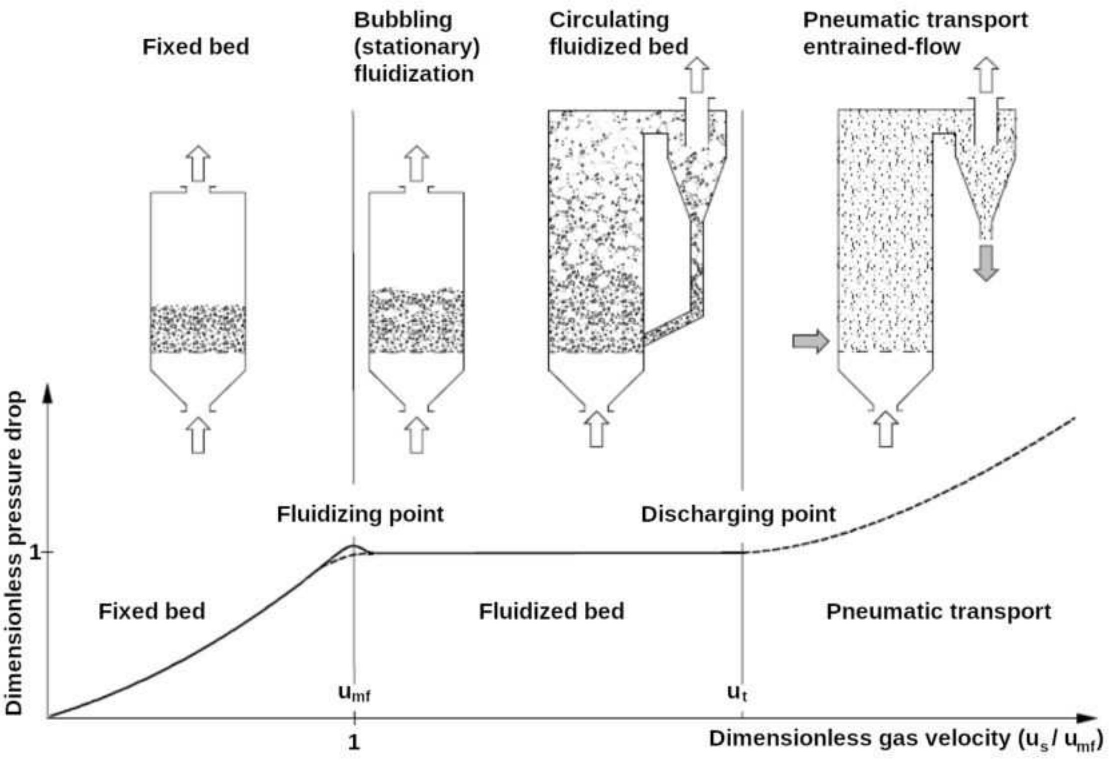

Figure 2.9: *Possible operating states of fluidized beds, based on fluidization velocities (adapted from [11, p. 210]).*

L_m refers to the height of the bed material, at which the fluidization rate is so low that the individual particles do not move. This is called a *fixed bed* [23, p. 3]. The fluid flows around the particles, but there is no lifting of the particles. The basic physical laws, as well as the mathematical formulation of the equilibrium conditions, which describe the floating state of a particle, are explained in more detail in Subsection 2.6.3. A schematic illustration of a fixed bed is shown in Figure 2.9 as well as in Figure 2.10a.

If the fluidization rate is increased, a point is reached at which the fixed bed begins to expand. The particles start to move and as shown in Figure 2.10b, the *minimum fluidization velocity* u_{mf} is reached. L_{mf} describes the height of the fluidized bed with minimum fluidization velocity [23, p. 3]. As the fluidization rate is further increased, the rate at which particles are discharged from the reactor is approached. Then the solid particles are discharged pneumatically at the top of the reactor. This speed is called *terminal velocity* u_t. It represents the upper end of a fluidized bed. Figure 2.10c shows a possible mode of operation of expanded fluidized beds. L_f describes height of the fluidized bed at a smooth fluidization velocity.

Figure 2.9 shows the velocities u_{mf} and u_t as well as the associated characteristic points of *fluidizing point* and the *discharging point*. The minimum fluidization velocity u_{mf} as well as the terminal velocity u_t are described in more detail in Subsection 2.6.3.

If the fluidization rate exceeds the terminal velocity, the lean phase fluidization with pneumatic transport is reached. Figure 2.10d illustrates the solid particles discharged at the top of the reactor because of a too high fluidization rate.

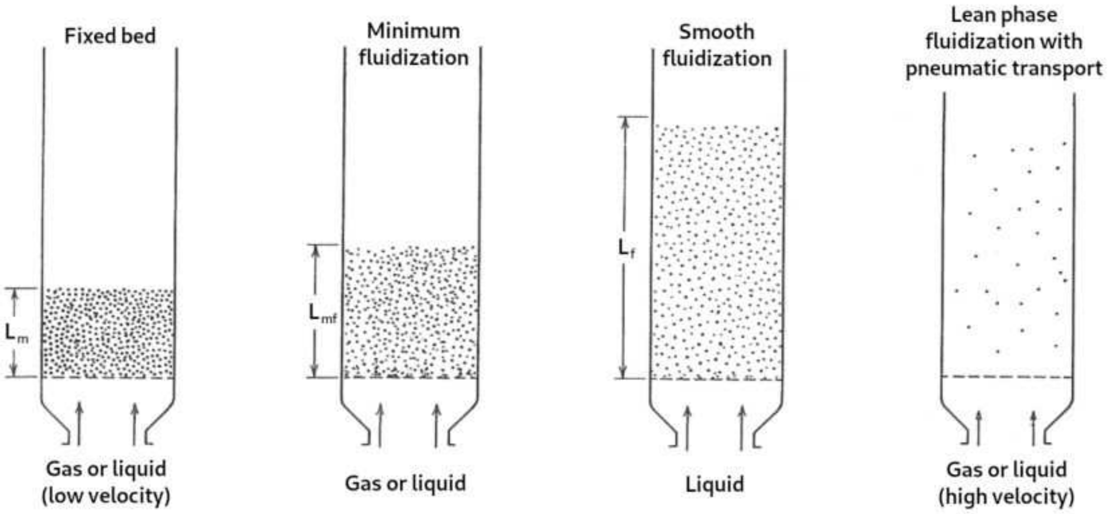

(a) *Fixed bed* **(b)** *Minimum fluidization* **(c)** *Smooth fluidization* **(d)** *Pneumatic transport*

Figure 2.10: *Quantitative representation of the possible states of a fluidized bed (adapted from [23, p. 2]).*

Apart from the fluidization rate, fluidized beds can basically be subdivided into two types. There are *homogeneous* fluidized beds and *inhomogeneous* fluidized beds [23, p. 3]. For homogeneous fluidized beds the individual particles, the so-called *disperse phase*, is equally distributed in the reactor. In the case of inhomogeneous fluidized beds, the disperse phase is not equally distributed in the reactor. In homogeneous fluidized beds, increasing the fluidization rate leads to continuous expansion of the fluidized bed. Homogeneous fluidized beds occur predominantly in the use of liquids as fluidization medium [23, p. 3]. Also with very fine-grained, small wide size distribution and non-cohesive material systems with low density difference, homogeneous fluidized beds can be realized.

Heterogeneous fluidized beds are also called *bubbling fluidized beds* [23, p. 3]. Bubbling fluidized beds occur predominantly when using gases as fluidization medium. If particles with

a wide size distribution or particles with a large differences in density are used, bubbling fluidized beds are dominant. Figure 2.11a shows an inhomogeneous, bubbling fluidized bed. The gas velocity in this state is significantly lower than the rate of descent of a single grain. The bubbling fluidized bed is characterized by intensive mixing in the vertical direction.
By using very slim reactors, special shapes of the bubbling fluidized beds can occur. Due to the small diameter of the reactor, bubbles form which occupy the entire cross section of the reactor. Representative are *axial slugs* and *flat slugs*. In Figures 2.11b and 2.11c, these two types of fluidized beds are shown. These are called *colliding fluidized beds* [23, p. 3].
In case of bubble-forming fluidized beds, if the fluidization rate is increased, the rate at which the particles are discharged from the reactor is approached. Before pneumatic discharge occurs, there may be a change in the flow structure in bubble-forming fluidized beds. Due to the high fluidization speed, small gas bubbles can combine to form bigger single gas bubbles [23, p. 3]. This can lead to formation of gas channels and solid strands, which are shown in Figure 2.11d. These are called *turbulent fluidized bed*. In this area, the pressure fluctuations decrease [23, p. 3] and the fluidized bed makes a much calmer impression.

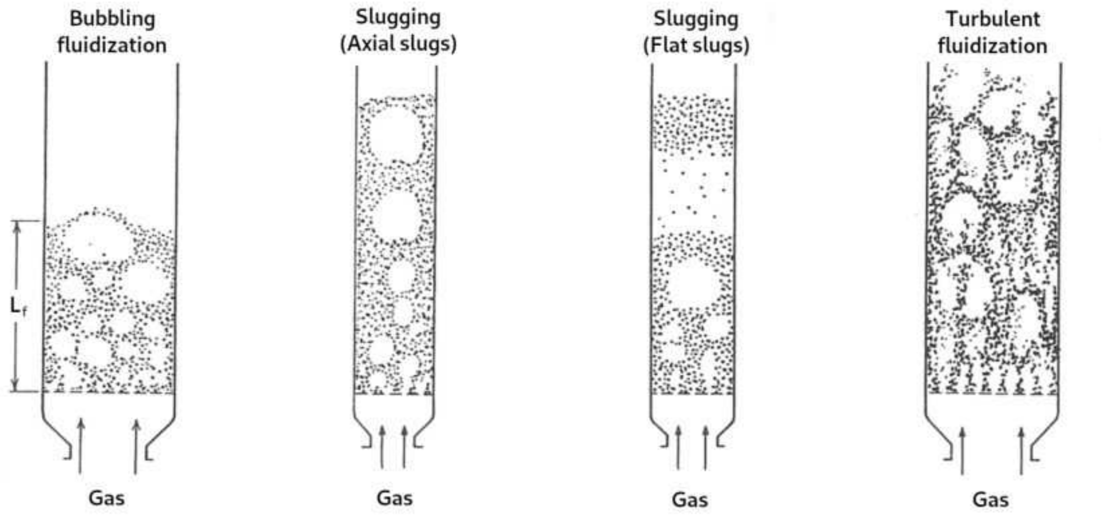

(a) *Bubbling fluidization* **(b)** *Axial slugs* **(c)** *Flat slugs* **(d)** *Turbulent fluidization*

Figure 2.11: *Quantitative representation of the different types of bubbles in bubble-forming fluidized beds (adapted from [23, p. 2]*

Referring to Figure 2.9, all possible flow states, which can occur in a fluidized bed, are summarized in Table 2.5.

Table 2.5: *Possible gas/solid flow conditions in a fluidized bed (adapted from [23, p. 3]).*

Flow state	Particle	Pressure drop	Fluid velocity
Fixed bed	do not move	increasing	low
Fluidized bed	move	constant	medium
Pneumatic transport	move	slightly increasing	high

2.5.4 Grouping according to Geldart

Derek Geldart was a British chemical engineer who worked as a professor of powder research at the University of Bradford [24]. His main scientific achievement was the introduction of Geldart grouping for the classification of fluidized bed processes in 1973 [25].
Depending on their different fluidization behaviour, bulk materials for gas/solid fluidized beds were subdivided by Derek Geldart into the so-called *Geldart groups*. These groups are plotted in a log-log plot of density difference (fluid-solid) versus mean particle size. Design methods for fluidized beds can be tailored based upon the Geldart grouping of the particle. Figure 2.12 shows this double logarithmic diagram according to which Derek Geldart carried out the classification.

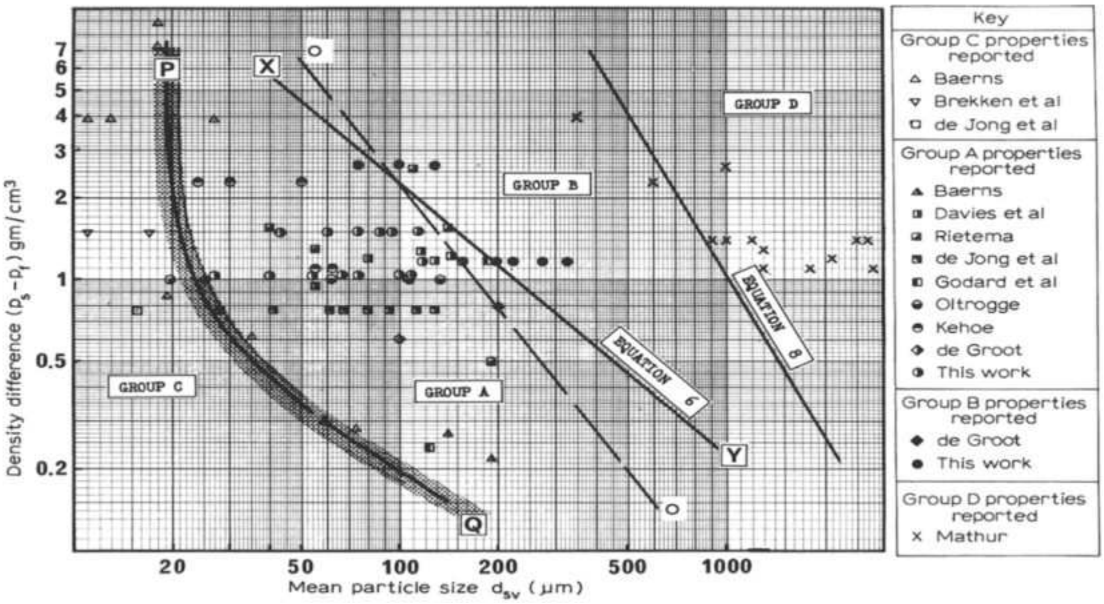

Figure 2.12: *Powder classification diagram for fluidization by air (ambient conditions) [25].*

The individual types of bulk materials can be reasonably distinguished by plotting the mean particle size and the density difference in the diagram. The bulk materials were divided into four groups (A - D) by Geldart [23, p. 27]:

- **Group A:** For this group the particle size is between approximately 20 µm to 100 µm, the particle density is typically less than approximately 1400 kg/m^3. Prior to the initiation of a bubbling bed phase, beds from these particles will expand by a factor of 2 to 3 at incipient fluidization, due to a decreased bulk density. This group includes most powdered catalysts.
- **Group B:** The particle size is between approximately 40 µm to 500 µm, the particle density approximately 1400 kg/m^3 to 4500 kg/m^3. Bubbling typically forms directly at incipient fluidization.
- **Group C:** This group contains extremely fine and thus very cohesive particles with a size of less than 20 µm to 30 µm. Due to the strong cohesive forces, these particles are very difficult to fluidize. These particles may require the application of an external force, such as mechanical agitation.

- **Group D:** The particles in this region are above 600 µm and typically have high particle densities. Fluidization of this group requires very high fluid energies and is typically associated with high levels of abrasion.

2.6 Characteristics of fluidized beds

2.6.1 Characterization of single particles

The bed material of fluidized beds consists of many individual particles. To characterize the individual particles, the particle size d, the particle form factor ϕ and the particle density ρ_p are defined [23, p. 7].
The diameter d is used to describe the particle size. Since virtually all of the technically interesting solids are particles that are not spherical, an equivaltent diameter has to be defined. There are a variety of definitions for how to define a suitable equivalency diameter for a particle. For many applications, the surface/volume-related diameter d_{sv} [23, p. 9] has been found to be suitable. The definition of d_{sv} is shown in equation 2.5 [23, p. 8].

$$\frac{V_p}{A_p} = \frac{\frac{4}{3} \cdot \pi \cdot (\frac{d_v}{2})^3}{4 \cdot \pi \cdot (\frac{d_s}{2})^2} = \frac{1}{6} \cdot \frac{d_v^3}{d_s^2} = \frac{1}{6} \cdot d_{32} = \frac{1}{6} \cdot d_{sv} \qquad \Rightarrow \qquad d_{sv} = 6 \cdot \frac{V_p}{A_p} \tag{2.5}$$

A_p is used to describe the surface area of a spherical particle with a surface-related diameter d_s. V_p denotes the volume of a spherical particle with a volume-related diameter d_v. According to its developer, the German scientist Joseph Sauter, the equivalent diameter d_{sv} is also known as the *Sauter mean diameter (SMD, d_{32})* [26, p. 83]. The equivalent diameter d_{sv} is defined as the diameter of a sphere, that has the same volume-to-surface area ratio, as a particle of interest [27, p. 45].
To determine the grain size, a sieve analysis is usually carried out, determining the equivalent diameter d_p being determined. The equivalent diameter d_p is also called *sieve diameter* [23, p. 9] and corresponds to the side length of the square of a sieve through which the particle passes. However, in most calculation formulas, the aforementioned SMD d_{sv} is used. There is no general correlation between d_{sv} and d_p [23, p. 9]. In order to be able to conclude a sieve analysis on the equivalent diameter d_{sv}, the following approximations have been found [23, p. 8]:

- For particles that do not deviate too much from the spherical shape:

$$d_{sv} \approx \phi \cdot d_p \tag{2.6}$$

- For particles that are significantly larger in one dimension than in the other dimensions, but not more than 2:1 (*egg-shaped*):

$$d_{sv} \approx d_p \tag{2.7}$$

- For particles that are significantly smaller in one dimension than in the other dimensions, but not less than 1:2 (*disk-shaped*):

$$d_{sv} \approx \phi^2 \cdot d_p \tag{2.8}$$

The shape of the particle is given by a form factor ϕ. The form factor is defined via the sphericity ψ, according to equation 2.9 [27, p. 51]. Proposed by the geologist Hakon Wadell in 1935 [28], the sphericity is the ratio of the same surface area of a sphere to the surface area of an random shaped particle A_p. As shown in equation 2.10, the inverse of this ratio is the form factor [26, p. 85]. The form factor is defined to be 1 for a sphere. For all other particle shapes the form factor is between 0 and 1 ($0 < \phi < 1$).

$$\psi = \frac{\pi^{\frac{1}{3}} \cdot (6 \cdot V_p)^{\frac{2}{3}}}{A_p} = \frac{d_v^2 \cdot \pi}{d_s^2 \cdot \pi} = (\frac{d_v}{d_s})^2 \tag{2.9}$$

$$\phi = \frac{1}{\psi} = (\frac{d_s}{d_v})^2 \tag{2.10}$$

There is currently no recognized method of determining form factors [23, p. 9]. A practically acceptable method is to determine d_{sv} and d_v separately [23, p. 9]. If both diameters are determined, the form factor can be calculated using equation 2.11.

$$\phi = \frac{d_{sv}}{d_v} \tag{2.11}$$

The particle density depends on the nature of a particle. A particle can have many or few pores. These pores can be open or closed pores. The density ρ_p, which is important for many calculations, is also known as *hydrodynamic density*. Equation 2.12 shows the definition of hydrodynamic density [23, p. 11]. M_p denotes the mass of the particle. The volume of the particle including its pores is referred to as V_p.

$$\rho_p = \frac{M_p}{V_p} \tag{2.12}$$

The hydrodynamic density ρ_p must not be confound with the *absolute material density* $\rho_{p,abs}$. The absolute material density is additionally defined by the volume of the pores V_{pore}. The absolute material density is greater than the hydrodynamic density ($\rho_{p,abs} > \rho_p$) [23, p. 11]. Equation 2.13 shows the absolute material density.

$$\rho_{p,abs} = \frac{M_p}{V_p - V_{pore}} \tag{2.13}$$

Table 2.6 shows some form factors for technically interesting materials.

Table 2.6: *Form factors for technically interesting materials (adapted from [23, p. 8]).*

Material	Form factor ϕ
Broken coal	0.70 - 0.75
Broken sand	0.70 - 0.85
Rounded sand	0.90 - 0.95
Limestone	0.65 - 0.75
Ordinary salt	0.80 - 0.85
Technical glass balls	0.98 - 1.00

2.6.2 Porosity and bulk density

Bed material, that is in a non-fluidized state, can be referred to as a loose bulk. A loose bulk consists of a dispersant and a disperse phase. The dispersant is also referred to as the *continuous phase* and the disperse phase as the *distributed phase*. The individual, each other touching particles of the bed material are the distributed phase. Air that fills the voids between the distributed phase is the continuous phase. Bulk density is required to calculate volumes or the weight of loose bulk materials.
The porosity ε indicates the relationship between the intermediate grain volume and the total volume of a bed [23, p. 14]. The intermediate grain volume results from the total volume of the bed material V_b minus the particle volume V_p. The porosity is defined in fluidized bed technology according to equation 2.14, where M describes the mass of all particles. In fluidized bed technology, the porosity is also called *fixed bed porosity* .

$$\varepsilon = \frac{V_b - V_p}{V_b} = 1 - \frac{V_p}{V_b} = 1 - \frac{M}{\rho_p \cdot V_b} \tag{2.14}$$

The bulk density ρ_b denotes the density of a mixture, which consists of a distributed phase and a continuous phase. The bulk density is determined according to equation 2.15. The bulk density is also called *apparent density* or *volumetric density* [23, p. 14].

$$\rho_b = \frac{M}{V_b} \tag{2.15}$$

From the two equations 2.14 and 2.15, the relationship between fixed bed porosity ε and bulk density ρ_b results, which is shown in equation 2.16 [23, p. 14].

$$\varepsilon = 1 - \frac{\rho_b}{\rho_p} \tag{2.16}$$

The fixed bed porosity ε mainly depends on the properties of the material. In summary, the following relations apply [23, p. 14]:

- **Particle shape:** The lower the form factor, the higher the fixed bed porosity.
- **Particle size:** The larger the particles, the lower the fixed bed porosity.
- **Grain size distribution:** The wider the distribution, the lower the porosity.

2.6.3 Velocity and pressure in fluidized beds

Important for fluidized beds are the transition from fixed bed to fluidized bed and the transition from fluidized bed to the pneumatic transport of the particles. These transitions can be described by critical fluidization velocities. The critical fluidization velocities are shown in Figure 2.13. This diagram is the most important diagram to describe the relationship between velocities and pressures in a fluidized bed.

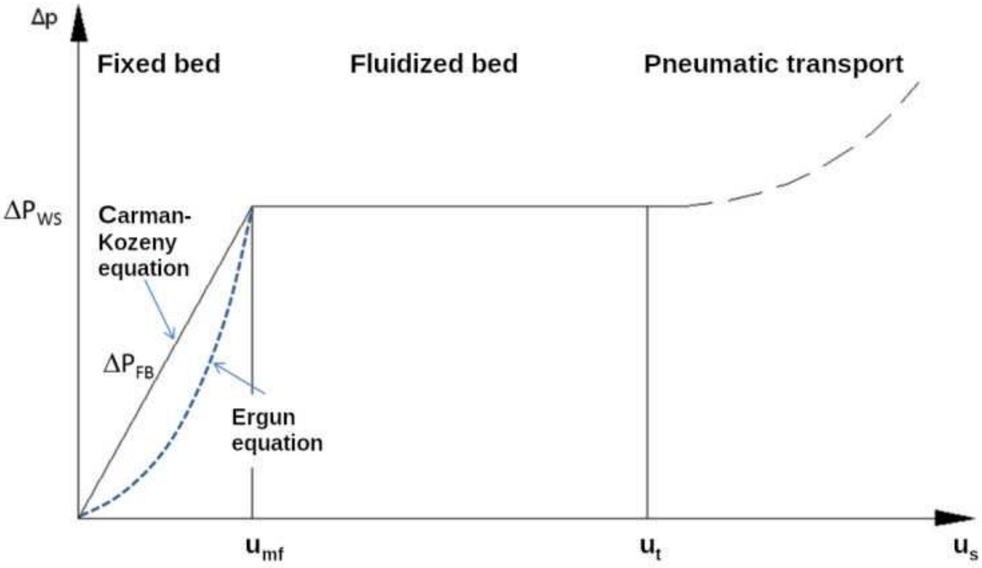

Figure 2.13: *Velocities and pressure drop in a fluidized bed (adapted from [23, p. 17]).*

As a reference, the so-called *superficial velocity* u_s is commonly used. The superficial velocity is is the velocity which would occur if there were no particles, meaning no fuel and no bed material, inside the reactor [23, p. 4]. Equation 2.17 shows the superficial velocity. The superficial velocity is therefore defined as the ratio of the gas volume flow $\dot{Q}$ to the cross sectional area of the reactor A [23, p. 16].

$$u_s = \frac{\dot{Q}}{A} \tag{2.17}$$

The two velocities u_{mf} and u_t are important for the description of fluidized beds. u_{mf} is the minimum fluidization velocity [23, p. 18] and u_t is the terminal velocity [23, p. 23]. The minimum fluidization velocity is the rate which describes the transition between a fixed bed operation and a fluidized bed. In the fixed bed area the pressure drop increases with increasing rate of fluidization. Depending on the Reynolds number Re, this can be a linear or a quadratic curve [23, p. 4]. If the minimum fluidization velocity is exceeded, then the pressure drop no longer changes and the area of the fluidized bed is reached. A characteristic of fluidized beds is that the pressure drop in the area of the fluidized beds remains constant over the entire area [23, p. 17]. If the fluidization velocity is further increased, finally the terminal velocity u_t is reached. The terminal velocity characterizes the upper end of a fluidized bed. After exceeding the terminal velocity, the weight forces of the particles are overcome and the particles are discharged from the reactor [23, p. 4]. The dashed line at the right side of Figure 2.13 describes the pressure drop which would occur when the discharged particles are

returned into the fluidized bed, as it is used in a CFB. In this area, the pressure drop over the velocity increases slightly [23, p. 4].
The *Carman-Kozeny* equation [23, p. 16] and the *Ergun* equation [23, p. 16] are used to calculate the pressure drop of a fluid caused by a fine-grained bed of particles. A model is used, in which the flow through a fixed bed takes place in parallel, twisted channels with a changing cross sectional area [23, p. 16]. The Carman-Kozeny equation is used for fluidized beds in which the Reynolds number Re is less than 1 ($\mathrm{Re} < 1$). Equation 2.18 shows the Carman-Kozeny equation for laminar flows.

$$\frac{\Delta p}{H} = 180 \cdot \frac{(1-\varepsilon)^2}{\varepsilon^3} \cdot \frac{\mu \cdot u_s}{d_{sv}^2} \tag{2.18}$$

In equation 2.18 the pressure drop across the fixed bed is denoted by Δp. H corresponds to the height of the fixed bed. The dynamic viscosity is denoted by μ. If the Reynolds number Re is greater than 1 ($\mathrm{Re} > 1$), a turbulent term must also be taken into account [23, p. 16]. Equation 2.19 shows the calculation according to Ergun.

$$\frac{\Delta p}{H} = 150 \cdot \frac{(1-\varepsilon)^2}{\varepsilon^3} \cdot \frac{\mu \cdot u_s}{d_{sv}^2} + 1.75 \cdot \frac{1-\varepsilon}{\varepsilon^3} \cdot \frac{\rho_g \cdot u_s^2}{d_{sv}} \tag{2.19}$$

The variable ρ_g denotes the gas density. The Reynolds number Re is calculated according to equation 2.20 [23, p. 16].

$$Re = \frac{u_s \cdot \rho_g \cdot d_{sv}}{\mu} \tag{2.20}$$

Both, the Carman-Kozeny equation and the Ergun equation, have proven to be sufficient in practice [23, p. 17].

Minimum fluidization velocity

For gas/solids fluidized beds, the pressure drop Δp in the fluidized bed can be approximated by equation 2.21 [23, p. 18]. M denotes the mass of the solid in the bed material, which is multiplied by the acceleration due to gravity g and related to the cross section area A of the reactor.

$$\Delta p = \frac{M \cdot g}{A} \tag{2.21}$$

To calculate the minimum fluidization velocity u_{mf}, approximate formulas based on experimental results are used [23, p. 20]. Equation 2.22 represents one of these approximation formulas, which has been well proven in practice. It is valid for a huge range of Reynolds number Re from 0.001 to 4,000 and has been proven for a wide range of different materials and grain diameters [23, p. 20].

$$u_{mf} = \frac{\mu}{\rho_g \cdot d_{sv}} \cdot [\sqrt{33.7^2 + 0.0408 \cdot Ar} - 33.7] \tag{2.22}$$

The Archimedes number Ar has to be calculated according to equation 2.23 [23, p. 16].

$$Ar = \frac{\rho_g \cdot d_{sv}^3 \cdot (\rho_p - \rho_g) \cdot g}{\mu^2} \tag{2.23}$$

Terminal velocity

Bubbling fluidized beds can be operated up to the terminal velocity u_t. If higher fluidization rates are required, the fluidized bed has to be carried out as a CFB in order to recirculate the particles discharged at the top of the reactor. Sometimes the terminal velocity is also known as *sedimentation velocity* or *levitation velocity* [23, p. 24].

Spherical particles For the mathematical description of the levitation velocity, an equilibrium of forces [23, p. 23] is applied to a single particle. The equilibrium of forces effecting the single particle is shown in more detail in Figure 2.14.

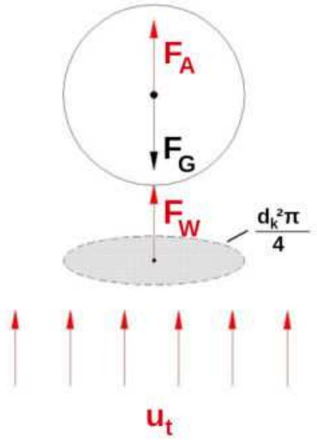

Figure 2.14: *The equilibrium of forces affecting the single particle (adapted from [23, p. 23]).*

A free-falling and undisturbed single particle in an infinitely extended liquid is considered. When the particle has reached its final velocity, no acceleration force acts on the particle [23, p. 24]. Then three remaining forces act on this particle:

- The **weight force** F_G of the particle.
- The **buoyancy force** F_A of the particle.
- The **resistance force** F_W of the particle.

The weight force is directed downwards, the buoyancy force and the resistance force are both directed upwards. Equation 2.24 describes the determination of the weight force F_G. The buoyancy force F_A is calculated according to equation 2.25. Equation 2.26 is used to calculate the resistance force F_W. The coefficient d_k denotes the diameter of a sphere. The dimensionless drag coefficient of a single sphere is given as c_w [23, p. 23].

$$F_G = m \cdot g = \frac{\pi}{6} \cdot d_k^3 \cdot \rho_p \cdot g \tag{2.24}$$

$$F_A = V \cdot \rho_g \cdot g = \frac{\pi}{6} \cdot d_k^3 \cdot \rho_g \cdot g \tag{2.25}$$

$$F_W = c_w \cdot A \cdot \frac{\rho_g \cdot u_s^2}{2} \tag{2.26}$$

The equilibrium of forces illustrated in Figure 2.14 can be expressed mathematically in equations 2.27 and 2.28. By using this equilibrium condition, the terminal velocity u_t can be calculated according to equation 2.29 [23, p. 24].

$$F_W = F_G - F_A \tag{2.27}$$

$$\frac{\pi}{6} \cdot d_k^3 \cdot g(\rho_p - \rho_g) = c_w \cdot \frac{d_k^2 \cdot \pi}{4} \cdot \frac{\rho_g \cdot u_t^2}{2} \tag{2.28}$$

$$u_t = \sqrt{\frac{4}{3} \cdot \frac{\rho_p - \rho_g}{\rho_g} \cdot \frac{d_k \cdot g}{c_w}} \tag{2.29}$$

The fluid resistance of a sphere is given as a function of the Reynolds number Re [23, p. 24]. The relationship between the Reynolds number and the drag coefficient was determined experimentally. The Reynolds number Re is calculated according to equation 2.30.

$$Re = \frac{\rho_g \cdot u_t \cdot d_k}{\mu} \tag{2.30}$$

This relationship makes it possible to distinguish three areas [23, p. 24]:

- **Laminar area:** $Re < 0.2$
- **Turbulent area:** $Re > 1000$
- **Transition area:** $0.2 < Re < 1000$

If the calculated Reynolds number Re assumes a value less than 0.2, then the model of the laminar flow around a sphere is used. This area is also called the *Stokes' area* because the velocity is calculated according to the *Stokes' law.* Equation 2.31 is used for the drag coefficient c_w and Stokes' law of drag, which is shown in equation 2.32, is used to calculate the terminal velocity u_t [23, p. 25].

$$c_w = \frac{24}{Re} \tag{2.31}$$

$$u_{t,Stokes} = \frac{(\rho_p - \rho_g) \cdot g \cdot d_k^2}{18 \cdot \mu} \tag{2.32}$$

The turbulent area begins for Reynolds numbers *Re*, which assume a calculated value of greater than 1,000 [23, p. 24]. In this area, turbulence occurs when the fluidization medium flows around the particle. This area is also referred to as the *Newton's area*. A fixed drag coefficient c_w is expected in Newton's area. The terminal velocity u_t is calculated according to equation 2.34.

$$c_w = 0.43 \tag{2.33}$$

$$u_{t,Newton} = \sqrt{\frac{4}{3} \cdot \frac{\rho_p - \rho_g}{\rho_g} \cdot \frac{d_k \cdot g}{0.43}} \tag{2.34}$$

The transition area is characterized by the fact that the Reynolds number *Re* is between the laminar and the turbulent area [23, p. 24]. The drag coefficient c_w is calculated according to equation 2.35.

$$c_w = \frac{24}{Re} + \frac{4}{\sqrt{Re}} + 0.4 \tag{2.35}$$

The determination of the terminal velocity u_t in the transition area, according to equation 2.29, is not possible. To calculate the terminal velocity, iteration techniques or other numerical approximation methods have to be used [23, p. 25].

Non-spherical particles For non-spherical particles, the formulas for spherical particles may not be used. To describe the rate of descent for non-spherical particles, approximations considering the form factor ϕ of the particles are used. It should be noted, that the form factor is not a suitable factor to satisfactorily describe the effects that occur by non-spherical particles. Nevertheless in the literature the form factor for laminar ranges is used for the calculation [23, p. 25].

2.7 Layer formation and agglomeration

The challenge of burning biogenic solid fuels, is to burn them as steady and as completely as possible [13, p. 691]. In fluidized beds, the bed material serves as a heat storage and heat exchanger. If fuel is brought into the combustion chamber, the fuel interacts with the bed material. The swirling bed material has close contact with the fluidization medium as well as with the fuel. This results in a very good heat exchange between the bed material and the particles of the fuel. The good heat transfer again results in a very homogeneous temperature distribution inside of the reactor [11, p. 211]. Ideally, the bed material is coating the fuel. Thus the supplied fuel is burned very steady and not punctually. Due to the homogeneous temperature distribution, it is possible to achieve a very constant and low-emission combustion. The homogeneous temperature distribution prevents hot spots inside the combustion chamber, whereby thermal nitrogen oxide formation is prevented. An advantage over other thermal systems is that plants with a fluidized bed have no moving parts inside of the combustion chamber. Due to the high temperatures in the combustion chambers, mechanically movable components are additionally subjected to high thermal loads. These components are often a source for failures.

The bed material is an essential component of fluidized bed plants and may also have catalytic properties [11, p. 216]. These catalytic properties are an important characteristic, especially for the reactions occurring during gasification. Due to the intensive contact with the fuel and the fluidization medium, the individual particles of the bed material interact with the fuel and the ash, resulting from thermochemical conversion, which leads to layering [29] on the surfaces of the particles. Investigations have shown that for many fuels, agglomeration and layer characteristics of the bed material did not reveal any major differences between gasification and combustion [30]. This indicates that layer formation processes of the bed material do not differ significantly between gasification and combustion [31].

The main problem with fluidized bed combustion and gasification is defluidization due to agglomeration. Regardless of the operating mode, the same agglomeration tendencies and layer formation mechanisms occur [30]. During the thermochemical conversion of the biomass in a fluidized bed, a large part of the ash leaves the reactor as flue ash, while a smaller part remains in the bed [32].

When examining samples from laboratory and industrial fluidized bed reactors, two main types of agglomeration were found. Partial defluidization of the fluidized bed and local peak temperatures also allow a combination of the two types of agglomeration. The two types of agglomeration are [32]:

- Agglomeration of bed material after **coating formation** from the gas phase.
- Agglomeration of bed material as **melt formation** of ash components.

The case of coating formation is more commonly observed in commercially operated fluidized bed combustors using woody-type of fuels. It is also referred to as *coating-induced* agglomeration. During this agglomeration, a uniform coating is formed on the surface of the particles. During certain critical conditions, like the coating thickness and/or the temperature, a so called *neck formation* may occur. This neck formation occurs between coatings of individual particles and initiates the agglomeration [32]. Figure 2.15a shows the agglomeration of bed material after coating formation from the gas phase.

In case of melt formation by ash melting, the particles of the bed material stick together by a melt phase. This melt phase roughly matches the chemical composition of the ash and is produced at normal operating temperature [32]. It is also referred to *as melt-induced* agglomeration. The ash melting behaviour has already been discussed in more detail in Subsection 2.1.4. Figure 2.15b shows the agglomeration of bed material as melt formation of ash components.

Layer induced bed agglomeration seems to be the main route for agglomeration in combustion of woody biomass fuels. During combustion of biomass, multiple layers with different properties and compositions have been found around the bed particles. However, the composition of the inner and outer layers appears to be different. On the one hand, the compositions of the inner layer depends on the composition of the bed and the fuel. On the other hand, the outer layers are more related to the fuel ash compositions [29].

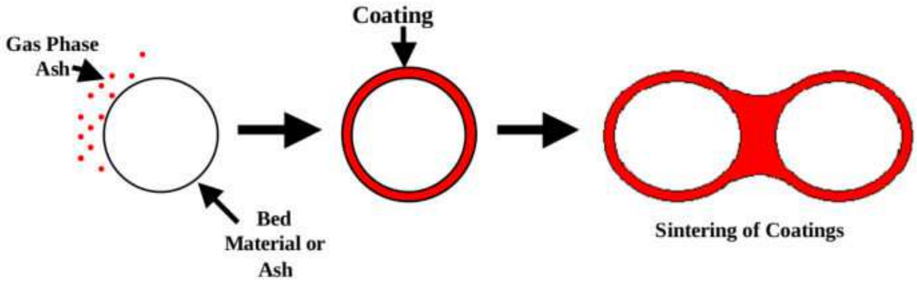

(a) *Agglomeration of bed material after coating formation from the gas phase.*

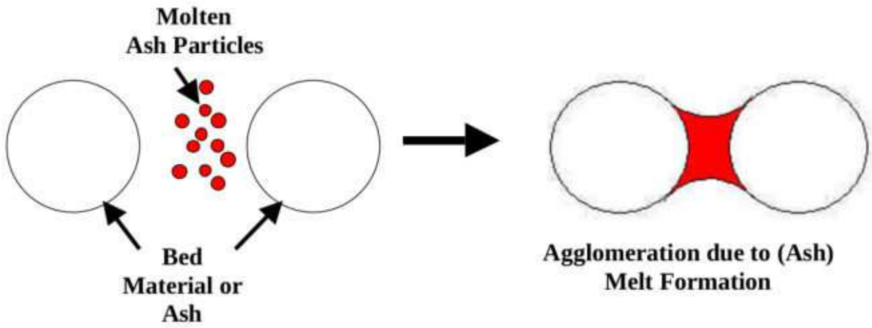

(b) *Agglomeration of bed material as melt formation of ash components.*

Figure 2.15: *The two types of agglomeration: Coating-induced and melt-induced agglomeration (adapted from [32]).*

2.8 Fields of application of fluidized beds

Fluidized beds are characterized by the fact that they are suitable for many applications. Fluidized bed plants are used in technical processes in which solids are to be brought into close contact with gases, liquids or other solids. Depending on the type of fluidized bed, which is explained in more detail in Subsection 2.5.3, circulating fluidized beds, for example, are characterized by relatively high velocities between the particles and the fluidization medium. The fluidized particles often collide with each other as well as with the wall of the reactor, resulting in an intensive mixing of the particles. The fluidized bed behaves like a fluid after exceeding the minimum fluidization velocity u_{mf}. As a result, the fluidized bed has a very homogeneous temperature distribution throughout the bed material. It also results in a very good heat exchange and a very good mass transfer. This is a special feature of fluidized beds. The following list gives some examples of possible applications of fluidized beds [20, p. 11]:

- Fluid bed drying
- Fluidized bed mixers
- Heating and cooling of bulk materials
- Coating of materials
- Fluidized bed adsorption
- Granulating, agglomerating, instantiating, enveloping;

- Roasting sulphide ores
- Reduction of metal oxides
- Coffee roasting
- Calcination
- Cracking

Fluidized bed combustion as well as fluidized bed gasification will be described in more detail below.

2.8.1 Fluidized bed combustion

Among the energy conversion processes for biogenic solid fuels, direct combustion in furnaces has the greatest importance to date. In incinerators, the chemically stored energy of the fuel is converted to the form of heat by thermochemical conversion phases described in Subsection 2.2.1. The recovered heat can then be used as secondary, useful or final energy.

The energetic conversion of the fuel takes place in fluidized bed combustion in a hot bed material. The bed material here consists of a granular inert material, usually a sand-ash mixture. Through nozzles, which are mounted in a so-called *inlet floor*, partially preheated air is injected into the bed and puts the particles in a kind of floating state. The fact that the bed material absorbs the released combustion heat, a very homogeneous temperature distribution is ensured in the entire fluidized bed [13, p. 905]. Fluidized bed combustion systems are therefore suitable for a wide range of fuels, in particular with regard to ash content and water content. At this point, reference is made to the elemental composition of biomass in Table 2.1 in Subsection 2.1.3.

One of the major advantages of fluidized bed combustion is the reduced formation of gaseous pollutants due to comparatively low combustion temperatures. Furthermore, by the addition of additives pollutant-forming elements, such as S and Cl, can be incorporated into the ash. This has the advantage that fluidized bed combustion systems are able to comply with valid emission limit values, without costly and expensive secondary measures. Additives may be, for example, limestone or dolomite [13, p. 906]. Fluidized bed combustion systems are significantly limited by the ash melting behaviour, described in more detail in Subsection 2.1.4, in particular by biogenic solid fuels. This can lead to agglomeration of the bed material, which can lead to complex and time-consuming cleaning. Likewise, there are limitations with regard to the maximum piece size of the supplied solid fuel. Depending on the fluidized bed design, the maximum piece size should be more or less clearly below 100 mm [13, p. 905].

Depending on the flow state, essentially two forms of fluidized bed combustion are of industrial significance. The stationary fluidized bed (SFB) combustion and the CFB combustion are explained in more detail below.

Stationary fluidized bed combustion

SFB combustion systems are operated at typical gas velocities of 1 m/s to 2 m/s (superficial velocity u_s) [13, p. 907]. They include a bed material with a mean grain diameter of about 0.7 mm to 1.0 mm [13, p. 907]. They are used for fuels of up to approximately 100 mm [13, p. 907] in size and allow almost complete oxidation of the biogenic solid fuel. The

thermal performance of such fluidized bed combustion systems is usually between 5 MW and around 50 MW [13, p. 907]. However, the majority of the ash does not remain in bed, but is deposited as flue ash in the dust separator. Dust separator facilities are essential in fluidized bed combustion due to the high particle load in the exhaust stream. The amount of particle load depends on the size of the plant, values between 20 g/m^3 and 50 g/m^3 [13, p. 907] are common. These values refer to standard conditions, i.e. at a temperature of 273.15 K and a pressure of 1.013 25 bar.
Figure 2.16 shows two types of SFB combustions.

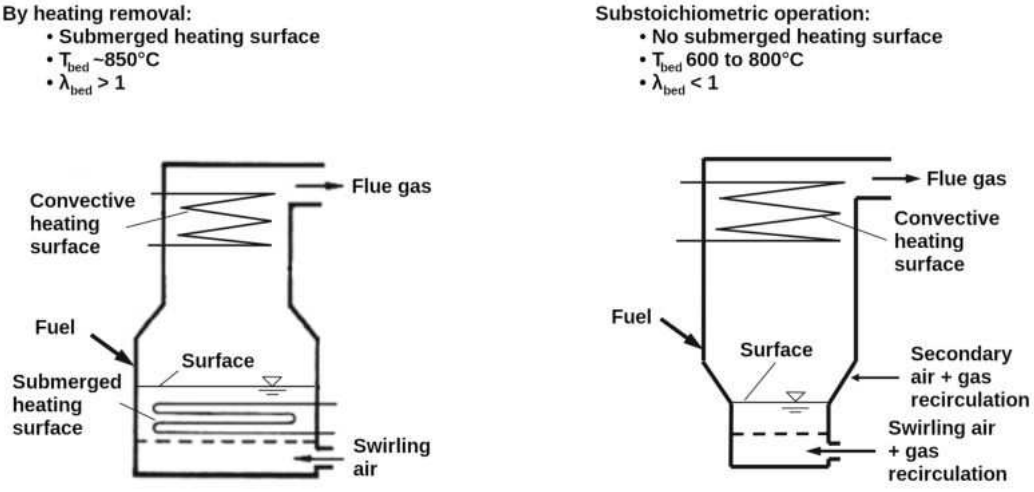

(a) *Stationary fluidized bed combustion with heat exchanger.*

(b) *Stationary fluidized bed combustion with recirculation of the flue gas.*

Figure 2.16: *Schematic representation of static fluidized bed combustion types to control the temperature inside of the reactor (adapted from [13, p. 908]).*

The temperature in the fluidized bed in Figure 2.16a can be adjusted by heat removal. This can be done by a built-in bed material heat exchanger (submerged heating surface).
In systems with a heat exchanger, the heating surface size is designed so that at nominal load a temperature of about 850 °C [13, p. 908] is reached. Most of the air is used as fluidizing air. Primary air ratio is slightly bigger than 1 ($\lambda \approx 1.1$) [13, p. 908]. The combustion can take place almost exclusively in the fluidized bed. Only a small part of the air is injected as secondary air into the space above the fluidized bed. Immersion heating surfaces have the disadvantage that at partial load, the temperature of the bed and thus the combustion temperature decreases. Furthermore, the immersion heating surfaces are subject to great erosion wear [13, p. 908].
For these reasons, newly built fluidized bed combustion systems therefore mostly operate without immersion heating surfaces. The way to control the temperature is shown in Figure 2.16b. In this case, a partial mass flow of the flue gas is supplied to the air supply again. This recirculation of the flue gas results in a substoichiometric air supply ($\lambda < 1$). The air ratio is in the range of 0.6 to 0.9 ($0.6 < \lambda < 0.9$) [13, p. 908]. Due to the recirculated flue gas gasification of the fuel takes place in the bed area. This happens at temperatures of approximately 600 °C to 800 °C [13, p. 908]. The post-combustion of the resulting gaseous products is carried out by secondary air in the free space above the fluidized bed.

Circulating fluidized bed combustion

As explained in more detail in the Subsections 2.5.3 and 2.6.3, the further increase of the gas velocity of the inflow medium leads to an increasing discharge of the bed material from the fluidized bed. For CFB combustion, the entrained bed material, therefore, must be returned to the fluidized bed. The installation of heat exchanger projecting into the fluidized bed, as shown in Figure 2.16a, is dispensed with in CFB combustion. The circulating bed material would lead to increased abrasion of the heating surfaces, whereby the heating surfaces would be worn very quickly. So that the bed temperature can still be regulated, a so-called *fluidized bed cooler* [13, p. 911] is used.
Figure 2.17 shows a schematic representation of a CFB.

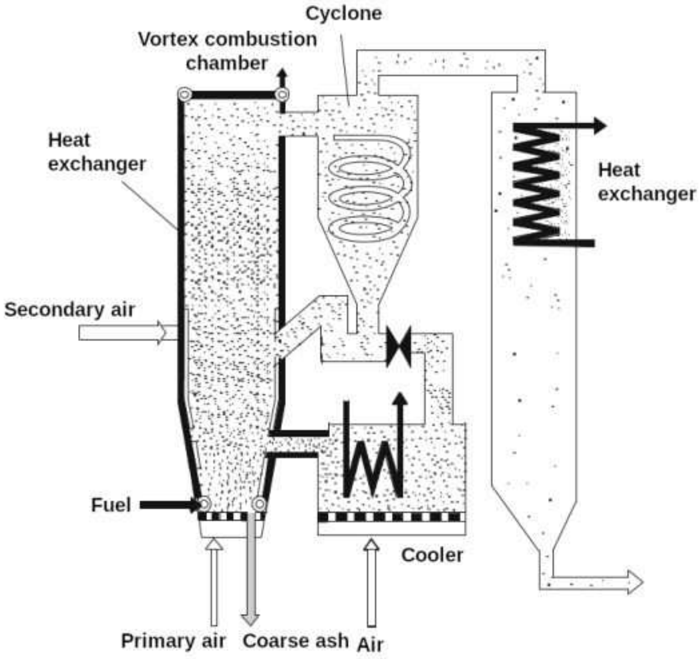

Figure 2.17: *CFB combustion with steam boiler (adapted from [13, p. 911]).*

In CFB combustors with fluidized bed cooler, a partial mass flow of the withdrawn circulation flow is passed through the radiator, whereby the temperature can be regulated [13, p. 910]. In such a fluidized bed high heat and mass transfer rates are achieved. CFB combustors are suitable for a wide range of fuels. In addition to coal combustion, CDF furnaces are primarily suitable for the energetic use of (biogenic) residues, by-products and waste of all kinds [13, p. 911]. In the combustion of fuels containing S and/or Cl, there is also the possibility of lime addition, in order to achieve in-situ desulfurization or chlorine separation [13, p. 911] in the fluidized bed. However, there are the same disadvantages that also occur in SFB combustion. For economic reasons, they are only used from approximately 30 MW firing heat output onwards.

2.8.2 Fluidized bed gasification

In addition to classical combustion, solid biomass can also be converted into a secondary energy source via gasification. The advantage of secondary energy carriers is, like described in 2.3, that they are available at a decoupled time, as well as spatially decoupled. The first large-scale application was a coal gasification. As explained in more detail in Subsection 2.5.1, this was developed by Fritz Winkler and put into operation for the first time in 1926 at BASF in a large-scale plant.

Fluidized bed gasifiers contain a bed of relatively fine bed material. In most cases, fine-grained quartz sand [13, p. 1079] is used as the bed material. However, it is also possible to use catalytically active bed material such as calcite, dolomite or olivine [13, p. 1081]. The gasification can be carried out under atmospheric or elevated pressure. The advantage of gasification under increased pressure is that with the same power output, the reactor dimensions can be reduced. As the pressure increases, the same amount of gas can be produced in an ever smaller reactor volume. Another advantage is that already compressed gas can be produced, which can offer advantages for some applications. A pressurized fluidized bed gasification works mostly in the range of 20 bar to 30 bar [11, p. 217]. However, the high level of plant engineering effort pays off only for larger plants.

As can be seen from the two Tables 2.3 and 2.4 in Subsections 2.3.3 and 2.3.4, basically the same conversion processes take place for both gasification and combustion. In contrast to combustion, however, the individual stages of thermochemical conversions are realized spatially and temporally separated.

Fluidized bed combustion is limited to the provision of the two forms of energy, heat and electricity. Figure 2.18 shows a possible process chain during the gasification of biogenic solid fuels.

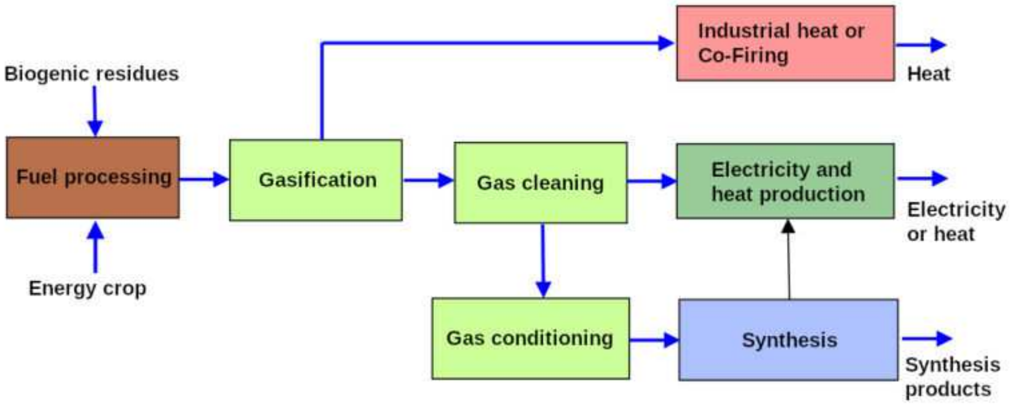

Figure 2.18: *Process chain of gasification for the production of electricity, heat and synthesis products (adapted from [11, p. 208]).*

Fluidized bed gasification, for example, offers the possibility of providing heat, electricity and synthesis products. The gas obtained by gasification of biogenic solid fuels is called *product gas*. In the literature, the terms *wood gas* and *syngas* are also used [11, p. 208].

An ideal gasification reactor for different types of biomass does not yet exist. In the past, some types of gasification reactors have been developed. Each of these gasification reactors has certain advantages and disadvantages with respect to the different gasified biomasses. Also with regard to the product gas quality, there are advantages and disadvantages with regard to the individual gasification reactor types.

The individual gasification systems presently available differ fundamentally and can be classified according to the following aspects [13, p. 1069]:

- **Type of heat supply:** Allothermal or autothermal gasification.
- **Type of medium for gasification:** Air, oxygen, water vapor;
- **Type of pressure conditions in the reactor:** Atmospheric pressure or overpressure.

Based on the gasification reactions shown in Table 2.3 in Subsection 2.3.3, technically meaningful gasification agents can be derived. As explained in more detail in Subsection 2.3.3, the gasification agent essentially serves to convert the carbon in the biomass or in the biomass coal into a gas. The types of gasification reactors are often distinguished in fixed bed gasifier, fluidized bed gasifier and entrained flow gasifier [13, p. 1069]. This subdivision is based on the fluid-dynamic behavior of the solid, as it flows through the gasification reactor against gravity. This subdivision has already been shown in more detail in Figure 2.13 in Subsection 2.6.3.

Stationary fluidized bed gasification

Stationary fluidized beds are characterized by the fact that the flow rate of the gas in the reactor is between the rate of u_{mf} and u_t for a single particle of the bed material. In stationary fluidized beds, a clearly recognizable fluidized bed is formed, which typically has a height of 1 m to 2 m [13, p. 1081]. In order to keep the output from the reactor as low as possible, a flow rate for the gas between 5 to 15 times the minimum fluidization velocity [13, p. 1081] has been useful. Figure 2.19a schematically represents a SFB gasification.

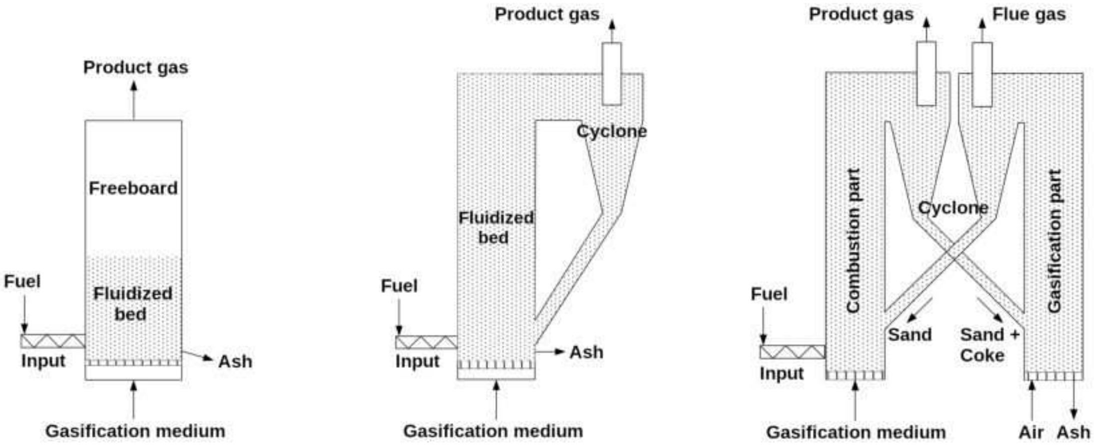

(a) *Stationary fluidized bed gasification.*

(b) *Circulating fluidized bed gasification.*

(c) *Dual fluidized bed gasification.*

Figure 2.19: *Schematic representation of fluidized bed gasifiers (adapted from [13, p. 217]).*

The field of application of SFB gasifiers is for fuel in a size range of 1 mm to 70 mm for the piece size. The gasification agents are usually air as well as mixtures of oxygen and steam. The thermal power SFB gasifier is located in size regions of several $\mathrm{MW_{th}}$ up to 50 $\mathrm{MW_{th}}$ [13, p. 1082].

In stationary fluidized beds, relatively well-defined reaction conditions, in particular with regard to temperature, are given. SFB gasification plants are particularly suitable for determining the influence of elevated pressure and the choice of the gasification medium used for the gasification reactions and the product gas quality [13, p. 1082]. For this reason, the design of SFB gasification is very well suited for laboratory-scale test facilities.

Circulating fluidized bed gasification

Similar to the SFB, the gasification of the biomass occurs in circulating fluidized beds at defined temperatures. In contrast to the SFB, thermochemical conversion takes place in a strongly expanded or CFB. Figure 2.19b shows the schematic structure of a CFB gasification. Typically, the bed materials in CFB gasification have a diameter of 0.2 mm to 0.4 mm [13, p. 1083]. The gas velocities in the fluidized bed are above the terminal velocity for the individual particles. Thus there is no recognizable bed surface in this type of fluidized beds. Therefore, this is called an *expanded fluidized bed* because the fluidized bed is expanded throughout overall the reactor. However, the fluidized bed does not form uniformly over the entire height. The result is a denser zone in the lower part and a thinner zone in the upper part. Due to the high gas velocities, the bed material is discharged from the reactor. With the help of one or more cyclones, the discharged bed material is separated from the gas stream and introduced back into the reactor. This creates a closed circulation of the bed material. The range of application is for fuels of 1 mm to 50 mm piece size with a thermal capacity of 10 MW to 100 MW [13, p. 1083].

The CFB gasification is an energy conversion process that has already been used several times commercially. Biomass fluidized bed gasification plants have been used for heat generation for years. These are used in paper and pulp production as well as lime burning for cement production [11, p. 219]. Another field of application for the CFB gasification of biomass is the co-firing of the produced product gas to existing coal power plants. The gas quality requirements are rather low. In this case, however, it must be ensured that tar condensation can not occur in the line connection between the fluidized bed gasifier and the power plant [11, p. 219]. The third area for commercial use of CFB gasification is biomass power generation using Integrated Gasification Combined Cycle (IGCC) technology [11, p. 219]. Here biomass is gasified with the help of air. The gas is then cleaned and fed to a gas turbine. The waste heat of the gas turbine is then used in a waste heat boiler to generate steam in order to generate additional power via a steam turbine. This allows very high electrical efficiencies.

Dual fluidized bed steam gasification

A particularly advanced but also complex type of biomass gasification is the dual fluidized bed (DFB) steam gasification with a circulating medium for heat transfer. This type of plant combines two spatially separated fluidized beds in one system. In the first fluidized bed, the gasification of the biomass is carried out. In the second fluidized bed, the heat necessary for the gasification is provided. The required heat is generated by burning a portion of the fuel or an auxiliary fuel. By a circulating bed material, the heat is exchanged between the two fluidized beds. The aim is to provide a medium calorific product gas, without using pure oxygen or to introduce the heat via an expensive high-temperature heat exchanger in the gasification fluidized bed [13, p. 1087]. Figure 2.19c schematically represents a DFB gasification.

The biomass is fed into the gasification fluidized bed and converted there with steam into a gaseous product. This creates a medium-calorific gas that is virtually free of nitrogen [11, p. 219]. In addition, the gasification fluidized bed and the combustion fluidized bed can be optimally designed independently of each other. Due to the separation in gasification and

combustion, the product gas flow is significantly lower than in conventional air gasification. The product gas stream is not mixed with the exhaust stream. The often necessary measures for the cleaning of the product gas are therefore much cheaper [11, p. 220].
The combustion fluidized bed typically operates at temperatures of 950 °C and is fluidized with air. The temperature in the gasification fluidized bed is lower by approximately 100 °C at approximately 850 °C [11, p. 219].
The fuel, necessary for the combustion, can be introduced into the fluidized bed together with the circulating bed material. Pyrolysis coke is used as a circulating bed material. If necessary, additional fuel can be introduced by external supply in the combustion fluidized bed. The flue gas produced during combustion is removed from the gasification fluidized bed separately from the product gas [13, p. 1085]. Figure 2.20 shows the basic principle of a DFB steam gasification with circulating heat transfer medium.

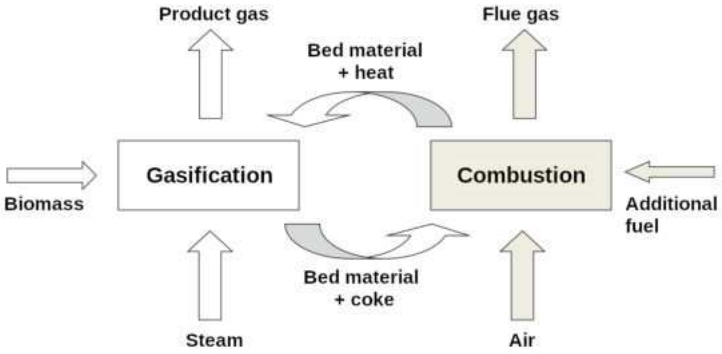

Figure 2.20: *Basic principle of a DFB steam gasification with circulating heat transfer medium, for the production of a medium-calorific product gas (adapted from [13, p. 1085]).*

Chapter 3

Aim of this thesis

The aim of this master thesis consists of three main tasks:

- Commissioning of a new bench scale fluidized bed pilot plant for the combustion of biogenic solid fuels.
- Investigation of fuel ash layers on different bed materials.
- Detailed documentation of the results obtained and development of improvements to the bench scale pilot plant for increased scientific output of future experiments.

3.1 Commissioning of a new bench scale fluidized bed pilot plant

A new bench scale fluidized bed pilot plant was build. This testing plant was built with the aim of burning and gasifying a wide variety of biogenic solid fuels as well as offer the opportunity of testing a wide range of different bed materials. The motivation is to better understand and investigate the fuel ash layers on different bed materials. Another motivation is to be independent from existing fluidized bed plants and their bed material samples.

The primary objective of this task is initially to put the existing bench scale fluidized bed pilot plant into operation. In order to achieve reproducible measurement results, it is necessary to ensure a constant operation of the bench scale fluidized bed pilot plant with controlled combustion under constant operating parameters.

Since this is a completely new bench scale fluidized bed pilot plant without any empirical values, one focus of this thesis is the documentation of the operation of the equipment to show which variation of the individual operating parameters leads to which changes during operation. The findings are explained with the aim of serving as a guide for later experiments on this bench scale fluidized bed pilot plant.

In addition, a three-dimensional modeling of the essential components of the system was created as technical drawings. The testing plant was modeled in a 3D CAD program in order to be able to draw on the knowledge gained visually and as technical drawings for possible later modifications or further bench scale fluidized bed pilot plants of the same type.

3.2 Investigation of fuel ash layers on different bed materials

An essential component of fluidized beds is the bed material. As described in more detail in Section 2.7, the bed material may also have catalytic properties. These catalytic properties are an important characteristic, especially for the reactions occurring during the gasification. Different bed materials are to be examined for their catalytic activity. The experiments on the bench scale fluidized bed pilot plant are also carried out with the aim of being able to give a qualitative statement about the temporal dependence of layer formation processes. Bed material samples were taken at regular intervals, which were then tested in a separate micro-scale test-rig for their catalytic activity in order to be able to check the influence on the activation of the bed material.

As described in more detail in Section 2.7, it is allowed to conclude from combustion experiments on the gasification technology.

3.3 Detailed documentation of the results obtained

During the experiments on the bench scale fluidized bed pilot plant, there were various complications in the experimental procedures. These complications resulted in various detail improvements and modifications of the system. The third main task of this master thesis is therefore the documentation of the knowledge gained from the experiments and the changes and modifications made on the bench scale fluidized bed pilot plant.

The aim behind this is that through the documentation, the knowledge and results gained from these experiments could be used for further bench scale fluidized bed pilot plants.

Chapter 4

Methods

This chapter is intended to give an overview of the methods of experimentation and describes the used equipment in more detail.
Before going into more detail about the bench scale pilot plant of the fluidized bed combustion, Section 4.1 explains the fuel and its processing in more detail. Section 4.2 gives an overview of the bed materials used during the experiments. In Section 4.3 the bench scale fluidized bed pilot plant is described in more detail, including the calibration of both screw conveyors and the sampling. The measuring devices, used for temperature, pressure and concentration of the flue gas are described in Section 4.4. Section 4.5 takes a closer look at the micro-scale test-rig, which was used to determine the catalytic activity of the bed material and bed material layers. The scanning electron microscope and the CAD program, used to create the CAD drawings and some documentation, are briefly presented in Sections 4.6 and 4.7. Finally, Section 4.8 gives an overview of the varied parameters during the experiments.

4.1 Fuel

Like large-scale fluidized bed plants, as mentioned in more detail in Section 2.8, the bench scale fluidized bed pilot plant can also be operated with many different fuels. The following criteria were taken into account when considering the choice of fuel for this bench scale fluidized bed pilot plant and the experiments:

- **Suitability in the bench scale fluid bed system:** The fuel must in principle be suitable for combustion in a fluidized bed plant.
- **Suitable preparation options:** The fuel should ideally be able to be prepared with the existing equipment. For example by a pelletizing machine.
- **Size:** Due to the mechanical conveyor of the testing plant via a screw conveyor, the fuel should not exceed certain dimensions or not fall below these dimensions.
- **Capacity:** Since the fuel supply of the screw conveyor of the bench scale fluidized bed pilot plant is limited in terms of the supplied mass flow, the fuel should be present in compressed form, to achieve the highest possible energy density.
- **Storability:** The processed fuel should be suitable for storage, without changing its mechanical or chemical properties.

- **Ash content:** Since the interaction of the bed material with the fuel is important for layer formation, the fuel must not be too low in ash in its burning behavior.
- **Price:** The fuel must be available in the required quantities at an affordable price.
- **Availability:** The fuel should be sufficiently available and it should be easily obtainable.

Due to these considerations, bark was selected as fuel. The bark was purchased in the form of pine bark from Hornbach, a local do-it-yourself market. For the experiments 10 bags with a volume of 60 L each were used [33].

4.1.1 Fuel processing

Despite the fact that the pine bark was purchased in the finest and therefore the smallest size available, it could not be used as a fuel without treatment in the fluidized bed testing plant. This is due to the fact that the two screw conveyors of the two fuel tanks are not designed for the big size of the individual pieces of pine bark. The pine bark was therefore suitably prepared. For this purpose the pine bark was milled in a hammer mill. Through the milling process, the particle size of the pine bark could be reduced from a few centimeters to a few millimeters. Thereby it was possible to feed the bark to the pelletizer. For milling, a hammer mill from Cissonius GmbH of type CF-420C [34] was used.
To prepare the pellets, a die with a hole diameter 6 mm was chosen. For the preparation of the bark, a pelletizer of the company Cissonius GmbH and the type PP-200 [35] was used. The pelletizer is shown in Figure 4.1. The ilustrated pelletizer is partially disassembled due to maintenance work.

Figure 4.1: *Pelletizer type PP-200 from Cissonius GmbH, to produce pellets of suitable size from the pine bark (partially disassembled).*

An important part of fuel processing is to let the pellets dry after the pelleting process. For this purpose, the pellets were spread directly after the pelleting process on a large plastic film and dried for several hours in the sun. This allowed the residual moisture of the fuel to escape. After the pellets were dried under atmospheric conditions, they could be filled and stored in standard plastic drums with lid and clamping ring to protect them from moisture. In the following master thesis, the fuel is also called *bark pellets*.

4.1.2 Fuel ash content

The fuel ash content of the bark pellets was determined according to standard ÖNORM EN ISO 18122 [36]. In order to obtain a qualitative statement about the ash content, three trays were weighed with fuel and ashed in the muffle furnace. For each of the fuel samples, the ash content was determined and the results of the three calculations were averaged. To calculate the ash content of the sample on an anhydrous basis A_d, equation 4.1 was used.

$$A_d = \frac{(m_4 - m_1)}{(m_3 - m_1)} \cdot 100 \tag{4.1}$$

The mass of the empty bowl is denoted by m_1. The mass of the bowl including the test quantity of the moist fuel is designated with m_2. m_3 denotes the mass of the bowl including the test quantity of the dried fuel. The amount after ashing the fuel is denoted by m_4. Table 4.1 shows the weighed quantities and the calculated fuel ash content of the individual samples.

Table 4.1: *The weighed quantities of the various fuel samples and the fuel ash contents, which are calculated according to equation 4.1.*

Sample	m_1 **in g**	m_2 **in g**	m_3 **in g**	m_4 **in g**	**Ash content** A_d **in %**
1	50.8044	131.2059	118.7539	53.1455	3.45
2	55.1175	122.3595	112.2404	57.1110	3.49
3	52.9695	118.1770	108.1570	54.8668	3.44
				average:	**3.46**

4.2 Bed material

The experiments were carried out with different bed materials. The following bed materials were used:

- Cristobalite (Sibelite)
- Na-feldspar
- Quartz

The minimum quantity of bed material was essentially determined by the dimensions of the the column base and the lower flange of the bench scale fluidized bed pilot plant. The detailed design of the bottom of the reactor is discussed in more detail in Subsection 5.2.8. In order to investigate the effects of the amount of bed material on the operation of the testing plant, the amount of bed material was varied between the individual experiments. Section 5.1 explains the individual experiments and their findings regarding the amount of bed material in more detail.

In order to obtain information about the particle sizes of the bed materials, a sieve analysis was carried out on the bed materials before the first use. Figure 4.2 shows the results of the sieve analyses to determine the grain size distributions.

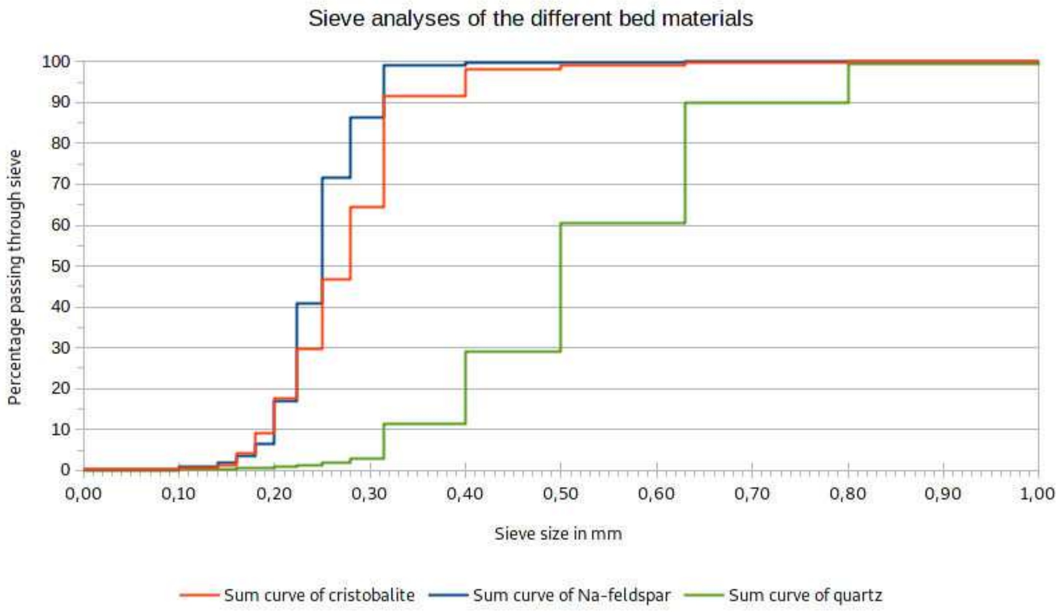

Figure 4.2: *Results of the sieve analyses to determine the grain size distributions of cristobalite, Na-feldspar and quartz.*

The sieve analysis of the different bed materials has shown, that Na-feldspar and cristobalite have approximately the same sum curve. The size distribution of quartz differs significantly from the other two bed materials. The particle size distribution has a deciding influence on the calculation of the equivalent diameter d_{sv}. With the help of the SMD, which has already been described in more detail in Subsection 2.6.1 and the geometric dimensions of the testing plant, characteristic parameters such as the minimum fluidization velocity u_{mf} and the terminal velocity u_t can be calculated. The calculation of the minimum fluidization velocity u_{mf} and the terminal velocity u_t has already been explained in more detail in Subsection 2.6.3. The results of the numerical calculation are explained in more detail in Section 5.3.

Based on the results of sieve analyses of the different bed materials, the average diameters of the individual bed materials can be calculated. Since all bed materials are particles whose shape differs from a sphere, the equivalent diameter d_{sv} is used to characterize them.

Since the particles of the different bed materials do not differ too much from spherical shapes, it is allowed to use formula 2.6 to calculate d_{sv}. The particle shape factor ϕ is required to calculate the equivalent diameter d_{sv}. The particle shape factor ϕ is a measure for assessing the shape deviation of an ideal sphere and was also explained in more detail in Subsection 2.6.1.

Some form factors for the technically interesting materials have already been given in Table

2.6. A form factor of 0.90 was used for cristobalite because the individual particles were very round. The form factor of Na-feldspar was assumed to be 0.85, since the individual particles of Na-feldspar were assessed somewhat more roughly than those of cristobalite. The form factor of 0.80 was chosen to calculate the equivalent diameter of the quartz. Table 4.2 lists the results of the calculation of the equivalent diameter d_{sv}.

Table 4.2: *Form factors and calculated equivalent diameters of the different bed materials.*

Bed material type	Form factor ϕ	Equivalent diameter d_{sv} in mm
Cristobalite	0.90	0.249
Na-feldspar	0.85	0.215
Quartz	0.80	0.434

4.3 Bench scale fluidized bed pilot plant

All experiments were carried out with the following testing plant, which is described below. As a testing plant, a new bench scale fluidized bed pilot plant without recirculating bed material was used. The testing plant is basically divided into two assembly units. The reactor and the components for flue gas treatment such as the cyclone and the flare are attached to an assembly unit. All components for supplying fuel and controlling the system are attached to the other assembly unit. The two assembly units are connected to each other via the downpipe for feeding the fuel.

Figure 4.3 shows the bench scale fluidized bed pilot plant as a 3D CAD model in the current state, meaning after finishing all experiments and with all modifications and improvements collected during the experiments.

Core of the testing plant is the cylindrical reactor with the combustion chamber and the attached cyclone for flue ash deposition. There are two fuel tanks, a small one and a big one, located at the top of the testing plant. Both fuel tanks are equipped with an inspection glass, so it is possible to see the level of the remaining fuel. The fuel is filled into the fuel tank from above. The inlet can be closed with a ball valve for safety reasons. Each of the fuel tanks is equipped with a screw conveyor to carry the fuel out of the fuel tank into the downpipes. The downpipes are interconnected with a Y-branch pipe, which is connected to the combustion chamber. Because of thermal expansion appearing during hot operations, it is necessary that the downpipes are equipped with compensators to reduce the occurring thermal load. Additionally, the two fuel tanks are statically decoupled by rubber foots. This is also to prevent transmission of vibrations caused by the spinning screw conveyors between the fuel tanks and the other components of the system. After some parts of the testing plant were redesigned, described at Section 5.2, it is possible that each of the two fuel tanks can be separated from the rest of the system separately via ball valves. The bed material enters the reactor by opening a ball valve, located at the top of the downpipe of the fuel supply of the big fuel tank. The capacity of the small fuel tank is approximately 15 dm^3 and the capacity of the large fuel tank is approximately 87 dm^3.

As mentioned in Section 3.1, the testing plant was built with the aim of burning a wide variety of biogenic solid fuels and also to be able to use different types of bed material. The testing plant allows to burn solid fuels in the form of pellets continuously under controlled conditions. To obtain meaningful results for the experiments, the testing plant is equipped

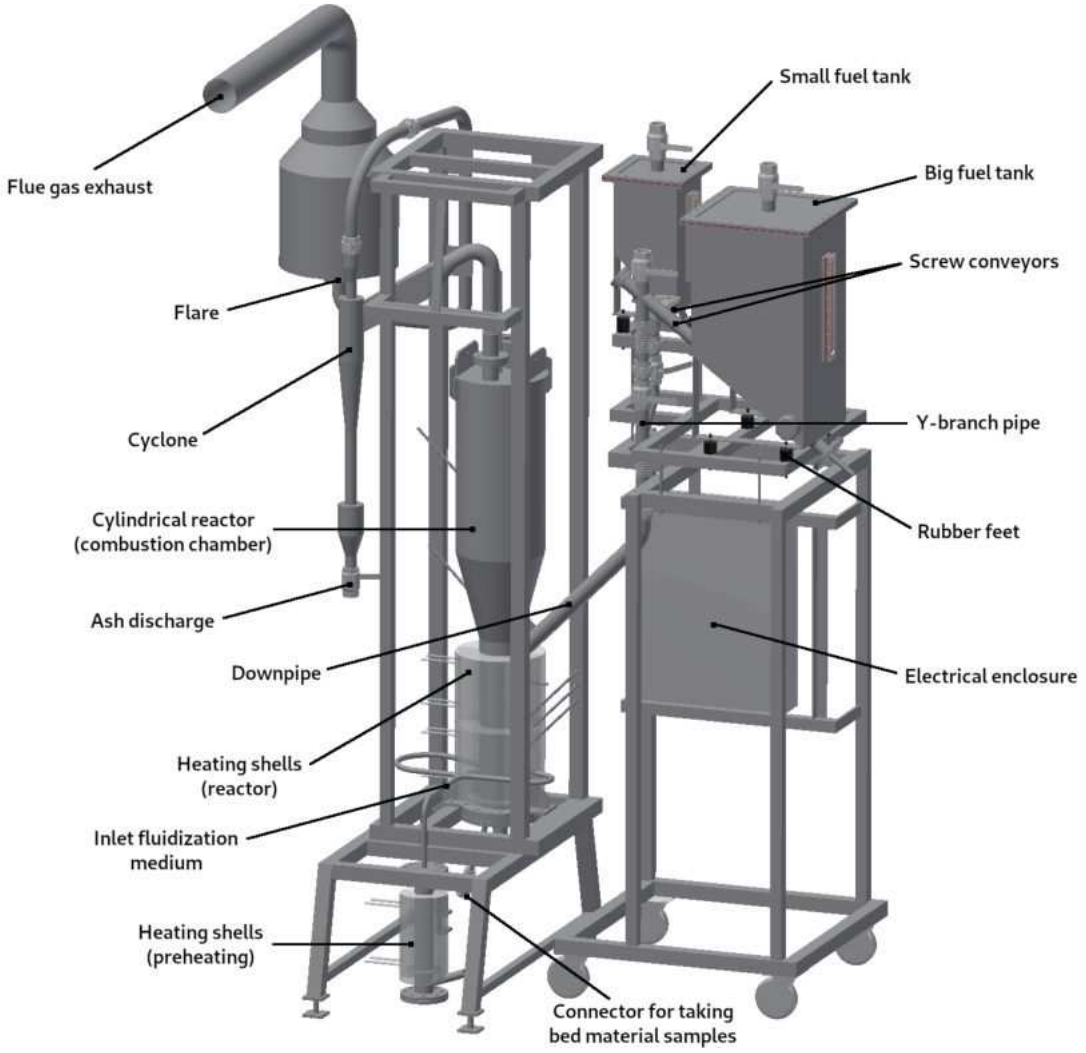

Figure 4.3: *3D CAD rendering of the bench scale fluidized bed pilot plant for the combustion of biogenic solid fuels.*

with various sensors. Figure 4.4 shows the arrangement of all the sensors used to measure the operating parameters during the experiments.

As shown in Figure 4.5a, there is a flange at the bottom of the combustion chamber, which serves to empty the bed material of the testing plant. At the top of the flange, there is a funnel welded in, which facilitates the emptying of the system. At the bottom of the pipe of the flange there is a centered ball valve for emptying the testing plant. In addition, there is a further pipe with a ball valve attached to be able to take bed material samples during operation. Also, at the lower end of the combustion chamber, there is the fluidization air inlet.

In contrast to other testing plants, this bench scale fluidized bed pilot plant does not have a closed nozzle bottom. The fluidization is realized via two pipes projecting into the combustion chamber, at the bottom of the reactor. Each of these two pipes has some nozzles. As shown in Figure 4.5b, the nozzles are directed downwards, to prevent bed material from entering the fluidization inlet. Before the air enters the reactor, it can be preheated in the air preheater

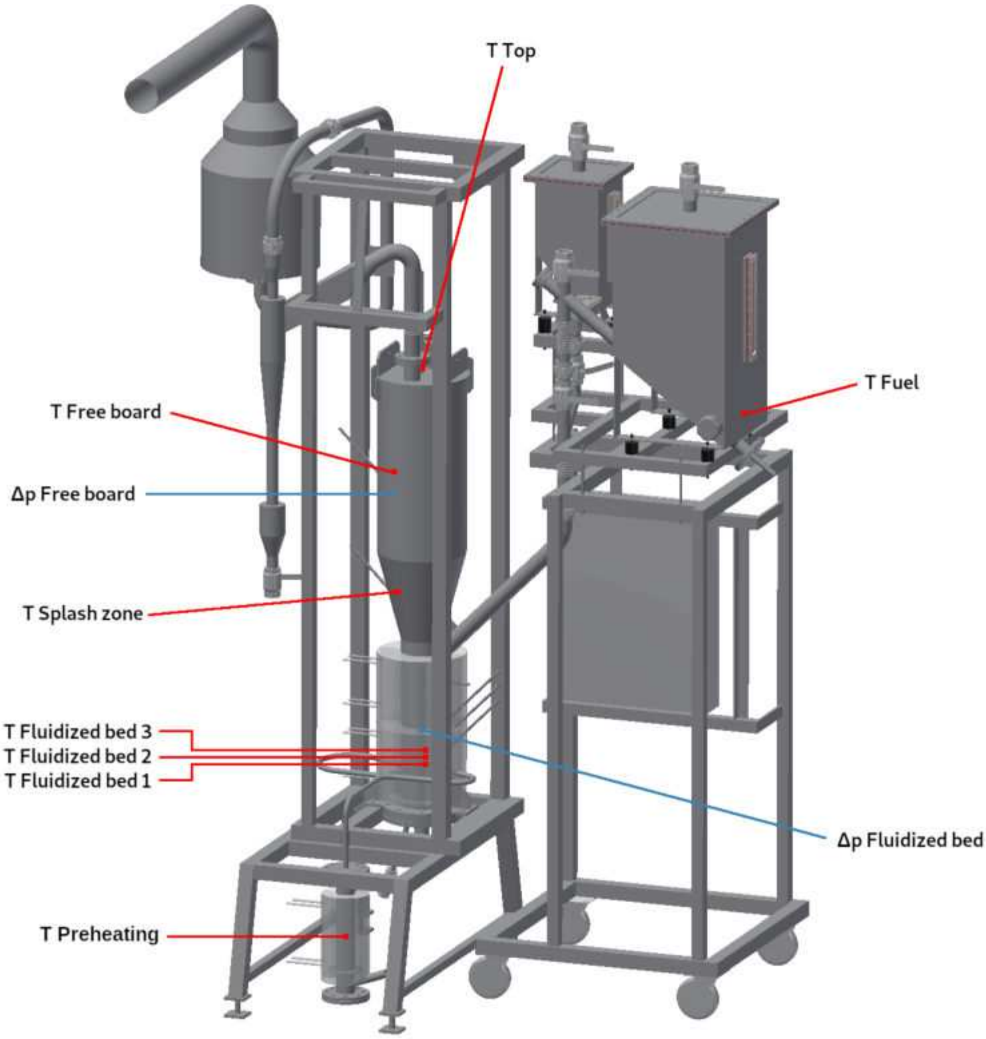

Figure 4.4: *3D CAD rendering of the bench scale fluidized bed pilot plant, showing the arrangement of temperature sensors and pressure sensors for monitoring the experiments.*

by heating shells.
The reactor is also equipped with heating shells, since it is not possible to heat the reactor only by using fuel. The heating shells are primarily used to compensate heat losses of the reactor and to ensure constant combustion at constant temperatures.
The heating shells are also necessary, to bring the reactor up to operating temperature under controlled conditions. It is important not to heat up the reactor too fast, to avoid thermal stress and fatigue. The reactor should be heated up at a constant heating rate of 30 °C per 10 min. The flue gas outlet is located at the top of the reactor. The flue gas is led into a cyclone. In the cyclone the solid particles are separated. These solid particles are the so-called flue ash. The ash can be separated after the end of the experiments via a ball valve. At the other end of the cyclone there is a line leading to a flare. The flare is supplied with natural gas via an additional pipeline to treat the flue gas thermally in the event of incomplete combustion, characterized by the presence of CO. After the flare, the flue gas is

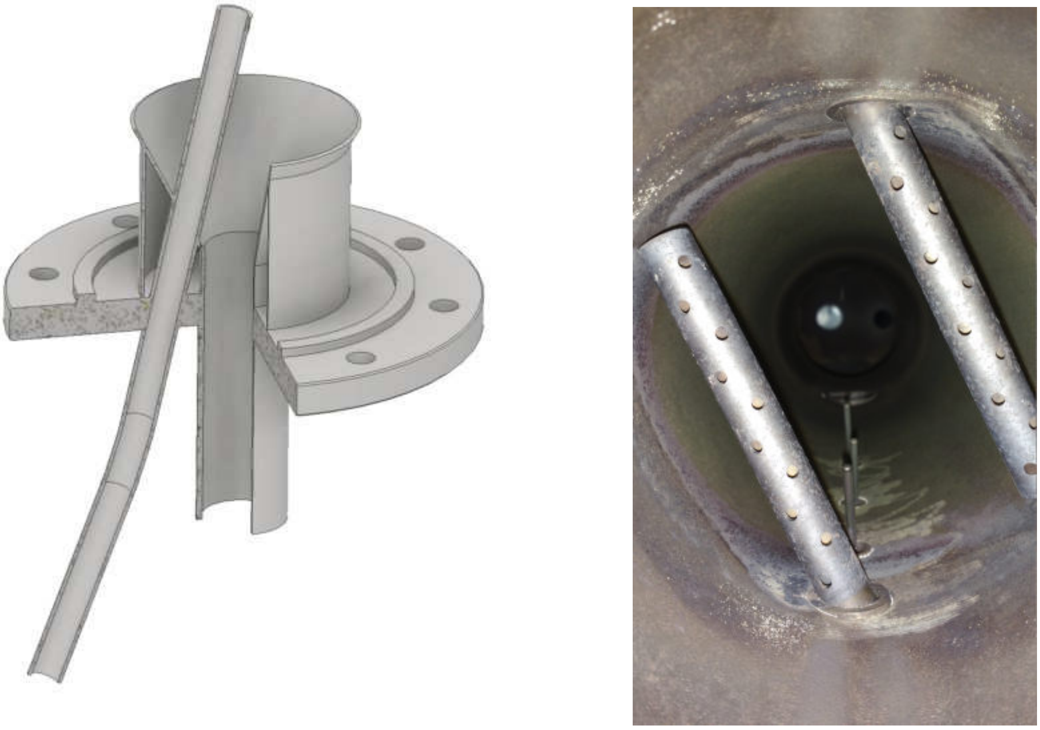

(a) *3D rendering of the flange, which shows the lower outlet for emptying and the tube for sampling during operation.*

(b) *Pipes with nozzles for fluidization, temperature sensors and the inspection glass. View from below.*

Figure 4.5: *Detail view of the flange and the nozzles for fluidization.*

directed into the chimney of the technical center. The two components, combustion chamber and cyclone, are suspended from the steel framework. In addition, the reactor is supported on the frame at the lower end via support braces.

At the upper end of the reactor, an inspection glass is attached. This provides the opportunity to see the process of combustion inside the reactor. A separate pipe, which is directed towards the inspection glass, is used to prevent the inspection glass from getting dirty by using a nitrogen purge.

For safety reasons the testing plant is equipped with an emergency stop. If this is triggered the entire column is flooded with N_2.

4.3.1 Calibration of the screw conveyors

Both screw conveyors were calibrated to provide information about the amount of fuel. For this purpose, each of the two screw conveyors was operated at defined frequencies and for a defined period of time in order to convey pellets. The weight of the conveyed pellets was weighed after each conveying process. A diagram was then drawn up for each of the two screw conveyors, in which the frequency was plotted with the associated conveyed weight of the pellets. This resulted in a calibration curve for each of the two screw conveyors. A linear regression curve was laid through this calibration curve. With the help of this linear regression curve, linear interpolation can be used to calculate the delivery rate of any frequencies. Figure

4.6 shows the two calibration curves of the two screw conveyors.

With the screw conveyor of the small fuel tank, the calibration was carried out over the entire possible frequency range from 10 Hz to 50 Hz. The screw conveyor of the big fuel tank was only calibrated up to a frequency range of 30 Hz, since higher frequencies were not required for the experiments.

The calibration of the two screw conveyors has shown that both, the screw conveyor of the small fuel tank and the screw conveyor of the big fuel tank, deliver fuel almost linearly over the entire frequency range. The deviations in the screw conveyor of the small fuel tank are slightly larger in the middle frequency range than in the screw conveyor of the big fuel tank. The functional equations of the straight line functions are shown above the regression line.

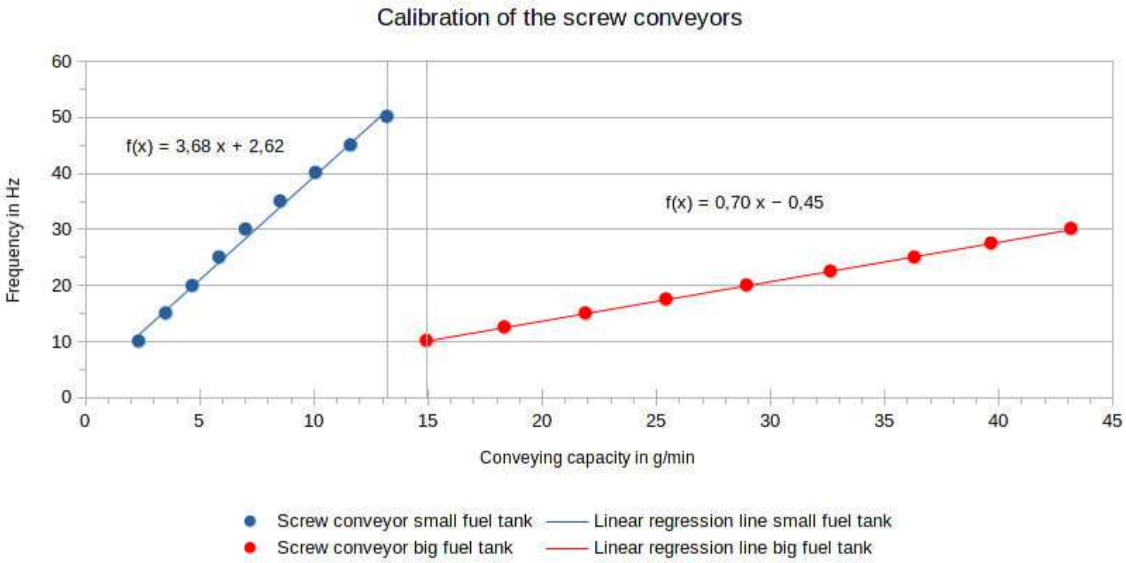

Figure 4.6: *Calibration curves and regression lines of the two screw conveyors of the small fuel tank and the big fuel tank.*

The screw conveyor of the small fuel tank can convey a maximum of 13.2 g/min fuel pellets at a maximum possible frequency of 50 Hz. The screw conveyor of the big fuel tank can be operated with a minimum frequency of 10 Hz. At this frequency a fuel delivery rate of 14.9 g/min was measured. The calibration curves of both screw conveyors are compared in Figure 4.6. The recorded values of both screw conveyors were recorded in a single diagram. This makes it clear, that the entire capacity range could not be covered in the existing configuration. Accordingly, it is not possible to achieve a delivery rate in the range between approximately 13 g/min and approximately 15 g/min with the existing configuration.

The limitations of the screw conveyors with regard to possible frequencies are discussed in more detail in Subsection 5.2.3.

4.3.2 Sampling

At the lower end of the testing plant there is a flange, which represents the bottom of the reactor. A 3D rendering of the flange is shown in Figure 4.5a. The flange has two outlet sockets. Each of the two sockets can be closed with a ball valve. In order to be able to provide information about the temporal dependence of the layer formation, bed material samples were taken at regular intervals.

Due to the design of the flange, there is a lot of bed material, which does not participate in the interaction with the fuel. Only after the bed material, which has not participated in the interaction with the fuel has been removed, samples of the bed material, which has participated in the interaction with the fuel, can be taken. This means that a lot of bed material has to be removed from the reactor.

In the first two experiments, only one bed material sample was taken after the end of the individual experiments. In the other experiments, a bed material sample was taken after each day of the experiments. In the third and fourth experiments, the same amount of bed material, that was taken for sampling on the first day in each case, was fed back into the fluidized bed. For this purpose, new bed material of the same type was added to the fluidized bed. Therefore, there always has been the same amount of bed material in the reactor on each days of the individual experiments. In the two long-term experiments, a bed material sample of 150 g was taken after each day. The removed amount of bed material was not put back into the reactor. For all samples that were taken, the bed material that did not participate in the interaction, was again filled into the reactor.

Due to the design of the flange, it would be possible to take bed material samples during operation. However, due to the amount that would have to be removed, no samples were taken during operation. Bed material samples were only taken after the fuel supply had ended. The experiments have shown that the bed material can be removed in the morning of the following day. About 12 h after the fuel supply was stopped, the bed material was below 50 °C. Also for safety reasons it was not reasonable to take bed material samples during operation.

After each experiment, the cool-down phase of the system began when the fuel supply was stopped. In order to allow the testing plant to cool down in a controlled manner, the fluidization was continued. To keep the abrasion of the individual particles of the bed material as low as possible, the fluidization rate has been significantly reduced compared to regular operation. During the cool-down phase, the volume flow of the fluidization was approximately 50 l/min. These values refer to standard conditions, i.e. at a temperature of 273.15 K and a pressure of 1.013 25 bar.

The design and the associated limitations of the bottom of the reactor are discussed in more detail in subsection 5.2.8.

4.4 Measurement equipment

The following section explains the measurement equipment used during the experiments, to monitor the operation of the testing plant.

4.4.1 Gas measurement equipment

A very small partial mass flow of the flue gas was withdrawn via a bypass to analyse the gas composition. The flue gas was withdrawn from the outlet at the top of the reactor before it entered the cyclone for dust separation. Because of this setup, it was necessary to install another filter in front of the gas detector.

A measuring device from Rosemount and type NGA 2000 [37] was used as the gas measuring device. For the gas composition, the product gas volume fraction in percentage could be recorded. The product gas volume fraction of O_2, CO_2, CO, CH_4 and H_2 were measured.

These measured values were recorded continuously using electronic data processing on a laptop with the LabVIEW [38] software. The Rosemount NGA 2000 measuring device was calibrated by the certified Test Laboratory for Combustion Systems of the Vienna University of Technology.
Since increased concentrations of CO can occur during the combustion of biogenic solid fuels, measuring the composition of the flue gas also serves personal safety. If an oxygen concentration of less than 6% [29] is measured in the flue gas, the torch must be lit to completely oxidize the CO to CO_2.

4.4.2 Temperature measurement equipment

Resistance thermometers were used as measurement sensors to record the individual temperatures. The system has eight screw-in sockets through which the sensors can be attached. Figure 4.5b shows some sensors protrude into the combustion chamber in order to record the temperatures in the bed material. The following temperatures could be recorded:

- **Temperatures of the bed material inside of the fluidized bed:**
    - T Fluidized bed 1
    - T Fluidized bed 2
    - T Fluidized bed 3
- **Further temperatures in the reactor:**
    - T Splash zone
    - T Free board
    - T Top
- **Preheating of the fluidization medium:**
    - T Preheating
- **Temperature of the big fuel tank:**
    - T Fuel

Like the concentrations of the flue gas composition, the measured values of the temperature sensors were recorded electronically using a laptop with the LabVIEW software. During the experiments, all logged values were recorded every 10 s. Figure 4.4 shows the arrangement of the temperature sensors.

4.4.3 Pressure measurement equipment

Similar to the temperature measurement, the pressure measurement was carried out on the system using screw-in sockets. The measured values of the pressure sensors are also recorded electronically using a laptop and the LabVIEW software. Two pressure differences were recorded on the system during operation. These were the pressure difference in the fluidized bed Δp *Fluidized bed* and the pressure difference in the free board Δp *Free board*. In order to achieve high pressure differences and meaningful measurement results, the two pressure sensors are located as high as possible at the temperature measurement points of *T Fluidized bed 3* and *T Free board*. Figure 4.4 shows the arrangement of the pressure sensors.

4.5 Micro-scale test-rig

A separate apparatus was used to check the catalytic activity of the bed materials sampled from the fluidized bed. The determination of the catalytic activity was carried out with a fixed bed reactor with the aid of the WGSR, which is shown in equation 4.2 [39].

$$CO + H_2O \rightleftharpoons CO_2 + H_2 \qquad \Delta H^0_{R,298} = -41.2kJ/mol \tag{4.2}$$

The WGSR describes the reaction of the reagents CO and H_2O (water vapor) to the products CO_2 and H_2. The enthalpy of the WGSR is slightly exothermal at −41.2 kJ/mol [40, p. 336]. The chemical equilibrium shifts with increasing temperature from the reaction products to the reaction reagents.

The WGSR is particularly important in gasification technology. For example in steam reforming, a process for the production of synthesis gas from carbon-containing fuels and water vapor. Steam reforming is used for example in coal gasification but also in the production of biohydrogen by biomass gasification. Historically, the WGSR is of particular importance in the Haber-Bosch process for ammonia synthesis, which has already been explained in Subsection 2.5.1 [41]. Figure 4.7 shows the schematic structure of the apparatus for determining the activity of the bed material.

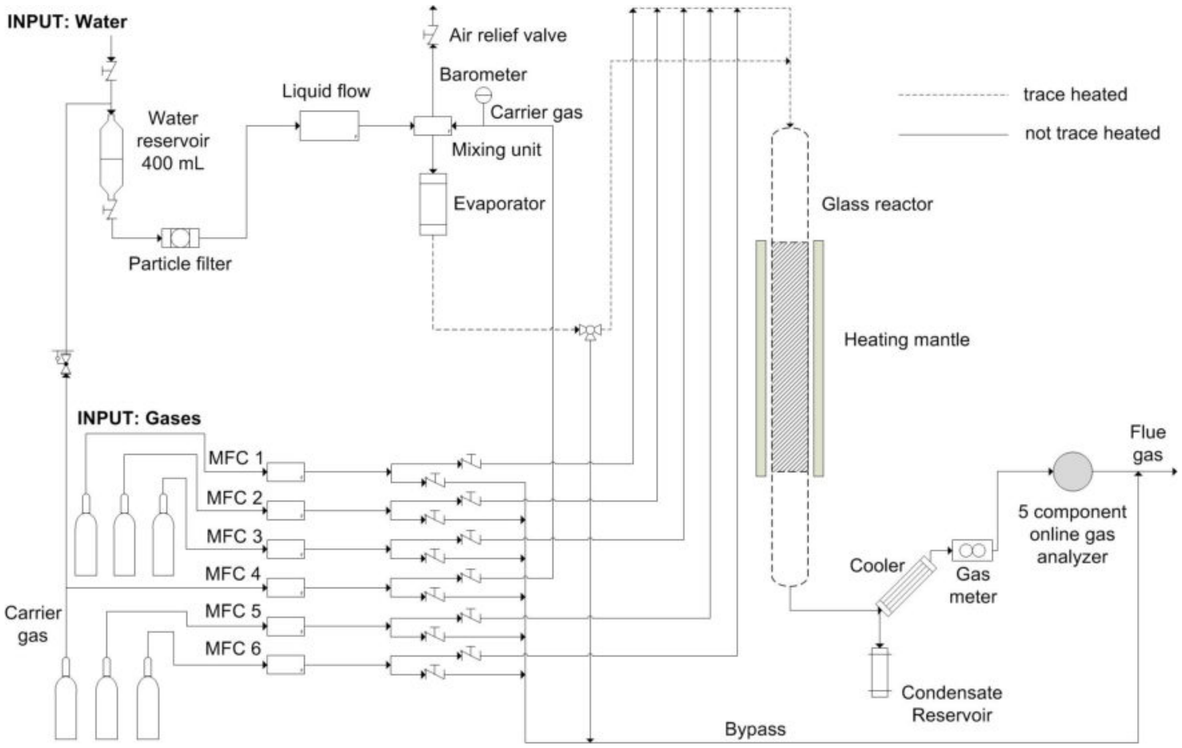

Figure 4.7: *The schematic structure of the apparatus for determining the activity of the bed material (adapted from [42]).*

All gases are fed into the reactor via mass flow controllers (MFC). Due to its inert properties, N_2 was used as a carrier gas for water vapor. The reactor essentially consists of a glass tube, which has an internal diameter of 4 mm and a length of 33 cm. This glass tube is surrounded by a heating shell in order to be able to heat the reactor to a temperature of 850 °C. This temperature was chosen because this is a common temperature for biomass gasification [13, p. 1068]. In the middle of the reactor, an exactly 5 cm high layer of the bed material sample is placed between glass wool.

The bed material should have a grain size of 200 µm to 250 µm. In order to obtain the required grain size, the bed material samples were sieved. Figure 4.8 shows a schematic representation of the reactor of the micro-scale test-rig.

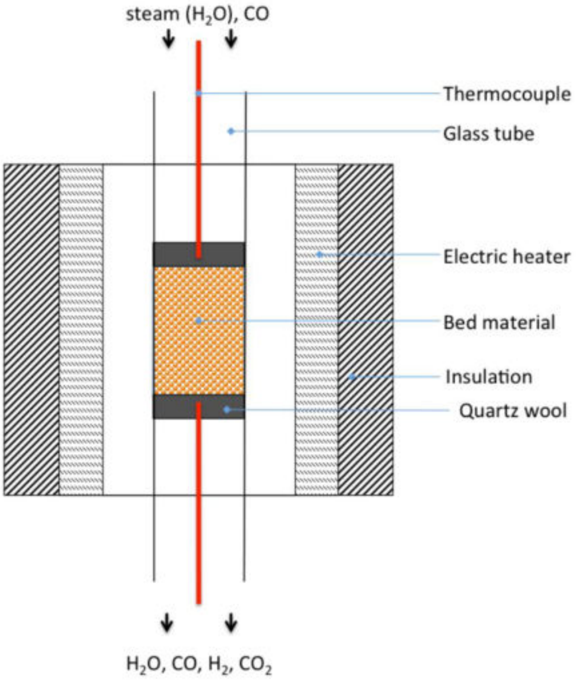

Figure 4.8: *The schematic structure of the apparatus for determining the activity of the bed material. [43]*

To investigate the catalytic activity, the carrier gas is fed into the reactor together with the H_2O (water vapor) and CO. If the bed material is catalytically active, the WGSR takes place and the two products H_2 and CO_2 are formed. The more catalytically active the bed material, the more H_2 and CO_2 is formed.

For a detailed description of the micro-scale test-rig, reference is made to the corresponding master thesis [43].

4.6 Scanning electron microscope

Some samples of the bed material of the individual experiments were examined using a scanning electron microscope (SEM). In order to be able to examine the bed material samples, the samples were embedded in epoxy resin. The samples were then polished to obtain cross sections of the bed materials. By polishing, it is possible to observe the individual layers that have formed on the particle surface of the bed material. Elemental analysis of the bed material layers was carried out with a Carl Zeiss Evo LS15 scanning electron microscope equipped with an Oxford X-Max 80 energy dispersive X-ray spectrometer (EDS). The measurements conducted were area analyses to obtain a distribution of elements.

For better comparison, Figure 4.9 shows bed material samples from experiments with similar scope conditions. In these experiments, bark was used as fuel, which was burned in a 5 kW bench scale fluidized bed pilot plant. Quartz with a size fraction from 106 µm to 125 µm was used as bed material. The fluidization rate was 80 l/min. These values refer to standard conditions, i.e. at a temperature of 273.15 K and a pressure of 1.013 25 bar. The amount of bed material was 540 g, which is only one tenth as much as in the experiments of this master thesis. Unfortunately, no fuel delivery rates or total fuel quantities for these experiments are given in the publication. The temperature of the bed material was 800 °C and thus roughly corresponds to the temperature that was used in these experiments. Bed material samples were taken and analysed after 4 h, 8 h, 16 h, 24 h, 32 h and 40 h [29].

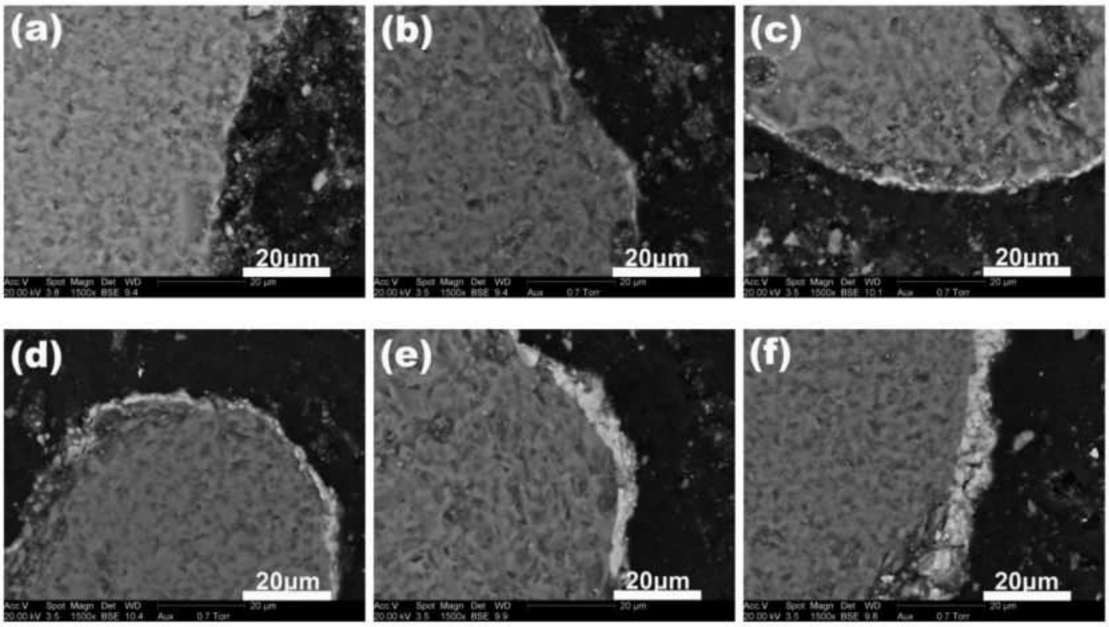

Figure 4.9: *SEM images of cross sections of bed material particles from a* 5 kW *fluidized bed combustion after an operation time of (a)* 4 h, *(b)* 8 h, *(c)* 16 h, *(d)* 24 h, *(e)* 32 h *and (f)* 40 h *[29].*

The individual images (a) to (f) of Figure 4.9 show cross sections of the bed material particles from different samples, which were taken at different times. The layer appears lighter in color, which has formed around the dark colored particle. It can be clearly seen that the layer thickness around the particle increases significantly with the time of interaction with the fuel.

In this master thesis bed material samples of the fourth, the fifth and the sixth experiment were selected for the SEM, since on the one hand different bed materials were used in these experiments and on the other hand the longest interactions of the individual bed materials with the fuel took place in these experiments.

In addition to the observations with the SEM, line scans with elemental mapping of the individual bed material samples were carried out. A line scan allows analysis over a selected line on the image. The analysis begins at the starting point of the line and finishes at the end of the line.

Epoxy compounds are a group of organic cyclic compounds that contain an epoxy bridge. An epoxy bridge consists of an oxygen bridge and carbon atoms [44, p. 522]. Therefore, by embedding the bed material samples in epoxy resin, elemental mapping is shown as an atomic

percentage on a carbon-free and oxygen-free basis over the length of the line.
Multiple lines were analyzed for each bed material sample. Representing each bed material, the evaluation is given along a single line. Line scans and the elementary analysis provide reliable information about the elementary composition of the layers of the bed material samples.

4.7 Computer-aided design

Most parts of the bench scale fluidized bed pilot plant were modeled in a 3D Computer-aided design (CAD) program. The computer program Autodesk Inventor 2020 Professional [45] was used for this 3-dimensional modeling.
The system was modeled using existing CAD drawings as well as parts lists and ordered material lists. The remaining, missing dimensions were taken manually from the existing testing plant. The essential components of the bench scale fluidized bed pilot plant were drawn from all these dimensions.

4.8 Variable parameters

As explained in more detail in Section 3.1, the bench scale fluidized bed pilot plant was a completely new testing plant on which hardly any experiments were carried out. For this reason, the experiments also serve as initial empirical values and the experience gained from them should serve as a guide for later experiments. The experiments carried out also paid attention to changing the various operating parameters and documenting their effects on ongoing operations.
The following list gives an overview of all parameters that are varied:

- **Fuel:**
  - Fuel type
  - Amount of fuel
- **Fluidization:**
  - Fluidization rate of the fluidization medium
  - Preheating temperature of the fluidization medium
- **Bed material:**
  - Type of bed material
  - Amount of bed material
  - Grain size distribution of the bed material

Bark pellets were used as fuel in all experiments. The bark pellets have already been discussed in more detail in Section 4.1. The amount of fuel depends essentially on the required combustion temperature inside the reactor. More fuel leads to higher combustion temperatures, a lower fuel supply leads to a lower combustion temperature. As explained in more detail in Section 4.3, the fuel is conveyed from the fuel tanks into the combustion chamber via two screw conveyors. The calibration of the screw conveyors in Subsection 4.3.1 has shown that the two screw conveyors are not optimally matched. The complications and problems of the screw conveyors are discussed in more detail in Subsection 5.2.1.

As described in more detail in Subsection 2.6.3 the fluidization rate of the fluidization medium essentially determines the operating mode of a fluidized bed. Depending on the volume flow, a fluidized bed reactor can be operated as a fixed bed or as a fluidized bed. An excessively high volume flow leads to pneumatic transport and thus to discharge of the bed material. During the experiments, the reactor was operated only as a fluidized bed. The bench scale fluidized bed pilot plant is equipped with several heating shells. On the one hand, the reactor can be heated with them, on the other hand there is the possibility of preheating the fluidization medium before it is fed into the reactor. In addition to these variable parameters of fluidization, the fluidization medium could also be changed. However, compressed air was used as the fluidization medium for all experiments.

The experiments were carried out with different bed materials. The individual experiments also differ with regard to the amount of bed material. The type of bed material based on the fundamental question of layer formation on the surface of the particles [46]. As mentioned in more detail in Section 4.2 cristobalite, Na-feldspar [47] and quartz [29] were used as bed materials. At the beginning of the experiments, no sufficient statement could be made about the optimal amount of bed material. Therefore different amounts of bed material were used during the experiments, in order to obtain information about the effects during operation. The grain size distribution of the bed material and the calculation of the SMD has already been discussed in more detail in Section 4.2 and in Subsection 2.6.1.

Chapter 5

Results and Discussion

In this chapter the results and the findings of this master thesis will be summarized.
Several experiments were carried out on the bench scale fluidized bed pilot plant. The experiments were carried out with different bed materials. The operating time of the experiments, as well as the amount of bed material of the individual experiments varied. Section 5.1 explains the individual experiments on the system. Only combustion experiments and no gasification or pyrolysis experiments were performed. All combustion experiments carried out are listed and the details and findings of these experiments are discussed.
With the knowledge and insights gained from these experiments, there were some modifications and improvements to the details of the bench scale fluidized bed pilot plant. These modifications and improvements are discussed in more detail in Section 5.2.

5.1 Experiments carried out on the bench scale fluidized bed pilot plant

This section is intended to provide a brief overview and summary of the experiments carried out on the bench scale fluidized bed pilot plant. The individual experiments are described in more detail in the Subsection 5.1.1 to Subsection 5.1.6. In total, six different experiments were carried out on the bench scale fluidized bed pilot plant.
Although bark pellets should be used for all experiments, the first two experiments are an exception regarding to fuel. In these two experiments, additional wood pellets had to be used during the heat-up phase. The reasons for this are explained in more detail in the individual experiment descriptions in Subsection 5.1.1 and Subsection 5.1.2. After each experiments was carried out, the total amount of fuel and the fuel feeding rate could be calculated using the calibration curves of the two screw conveyors, described in Subsection 4.3.1. The total amount of fuel, burned during the experiments, differs quite clearly. With the exception of the first experiment, between 0.34 kg and almost 0.68 kg of fuel were burned per hour. This big difference is due to the operational management of the individual experiments and will be explained in more detail later.
The experiments also differ in terms of operation time. The duration of the experiments varied, with the exception of the first experiment which had to be canceled, from a duration of approximately 10.5 h in the second experiment to a duration of well over 60 h in the fifth experiment. The first four experiments were carried out with the aim of bed material variation. In order to achieve a sufficient layer formation, the fifth and sixth experiments were

Table 5.1: *Overview of all experiments with the associated operating parameters.*

Operating parameter	**Bed material variation**				**Long-term experiment**	
	1	**2**	**3**	**4**	**5**	**6**
Bed material						
Type of bed material	Cristobalite	Cristobalite	Na-feldspar	Quartz	Na-feldspar	Cristobalite
Grain size (d_{sv})	249 µm	249 µm	215 µm	434 µm	215 µm	249 µm
Amount of bed material	5.5 kg	5.5 kg	5.5 kg	4.5 kg	6.0 kg - 5.4 kg	6.0 kg - 5.55 kg
Fuel						
Type of fuel	bark pellets (wood pellets)	bark pellets (wood pellets)	bark pellets	bark pellets	bark pellets	bark pellets
Fuel feeding rate	< 0.34 kg/h	0.34 kg/h	0.53 kg/h	0.56 kg/h	0.68 kg/h	0.45 kg/h
Total amount of fuel	< 0.5 kg	2.4 kg	6.4 kg	6.7 kg	34.1 kg	18.1 kg
Operating time						
Duration with preheating	~5 h	~10.5 h	~16 h	~16 h	~63.5 h	~50.5 h
Fuel supply	~1.5 h	7 h	12 h	12 h	50 h	40 h
Day(s)	1	1	2	2	5	4
Temperature (bed material)						
Target temperature	750 °C	700 °C	(1) 750 °C (2) 800 °C	(1) 750 °C (2) 800 °C	(1-4) 750 °C (5) 820 °C	(1-4) 770 °C
Peak temperature	-	950 °C	950 °C	950 °C	950 °C	-
Fluidization						
Fluidization medium	air	air	air	air	air	air
Flow rate *	-	~140 l/min - ~180 l/min	~95 l/min - ~140 l/min	~85 l/min - ~120 l/min	~65 l/min - ~100 l/min	~90 l/min - ~120 l/min
Miscellaneous						
Annotation	Termination of the experiment	Repetition of the first experiment	Extend experiment time	Reduce bed material	Extend experiment time, reduced flow rate	Termination after the fourth day of experiment

* Refer to standard conditions: 273.15 K and 1.013 25 bar

carried out as long-term experiments. The third, fourth, fifth and sixth experiment lasted several days. In this context it should be mentioned, that it was not allowed to operate the testing plant overnight for legal reasons. For this reason, these longer experiments had to be spread over several days. A continuous supply of fuel for more than 10 h a day was therefore not possible. In experiments that lasted several days, the system had to be brought up to operating temperature every day. The experiments have shown, that the heat-up phase lasted approximately 3 h before the fuel supply can be started. The duration of the pure fuel supply varied between 7 h and 50 h in the experiments.

The effects of the volume flow in fluidized beds have already been discussed in more detail in Subsection 2.6.3. In order to recognize the effects of fluidization, the individual experiments were carried out at different fluidization rates. The volume flow for fluidization was between 65 l/min and 180 l/min. These values refer to standard conditions, i.e. at a temperature of 273.15 K and a pressure of 1.013 25 bar. The effects of the fluidization rates and other parameters are explained in more detail in Subsection 5.1.7. As explained in more detail in Subsection 5.2.2, the heating shells did not work as expected. At higher temperatures there were short circuits, which made it necessary to switch off the heating shells. For this reason, the heating shells were mainly used to preheat the fluidization medium. The heating shells, which are located around the reactor, were not used during the combustion experiments. When explaining the individual experiments, the preheating temperatures can be read in the associated diagrams.

The amount of bed material varied between 4.5 kg and 6.0 kg. The effects of the amount of bed material on the operation of the system are explained in more detail in the detailed description of the individual experiments.

Table 5.1 is intended to give an overview of all experiments with the associated operating parameters. As can be seen in Table 5.1, the first experiment and the last experiment column are missing some entries. The explanation for this is that the first experiment was canceled. The details are explained in more detail in Subsection 5.1.1. Originally, in the last experiment, the fuel supply should also be 50 h, but this sixth experiment was also ended prematurely.

5.1.1 First experiment (bed material variation - cristobalite)

The first experiment, which was carried out on the testing plant, turned out to be very helpful to learn many details about the system, its operation and how to handle the bench scale fluidized bed pilot plant.

In the first experiment, cristobalite was used as bed material. Since there was no indication of the optimal amount of bed material, the dimensions of the testing plant were used as a reference for the amount of bed material. As already described in more detail in Section 4.3, the bench scale fluidized bed pilot plant has no closed nozzle bottom. The fluidization is implemented via two tubes protruding into the column, which have openings directed downwards. These are shown in detail in Figure 4.5. As shown in Figure 4.5b, there are three measuring elements above the nozzles for measuring the temperature of the fluidized bed. Furthermore, a measuring element can be seen to record the pressure in the fluidized bed. In the first experiment, enough bed material was introduced into the reactor that all three measuring elements for temperature measurement were fully covered by the bed material, without fluidization. The amount of bed material in the first experiment was 5.5 kg.

To carry out the experiment, the system was first brought to operating temperature without the addition of fuel. In order to minimize thermal stresses and to keep the loads on the materials low, a heating rate of 30 °C per 10 min was set. At the beginning of the first experiment, fluidization was carried out with air at a fluidization rate of 200 l/min. These values refer to standard conditions, i.e. at a temperature of 273.15 K and a pressure of 1.013 25 bar. Figure 5.1 shows the measured temperature profiles during the first experiment. The abscissa shows the duration of the experiment. The fuel supply was set as the starting point for the experiment. The time before is given with a negative sign and indicates the heat-up phase.

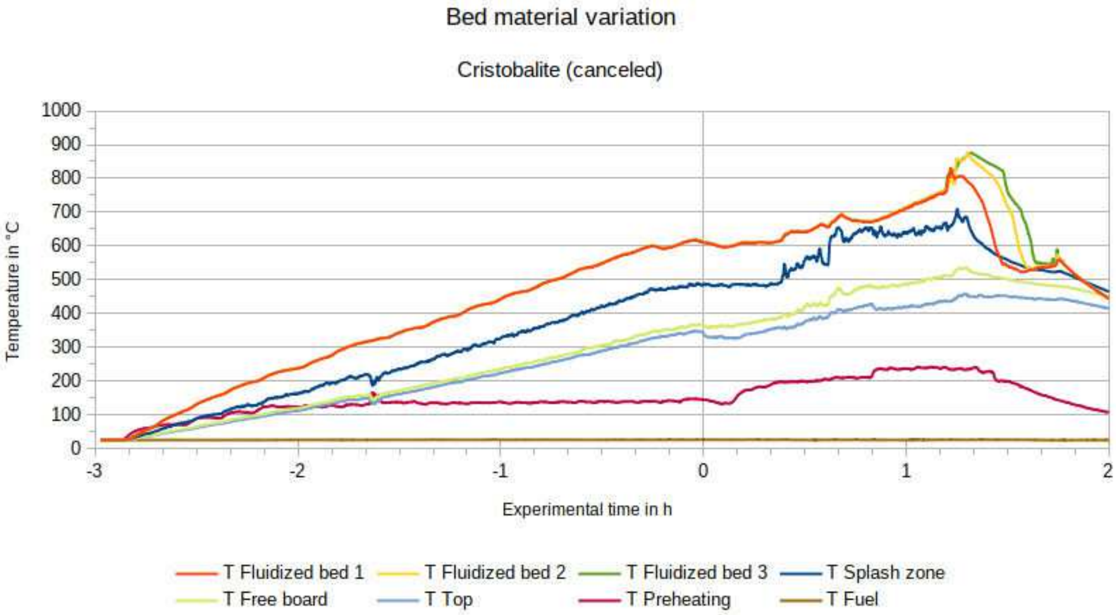

Figure 5.1: *Temperature curves over the time of the first experiment with cristobalite.*

As shown in Figure 5.1, the reactor could be heated up to a fluidized bed temperature of 600 °C with a constant heating rate of 30 °C per 10 min. After a temperature of the bed material of 600 °C was reached, it was not possible to further heat up the reactor, although this should be possible with the installed heating shells. As it turned out, the heating shells caused a short circuit, which triggered the main fuse of the heating shells several times. As a result, the entire system was without electricity. Further explanations of the heating shells are explained in more detail in Subsection 5.2.2.

According to the specifications for the experiment, the reactor temperature should first be brought to 600 °C before the testing plant is operated with fuel. After this temperature was reached, the fuel supply could begin. First, pellets from bark were fed. This can be seen in Figure 5.1 at a time of 0 h. However, since the temperature suddenly dropped at a bed temperature of approximately 700 °C, pellets made of wood were added, which were stored in the second fuel tank. The wood pellets were fed in because the plant was successfully operated with wood pellets in a first test run. The temperature could be increased further by the simultaneous supply of bark and wood pellets. This can be seen in Figure 5.1 at a time of approximately 40 min.

The combustion temperature in the reactor then rose very constantly up to a temperature of 770 °C. From 770 °C, the temperature rose quite quickly, up to approximately 820 °C. From here, the temperature values *T Fluidized bed 1*, *T Fluidized bed 2* and *T Fluidized bed 3* of the fluidized bed were no longer in the same temperature range. This can be seen particularly well in Figure 5.1, since the graphs of these three temperatures are no longer exactly

congruent. In particular, the temperature *T Fluidized bed 1* of the bed material differs from the other two temperatures *T Fluidized bed 2* and *T Fluidized bed 3*. After *T Fluidized bed 2* and *T Fluidized bed 3* reached the peak value of 880 °C, the fuel supply was stopped. As a result, the temperatures initially went slowly and then abruptly downwards.
The reason why the temperatures in the fluidized bed differed in such a way was not known at that time. However, everything indicated defluidization through an agglomerated fluidized bed. After the system had cooled down, the bed material could be removed. Figure 5.2 shows the removed bed material.

Figure 5.2: *The picture shows a small agglomerate of bed material, which was taken from the fluidized bed after the first, canceled experiment.*

Figure 5.2 clearly shows that parts of the bed material formed agglomerates. However, not all of the bed material was agglomerated, only a few small lumps formed. The size of the agglomerates was only a few mm up to 1.5 cm. The strength of the agglomerates was also not very high. Hardly any force was required to separate the adhering particles.
On the other hand, it seems interesting that the combustion obviously took place very consistently until the experiment was stopped. The combustion mainly produced CO_2 and hardly any CO.
Figure 5.3 shows the measured values of the gas measuring device associated with the first experiment. As can be seen in this diagram, mainly carbon dioxide concentrations were measured. The concentrations of CO were less than 2% and only for short periods. The concentrations of CH_4 and H_2 were hardly measured and were less than 1% of the flue gas over the entire duration of the experiment.
The first experiment turned out to be particularly educational. Even if the first experiment had to be canceled, it provided important information in particular on how the processes of future experiments should proceed and how the measurement results should be interpreted with regard to the course of the experiment.

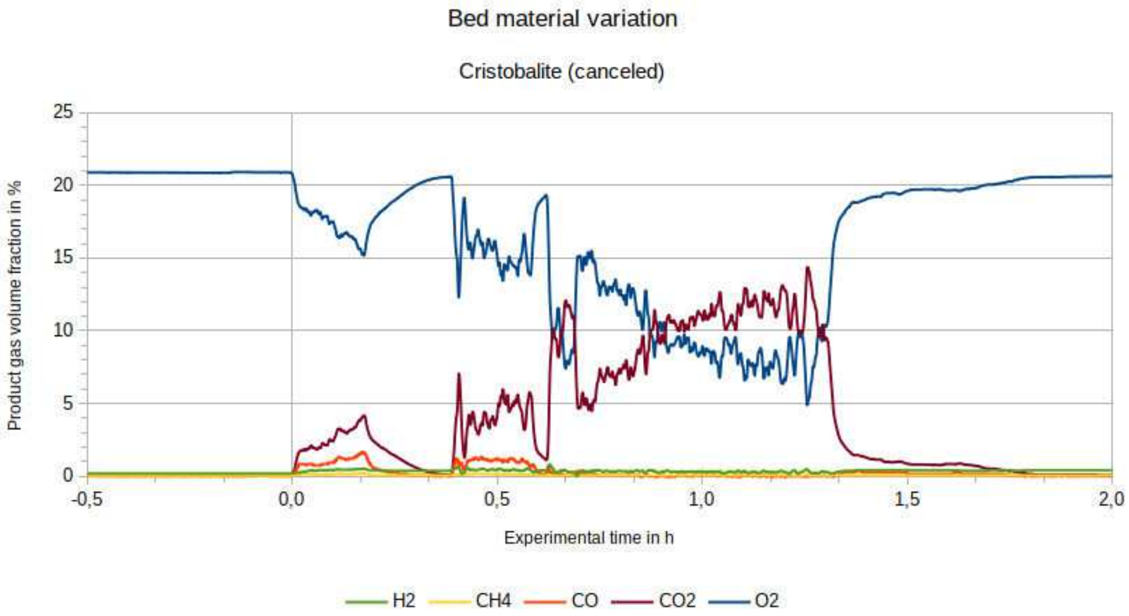

Figure 5.3: *Flue gas volume fraction over time of the first experiment with cristobalite.*

5.1.2 Second experiment (bed material variation - cristobalite)

After the first experiment had to be stopped, it was decided to carry out the second experiment again with the same operating parameters and under the same conditions as for the first experiment.

Before the second experiment was carried out, the testing plant was thoroughly cleaned. For this purpose, all measuring lines, the flange at the lower end of the column and the combustion chamber inside the testing plant were cleaned. Particular care was taken to ensure that the combustion chamber and the pipes for fluidization were cleaned of all residues from the first experiment. The combustion chamber was cleaned with a hearth brush, which is also used by chimney sweeps. The intensive cleaning of the testing plant is intended to ensure that there are no residues from previous experiments in the testing plant, which could influence or falsify the results of further experiments.

Cristobalite was used again as bed material. The time course of the individual temperatures can be seen in Figure 5.4.

Figure 5.4 shows that also in this experiment it was not possible to heat up the reactor to temperatures above 600 °C by only using the heating shells. An attempt was made to reactivate the electrical fuse of the heating shells a few times, but each time the fuse was triggered again a few seconds later. For this reason, the fuel supply was started again. In this experiment, the testing plant was operated at a temperature of the fluidized bed material of 700 °C. This temperature was attempted to be kept as long as possible in order to maintain constant combustion conditions. The experiment showed that constant operation at a temperature of 700 °C can be maintained very well. Towards the end of the experiment, a temperature of 950 °C should be reached in order to expose the bed material to higher temperatures in order to check whether agglomeration occurs. The heating rate until this temperature is reached should be approximately the same heating rate as when the system was started up. This corresponds to a heating rate of 30 °C per 10 min. As can be seen in Figure 5.4, this was

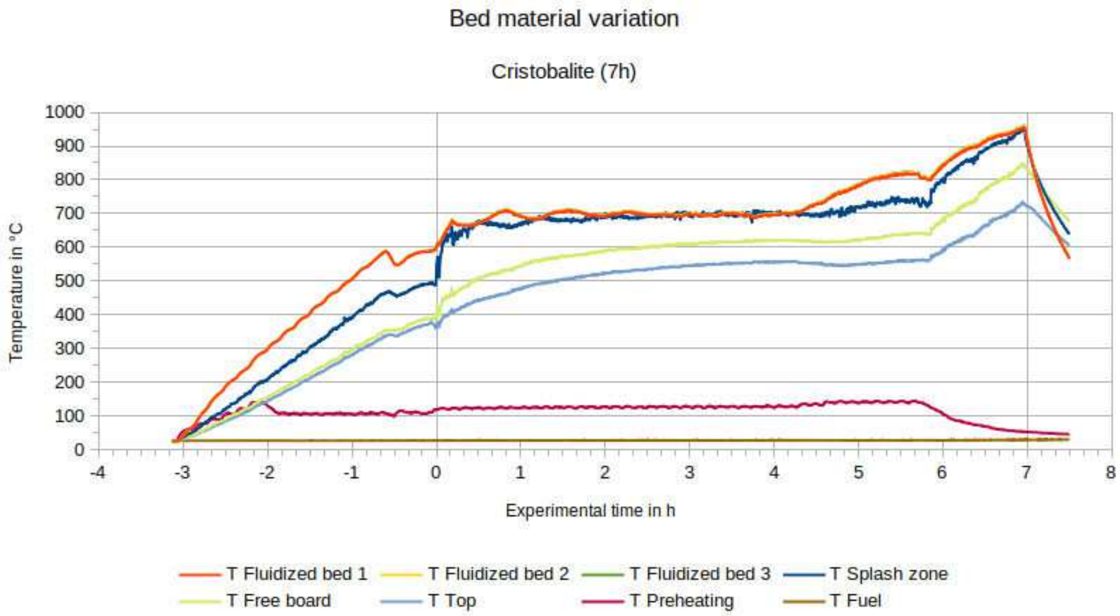

Figure 5.4: *Temperature curves over the time of the second experiment with cristobalite.*

not possible. The heating rate was significantly below the required heating rate. This was due to the fact that the maximum conveying capacity of the screw conveyor of the small fuel tank was reached. From a measured temperature of 817 °C of the bed material, it was no longer possible to further increase the combustion temperature inside the reactor. The screw conveyor has already been operated at the maximum possible frequency of 50 Hz.

After a temperature of 817 °C has been reached, an abrupt drop in the temperature of the bed material can be seen. An attempt was made to increase the lower temperature by using the heating shells. Unfortunately, this was not possible because the ground fault interrupter tripped a few times. This meant that the screw conveyor was also without electricity and therefore no more fuel could be introduced into the reactor. The temperature continued to drop.

Because of this, as in the first experiment, wood pellets from the second, the big fuel tank, were additionally used. Since the electric motor of the big fuel tank has a different gear ratio than the electric motor of the small fuel tank, the temperature rose significantly faster due to the higher fuel input. As can be seen in Figure 5.5, this led to an increase in the carbon monoxide concentration in the flue gas.

For this reason, the volume flow of the fluidization medium has been increased to ensure a combustion atmosphere. In this experiment, fuel was fed for exactly 7 h. The temperature of the bed material was kept at a rather moderate temperature of 700 °C during most of the experiment. The primary purpose of this experiment was to repeat the first canceled experiment. As was shown after the cooling process and emptying of the system, no agglomeration of the bed material occurred in this experiment, despite the same operating conditions as in the first experiment. Why the bed material of the first experiment agglomerated and formed small lumps could not be sufficiently clarified. A possible explanation could be previous test runs on the system. Before the first experiment was carried out, a test run of the new bench scale fluidized bed pilot plant with straw as fuel was carried out [48].

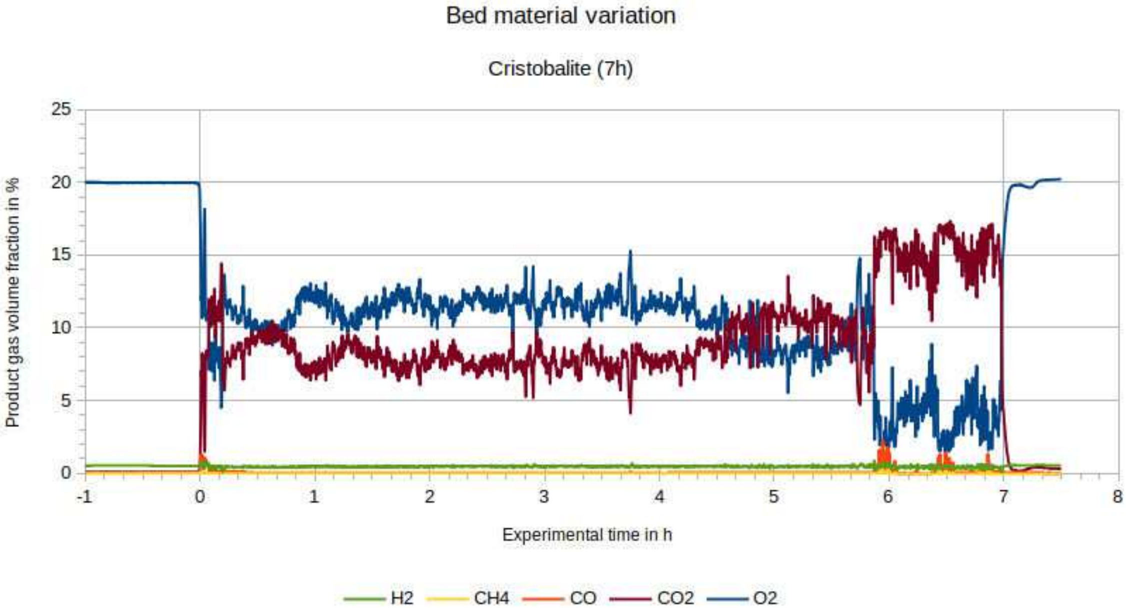

Figure 5.5: *Flue gas volume fraction over time of the second experiment with cristobalite.*

Straw has a very low ash melting point [11, p. 218]. It could be possible that the agglomeration caused by residues from this test run led to the agglomeration of the bed material of the first experiment. However, since no further investigations of the bed material have taken place, this statement cannot be scientifically proven.

5.1.3 Third experiment (bed material variation - Na-feldspar)

Since no results about the time-dependent catalytic activation have been made, it was decided to carry out the third experiment over a longer period of time. The idea was to let the bed material interact with the fuel for a longer time. The default was 12 h of fuel supply. Since no experiments are allowed to be carried out on the testing plant in the technical center at night, the fuel was supplied over two days for 6 h each. In contrast to the first two experiments, Na-feldspar was used as bed material. The amount of bed material was chosen at 5.5 kg, the same as in the first two experiments. Before starting this experiment, both fuel tanks were filled with bark pellets. This should give more flexibility in the delivery rate of the fuel supply. Figure 5.6 shows the temperature profiles of the third experiment. For a better overview, the diagram only shows the times at which combustion took place as well as the first heat-up and the last cool-down phase.

The fluidized bed temperature was set at 750 °C for the first day of the third experiment. Subsequently, as in the second experiment, the third experiment should be finished with a ramp to test for agglomeration at higher temperatures. Therefore a peak temperature of 950 °C should be reached towards the end of the experiment.

As can be seen in the Figure 5.6, especially on the first day, the target temperature of the fluidized bed could not be kept nearly as constant as in the second experiment. This is mainly due to the fact that fuel delivery often had to be switched between the big and the small fuel tank. This is due to the fact that the screw conveyor of the small fuel tank could not conveying enough pellets under full load to reach the required fluidized bed temperature of

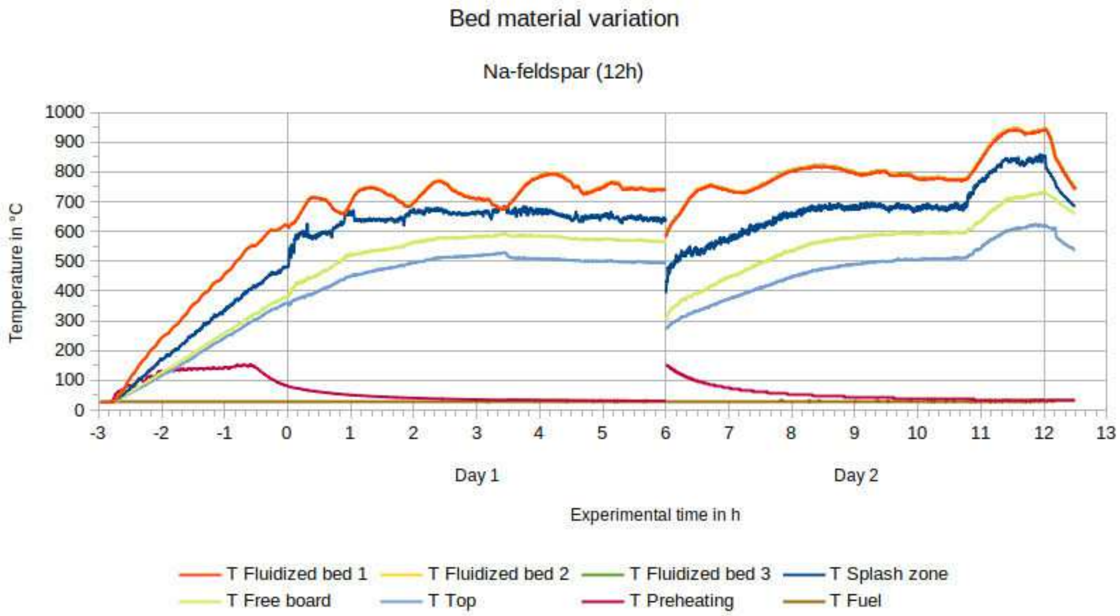

Figure 5.6: *Temperature curves over the time of the third experiment with Na-fedlspar.*

750 °C. The screw conveyor of the big fuel tank, on the other hand, was conveying too much fuel at its minimal possible frequency. The fluidized bed temperature rose significantly above 750 °C.

In contrast to the second experiment, the fluidization rate of the fluidizing air was significantly reduced in the third experiment. In the second experiment, where the fluidization rate was 140 l/min to 180 l/min, the third experiment was fluidized at a fluidization rate of 95 l/min to 140 l/min. On the second day of the third experiment, an attempt was made to keep the fluidization rate well below 120 l/min. The reduced flow rate made it possible to transport the fuel into the combustion chamber almost exclusively using the screw conveyor of the small fuel tank.

As expected, a lower fluidization rate resulted in less heat output from the reactor. This made it possible to reach significantly higher temperatures only by using the screw conveyor of the small fuel tank. As can be seen in Figure 5.6, the fluidized bed temperature fluctuates far less than the fluidized bed temperature on the first day of the third experiment.

Towards the end of the third experiment, as in the second experiment, the bed material was heated to a temperature of 950 °C. This was not possible with the screw conveyor of the small fuel tank, therefore the screw conveyor of the big fuel tank with a higher delivery rate was used. Figure 5.7 shows the flue gas concentrations measured during the third experiment.

The oxygen concentration mainly correlates with the concentration of CO_2. The lower the oxygen concentration, the higher the carbon dioxide concentration. The experiment has shown that as long as the oxygen concentration is above the self-imposed limit of 6% [29], a very controlled and complete combustion takes place.

The fluctuations in the concentrations of O_2 and CO_2 arise due to the changing frequencies of the screw conveyors. The temperature was kept as constant as possible. Every time the flow rate changes, combustion is therefore not constant, i.e. incomplete, which leads to changes the concentrations in the flue gas composition.

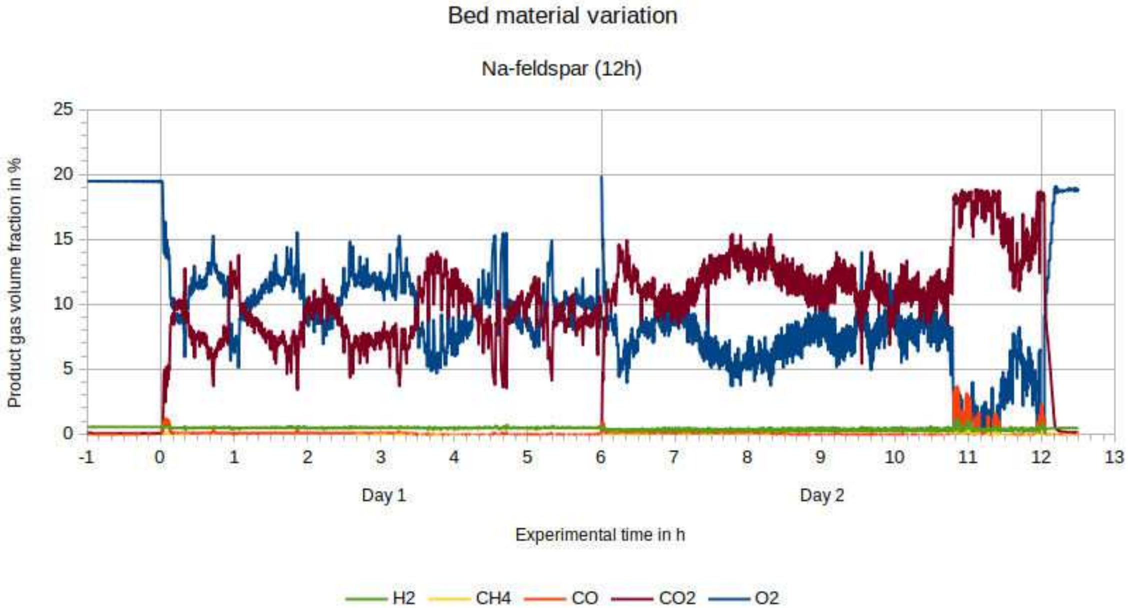

Figure 5.7: *Flue gas volume fraction over time of the third experiment with Na-feldspar.*

5.1.4 Fourth experiment (bed material variation - quartz)

Like the third experiment, the fourth experiment was carried out with the same time for the fuel supply. The experiment was divided into two days. Fuel was burned for 6 h a day. Quartz was used as bed material.

After no catalytic activity of the bed material was found after the end of the third experiment, it was decided to use less bed material for the fourth experiment. The reasoning behind this was, that the use of less bed material with approximately the same amount of fuel, should result in an increased interaction of the fuel with a single particle of the bed material. For this reason, a quantity of 4.5 kg of bed material was used for the fourth experiment. Due to the small amount of bed material, the top sensor for the fluidized bed temperature was not completely covered with bed material without fluidization. As it turned out, however, the sensor was completely encased in the bed material due to the expansion of the fluidized bed in the fluidized state. Thus, there were no problems in measuring the three different fluidized bed temperatures inside the combustion chamber.

The setting for the combustion temperatures was chosen, as for the third experiment, on the first day at a temperature of 750 °C and on the second day at a temperature of 800 °C. Towards the end of the second day, as in the previous experiments, a temperature of 950 °C was reached. As in the third experiment, only bark pellets were burned as fuel. Wood pellets were not used.

When filling the system with bed material, it was checked how the fluidization rate affects quartz and the smaller amount of bed material. Through the inspection glass it was observed that higher fluidization rates, despite the generally larger grain size of the quartz, lead to a discharge of the fine particles. At fluidization rates greater than 200 l/min, the bed material swirled very strong. Emptying the cyclone, before starting the experiment, showed that fine particles of the bed material had been deposited in it.

As the third experiment has shown, the rate of fluidization was set as relatively high in the previous experiments. For this reason, it was decided to fluidize with even lower volume rates in this experiment. The fluidization rates for the fourth experiment were between 85 l/min and 120 l/min. As it turned out after the end of the fourth experiment, even more fuel was burned compared to the third experiment. Details of the quantities of fuel delivered can be found in Table 5.1.

Due to the smaller amount of bed material, it was a challenge to operate the fluidized bed under constant conditions and therefore at constant combustion temperatures. As a result, the amount of fuel supply had to be adjusted frequently during operation. This was done by changing the frequencies of the two screw conveyors. The temperature curves of the fourth experiment can be seen in Figure 5.8.

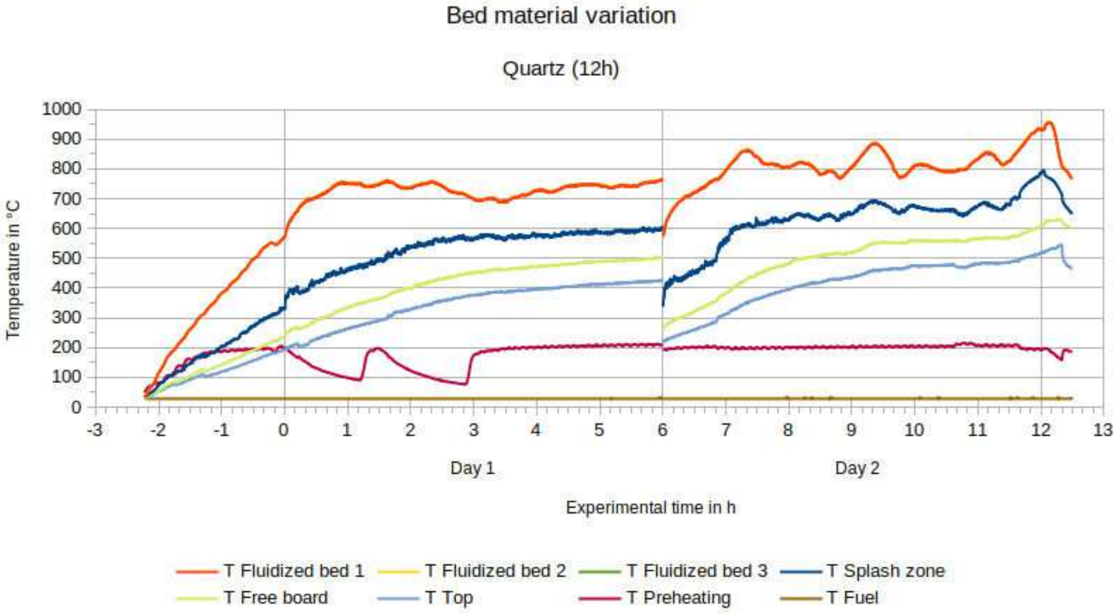

Figure 5.8: *Temperature curves over the time of the fourth experiment with quartz.*

The frequent adjustment of the frequencies of the screw conveyors resulted in less uniform combustion, compared to the third experiment. This was reflected in the flue gas composition. The measurements of the flue gas concentrations can be seen in Figure 5.9.

The concentrations of CO are higher compared to previous experiments. The fluctuations in the fuel supply are particularly noticeable on the second day.

At the end of the fourth experiment, a peak temperature of 950 °C was reached. To reach this temperature, the screw conveyor of the big fuel tank was used to be able to feed more fuel into the reactor. As expected, the addition of fuel increased the carbon monoxide concentration. The fluidization rate was increased to provide more oxygen to the combustion. It was expected that more heat would be removed from the reactor. Therefore the fuel supply was increased further. After the required target temperature of 950 °C was reached, the fuel supply was stopped.

Contrary to expectations, the temperature in the reactor continued to rise. This can be explained by the fact that many pellets got into the combustion chamber but did not yet burn completely. If the temperatures from Figure 5.8 are compared with the flue gas concentrations in Figure 5.9, it can be concluded that the fuel was mainly gasified and not burned.

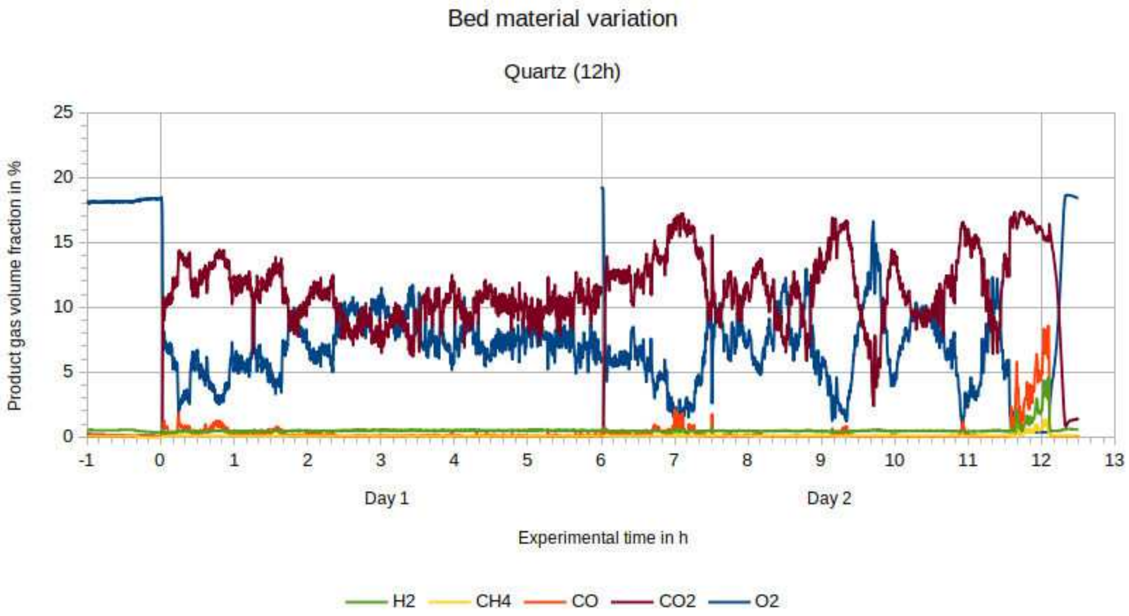

Figure 5.9: *Flue gas volume fraction over time of the fourth experiment with quartz.*

Due to the abundance of fuel and the absence of oxygen, the fuel could not be completely oxidized. This led to gasification, causing the volatile components to be released out of the fuel. The remaining coke was largely converted to CO. This can be confirmed by Figure 5.9, where the carbon monoxide content of the flue gas was measured with up to 8%. Increased concentrations of CH_4 and H_2 could also be measured.

Another disadvantage of the reduced volume flow of the fluidization appears after cool down and opening the system. The soot in the flue gas increased due to the lower oxygen content. Because a partial volume flow of the flue gas is used for flue gas measurement, the filter of the measuring device was clogged more quickly. The filter of the flue gas measurement essentially consists of a close-meshed metal sieve and a glass wool filter, which is located in front of the metal sieve. All of the soot settled on the glass wool filter. This caused the filter to become clogged. For this reason, the glass wool in the filter had to be changed after the first day of the experiment. The problems of filters for flue gas measurement are discussed in more detail in Subsection 5.2.7.

Since no catalytic activity could be determined on the samples taken from the micro-scale test-rig using the WGSR, it was decided to additionally examine some bed material samples using a SEM. Figure 5.10 shows SEM images of cross sections of quartz. In Figure 5.10, the images (a), (b) and (c) show three different magnifications.

The bed material samples correspond to the samples as they were taken after the full test period of each experiment, which are listed in Table 5.1. The illustrations of the individual cross sections are representative of every bed material that has been examined. Several particles were examined per bed material sample. Each Figure shows three images of the same bed material sample.

The SEM analyzes confirm the results of the kinetic experiments on the micro-scale test-rig. As expected, there are no clear visualizations of layer formation on the images of the SEM analysis.

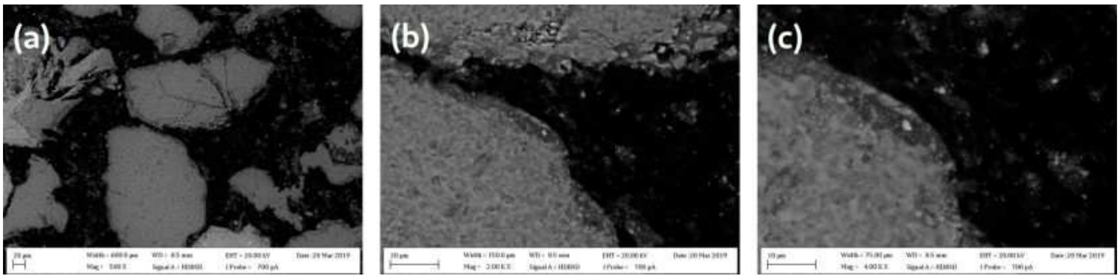

Figure 5.10: *Different enlargements quartz of the fourth experiment, after a fuel supply of* 12 h.

For further investigation, line scans with elemental mapping of the bed material were carried out. Figure 5.11 shows a bed material sample of quartz. The arrangement of the two lines *Line Data 11* and *Line Data 12* are marked in Figure 5.11.

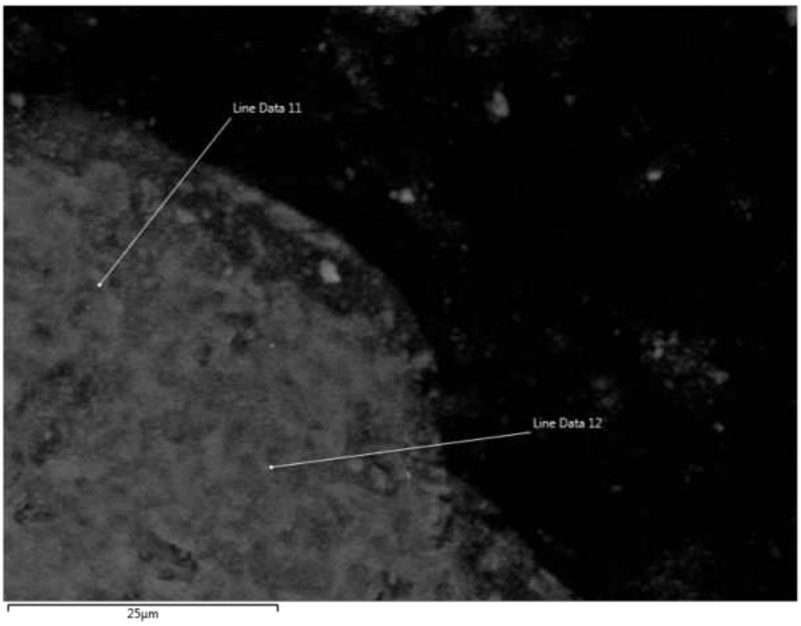

Figure 5.11: *Arrangement of the lines on the polished surface of the bed material samples of quartz.*

Representative for the line scans of quartz, Figure 5.12 shows the elementary mapping of *Line Data 11* after 12 h of fuel supply. The line scan does not show the scan of the entire length, but only a section from 7 µm to 17 µm. A slight increase in Ca and K can be seen at a length from the starting point of approximately 12 µm. This suggests an initiation of layer formation.

The two elements K and Ca are of particular importance for the assessment of the layer formation, since they serve as an indicator for the layer growth. In order to keep the graphical representation of the evaluation as clear as possible, only the elements Na, Si, Ca, K, P and Al were shown in the corresponding diagrams.

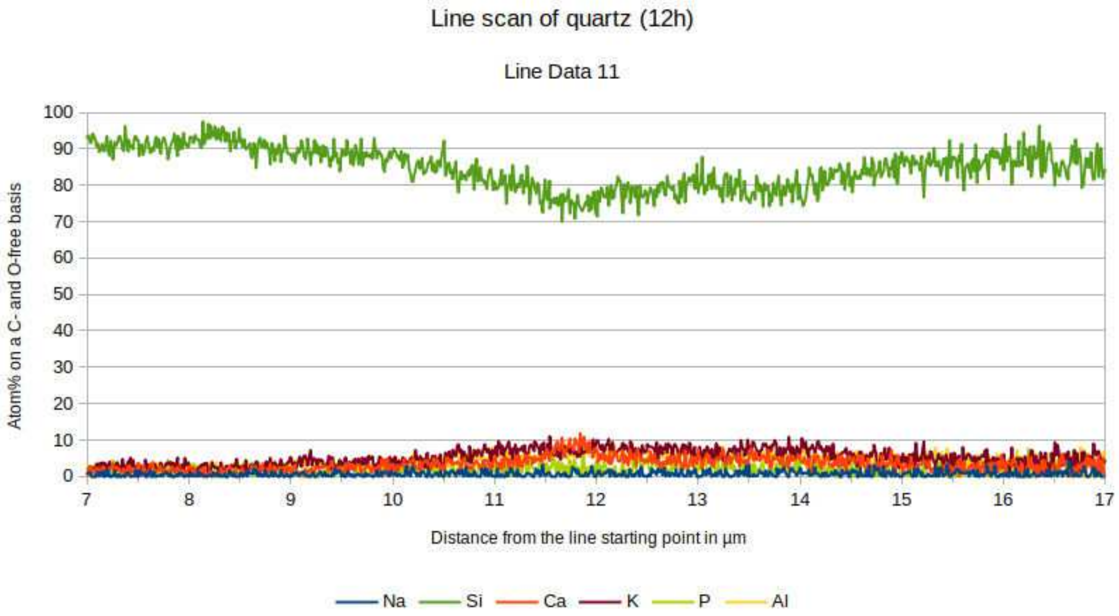

Figure 5.12: *Line scan in atomic percentage on a carbon-free and oxygen-free basis depending on the starting point of Line Data 11, for quartz after* 12 h *of fuel supply.*

5.1.5 Fifth experiment (long-term experiment - Na-feldspar)

Since no clear catalytic activity of the bed material could be detected in the previous experiments, the decision was made for the fifth experiment to significantly increase the duration of the interaction between fuel and bed material. For this purpose, the operating time of the fuel supply was increased to 50 h. As already mentioned, combustion experiments in the technical center must not run overnight, for this reason the fifth experiment was divided into five days. Fuel was fed into the reactor for 10 h each of the five days.

A further consideration was, that bed material should be sampled after each day of the experiment, in order to be able to show a chronological course of the activation of the bed material. It was decided to take a 150 g sample from the bed material after each day. These samples where then checked for catalytic activity with the micro-scale test-rig.

For this experiment, as in the third experiment, Na-feldspar was used as bed material. In contrast to the previous experiments, the amount of bed material was increased slightly. The fourth experiment showed that less bed material caused significantly greater fluctuations in the operational management of the system. If 150 g of bed material are removed per day, there are still 5.4 kg of bed material in the reactor at the end of the experiment. From this amount it is already known that the reactor can be operated constantly.

The temperature of 750 °C has proven to be a reasonable operating temperature for combustion in the fourth experiment. Therefore, this temperature was chosen for this experiment too. Towards the end of the fifth experiment, the reactor was heated up to a peak temperature of 950 °C to test whether agglomeration occurs. As in the previous experiments, bark pellets were used as fuel. Compared to the fourth experiment, the fluidization rate was again significantly reduced. The idea behind this was to keep the abrasion of the individual particles as low as possible during operation. Previous experiments have shown that lower fluidization rates make it possible to reach higher temperatures exclusively using the screw conveyor of the small fuel tank. In some cases the system was operated with a fluidization rate of only 65 l/min. Figure 5.13 shows the temperature profiles of the fifth experiment.

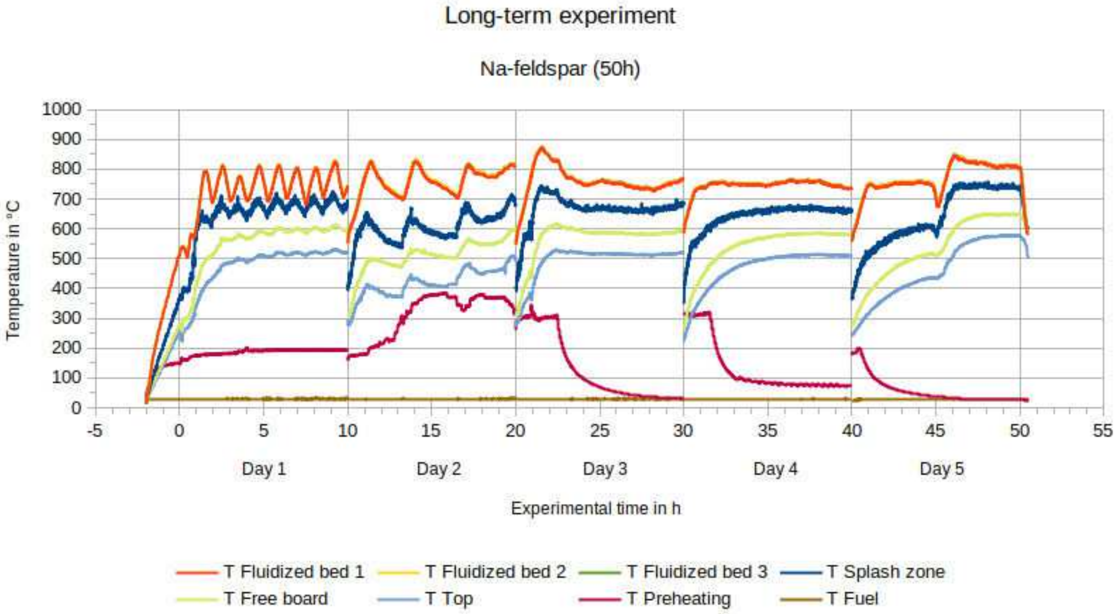

Figure 5.13: *Temperature curves over the time of the fifth experiment with Na-feldspar.*

As shown in Figure 5.13, the temperature fluctuated greatly on the first day of the experiment. This is due to the fact, that no experience has yet been gained on how the system behaves with the amount of 6 kg of bed material during operation. It had to be switched very often between the screw conveyor of the small fuel tank and the screw conveyor of the big fuel tank. Contrary to expectations it turned out that despite the lower fluidization rates, the conveying capacity of the screw conveyor of the small fuel tank was not sufficient to reach a temperature of 750 °C in the combustion chamber. The amount of 6 kg of bed material had a negative impact. The screw conveyor of the big fuel tank, on the other hand, delivered too much fuel at a minimum possible delivery rate, to prevent the temperature from rising.
Another side effect of using a lot of bed material during operation was that the system reacted very slowly to changes. A change in the amount of fuel or a change in the volume flow of the fluidization led to a change in the ongoing combustion process only after a significant time delay. For example, increasing the fuel supply did not immediately increase the combustion temperature. An increase in the fuel supply only increased the temperature after a few minutes. A reduction in the fuel supply led to a reduced temperature only after a few minutes delay. This can be seen particularly clearly in Figure 5.13 on the first day, where the system overshooted and the temperatures of the bed material *T Fluidized bed 1*, *T Fluidized bed 2* and *T Fluidized bed 3* fluctuate very much.
On the third day of the fifth experiment, there were still 5.7 kg of bed material in the system. With this smaller amount of bed material, it was possible to reach the combustion temperature of 750 °C with the screw conveyor of the small fuel tank. This was possible due to the lower fluidization rate, which resulted in less heat being removed from the reactor. On the third day of the fifth experiment, the rate of fluidization was significantly reduced, when heating up the testing plant. As would be expected, this resulted in an overshoot of

the system due to the increased amount of bed material. The very high temperatures at the beginning of the third day of the experiment can be seen in Figure 5.13.
As shown on the individual days of the experiments, it becomes easier to operate the system under constant conditions as the amount of bed material decreases.
In the fifth experiment, the temperature of the preheating of the fluidization medium was increased for the first time. In the previous experiments, the fluidization medium was preheated to a maximum of 200 °C. On the second day of the fifth experiment, the fluidization medium was preheated to 400 °C, the next two days to 300 °C. The preheating was switched off during the running operation, in order to investigate the effects on the running operation. The experiment has shown that preheating the fluidization medium has no noticeable effect on the operational management of the testing plant. The energy introduced in the form of heat via the preheating of the fluidization medium has no noticeable effect on the combustion temperature inside the reactor. It could be observed that the temperature inside the reactor depends mainly on the fluidization rate of the fluidization medium and the fuel feeding rate. Figure 5.14 shows the diagram with the associated concentrations of the measured flue gas.

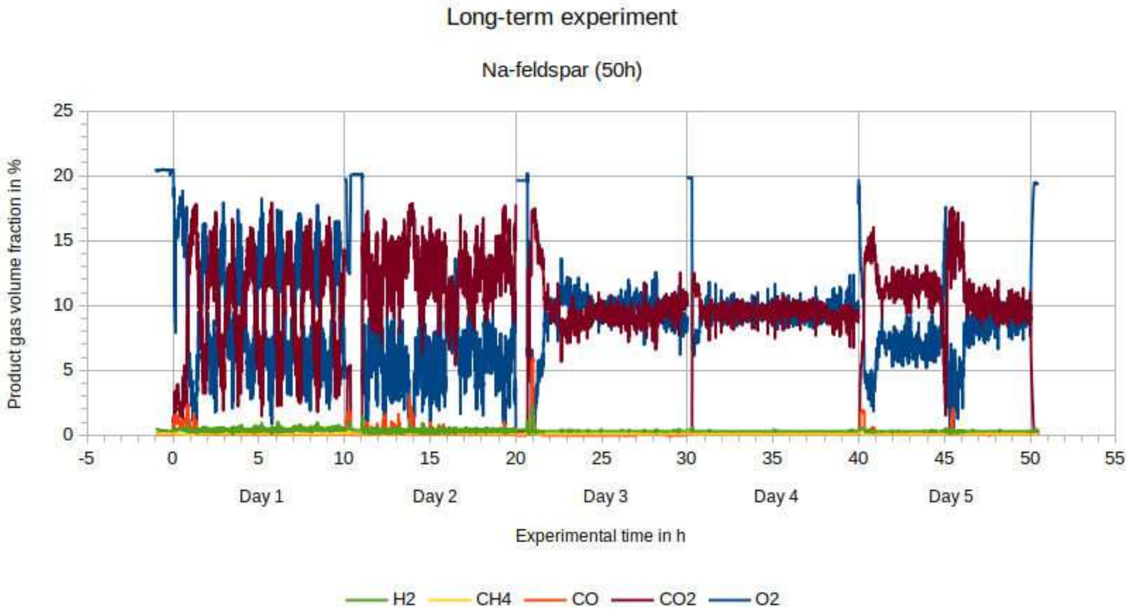

Figure 5.14: *Flue gas volume fraction over time of the fifth experiment with Na-feldspar.*

On the last day of the fifth experiment, the screw conveyor of the small fuel tank was blocked and could therefore no longer feed fuel into the combustion chamber. In order not to have to stop the experiment, the screw conveyor of the big fuel tank was put into operation. Despite the fact that the screw conveyor of the big fuel tank was conveying at minimal frequency, the combustion temperature rose to approximately 820 °C. This temperature level was maintained to run the fifth experiment to the end. After the fifth experiment was finished, the system had to be partially disassembled in order to repair the damage to the screw conveyor of the small fuel tank. The necessary repairs and conversions are described in more detail in Section 5.2. In Figure 5.13 this can be seen at a time of approximately 45 h. Switching to the screw conveyor of the big fuel tank resulted in incomplete combustion for a short time, which can be seen in Figure 5.14 from the concentrations of the flue gas measurement.

As in the fourth experiment, no catalytic activity could be determined with the micro-scale test-rig using the WGSR after none of the five days. Figure 5.15 shows SEM images of cross-sections of Na-feldspar. The images (a), (b) and (c) show three different magnifications. There are no clear visualizations of layer formation on the images of the SEM analysis.

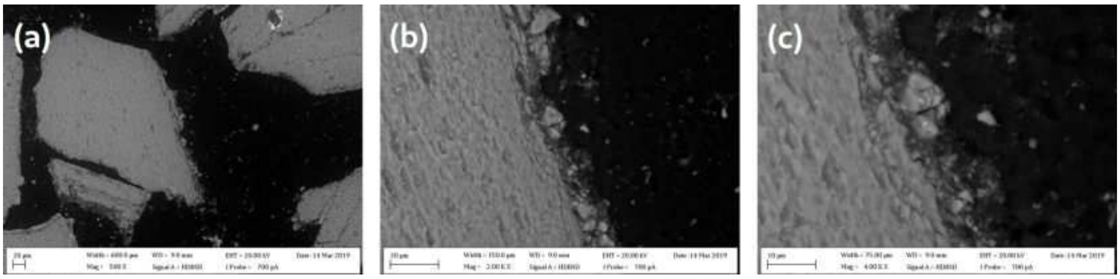

Figure 5.15: *Different magnifications of Na-feldspar of the fifth experiment, after a fuel supply of* 50 h.

Like in the fourth experiment, line scans with elemental mapping of the bed material were carried out for further investigation. Figure 5.16 shows a bed material sample of Na-feldspar. The arrangement of the two lines *Line Data 18* and *Line Data 19* are marked in Figure 5.16.

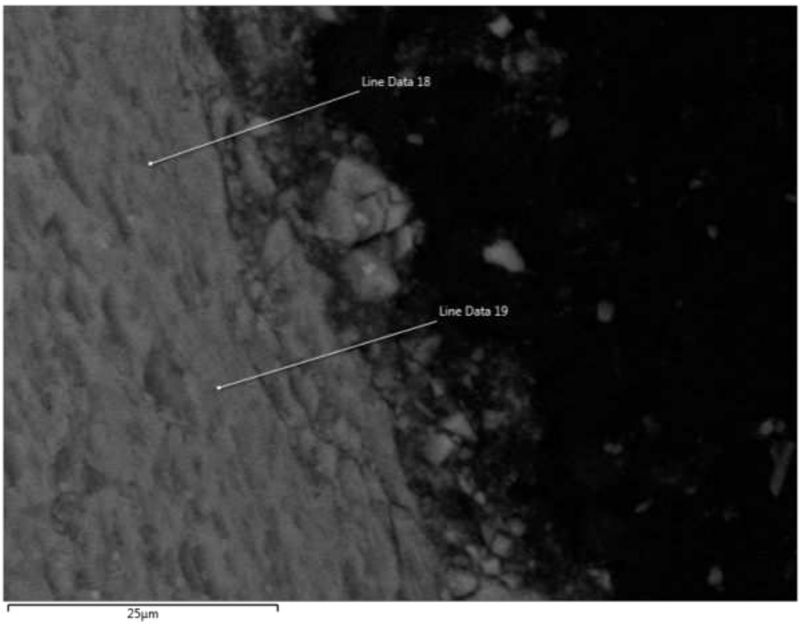

Figure 5.16: *Arrangement of the lines on the polished surface of the bed material samples of Na-feldspar.*

Representative for the line scans of Na-feldspar, Figure 5.17 shows the line scan of *Line Data 19* after 50 h of fuel supply. The entire length of *Line Data 19* is shown in Figure 5.17. Compared to the line scan of quartz shown in Figure 5.12, Figure 5.17 shows that despite the long fuel supply of 50 h and over 34 kg of total amount of fuel, no meaningful layer formation can be determined.

The flue ash was removed from the cyclone after each day of the experiment. Over the entire duration of the fifth experiment, 327.7 g of ashes were separated in the cyclone. This

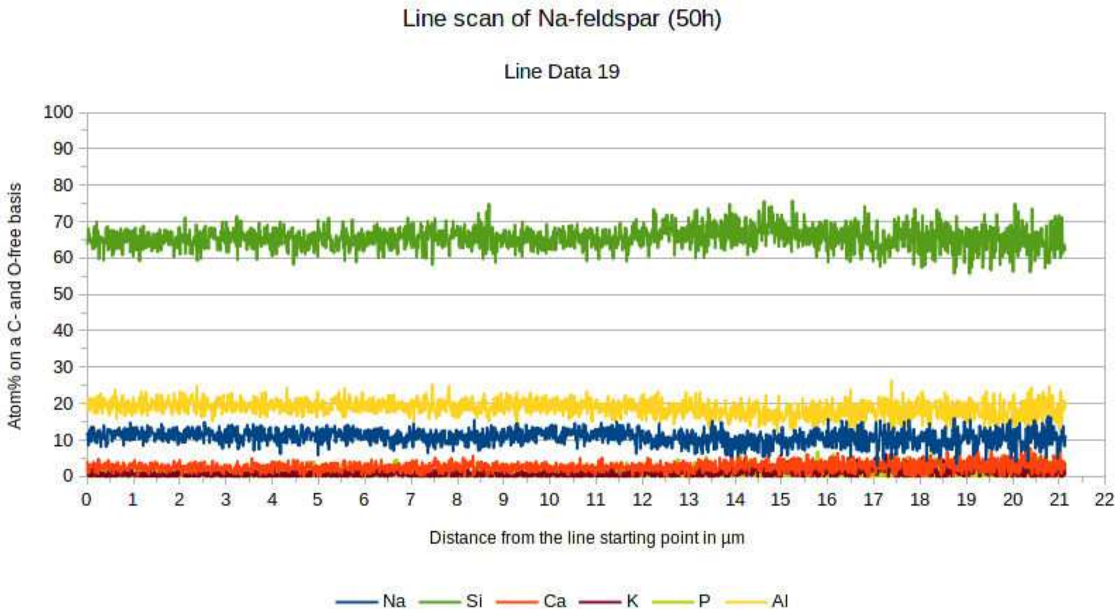

Figure 5.17: *Line scan in atomic percentage on a carbon-free and oxygen-free basis depending on the starting point of Line Data 19, for Na-feldspar after* 50 h *of fuel supply.*

weight corresponds to 0.96% of the total weight of the bark pellets that were burned in this experiment. Assuming the ash content of 3.46% of the fuel, calculated in Subsection 4.1.2, the remaining 2.5% of the ash should have participated in interaction with the bed material. This 2.5% ash result in a theoretically weight of 0.85 kg of ash for the total amount of 34.1 kg of the burned fuel. The separation efficiency of the cyclone is not taken into account in this calculation. Also the amount of ash that accumulates, for example, on the walls inside the testing plant is also unknown.

5.1.6 Sixth experiment (long-term experiment - cristobalite)

The sixth experiment represents the first experiment that was carried out with the modified screw conveyor and the modified downpipe of the small fuel tank. The sixth experiment ran under the same conditions and at the same specifications as the fifth experiment. However, as in the first two experiments, cristobalite was used as bed material. The amount of bed material and the type of fuel correspond to those of the fifth experiment. Only the specification for the combustion temperature was slightly increased at 770 °C, because this temperature was easier to maintain. Figure 5.18 shows the temperatures over the time of the sixth experiment.

In the sixth experiment, all the findings and the knowledge gathered from the previous experiments were incorporated. As shown in Figure 5.18, a very constant and trouble-free operation at constant temperatures was possible. The volume flow of the fluidization medium was increased slightly compared to the fifth experiment. On the one hand, this resulted in more heat being removed from the reactor, but on the other hand, it ensured stoichiometric complete combustion. This resulted in a complete combustion of the fuel in which hardly any carbon monoxide concentrations could be measured in the flue gas. Figure 5.19 shows the measured flue gas concentrations.

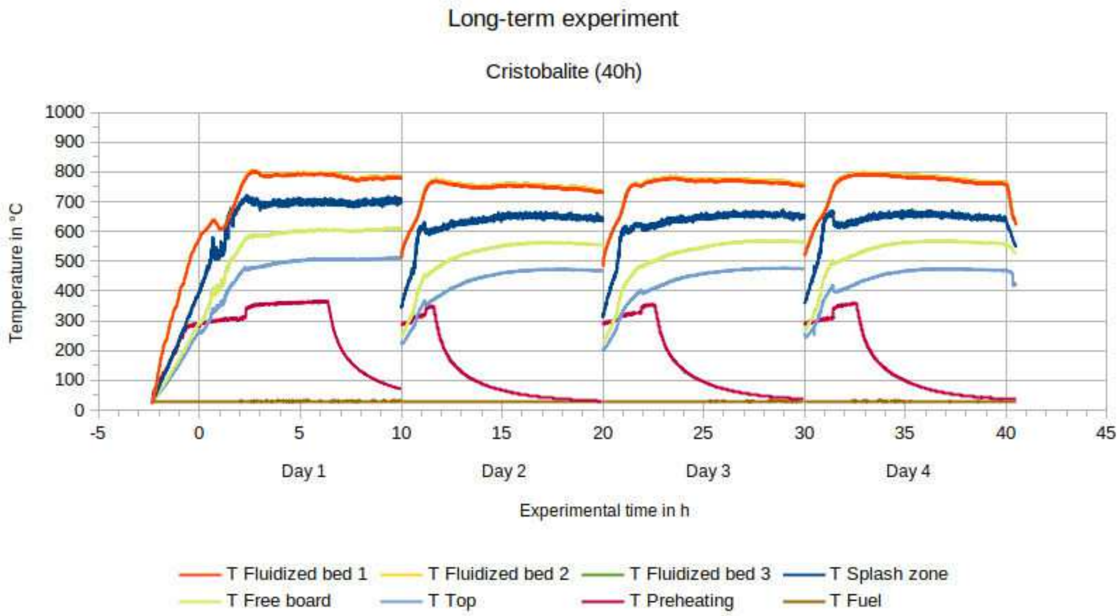

Figure 5.18: *Temperature curves over the time of the sixth experiment with cristobalite.*

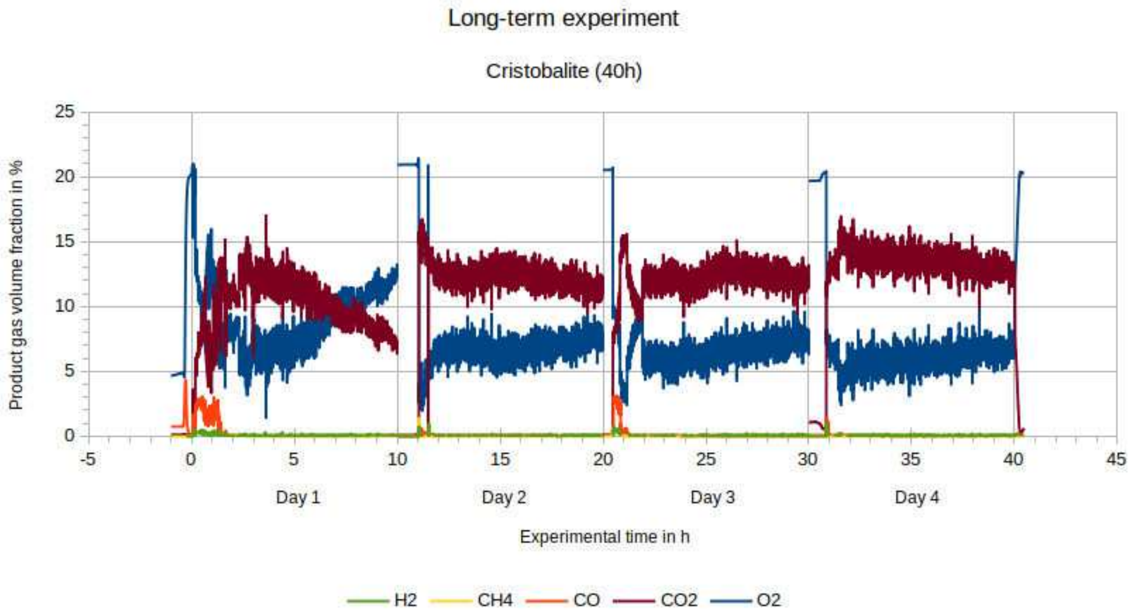

Figure 5.19: *Flue gas volume fraction over time of the sixth experiment with cristobalite.*

As with the fifth experiment, samples of 150 g of the bed material were taken after each day of the experiment. These were examined for their catalytic activity in the micro-scale test-rig. In addition to examining the bed material on the micro-scale test-rig, bed material samples were examined with the SEM. Figure 5.20 shows SEM images of cross sections of cristobalite at different magnifications.

As in the previous SEM analyzes, this also confirms the results of the kinetic experiments

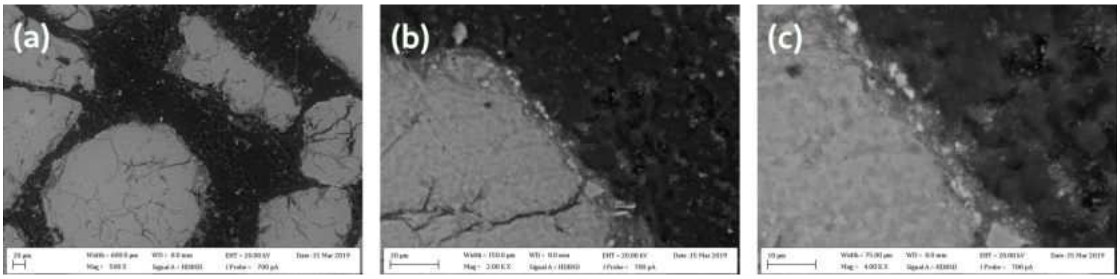

Figure 5.20: *Different magnifications of cristobalite of the sixth experiment, after a fuel supply of* 40 h.

on the micro-scale test-rig. The SEM analyzes show, that there are no clear visualizations of layer formation on the images. Figure 5.21 shows the polished particle surface of the bed material sample of cristobalite.

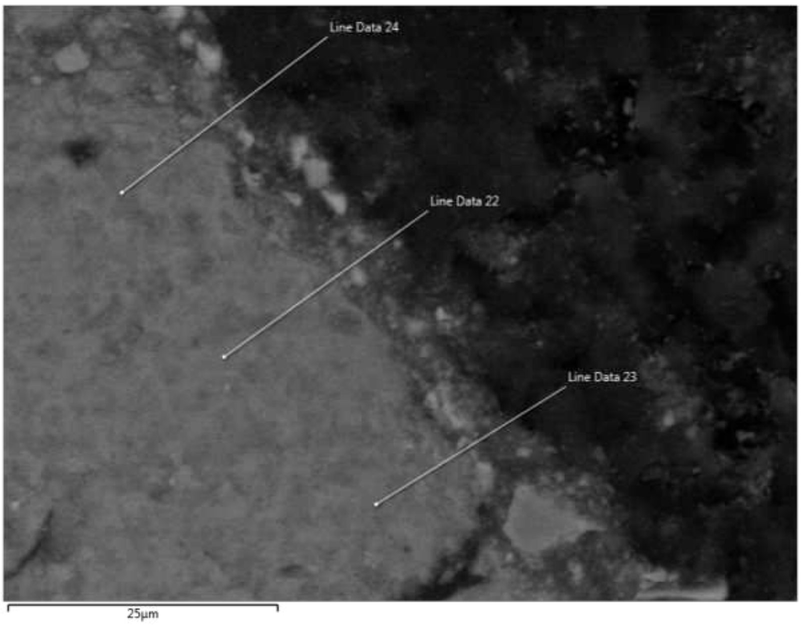

Figure 5.21: *Arrangement of the lines on the polished surface of the bed material samples of cristobalite with a magnification of 4,000.*

Representative for the line scans of cristobalite, Figure 5.22 shows the line scan in atomic percentage on a carbon-free and oxygen-free basis of *Line Data 22* after 40 h of fuel supply. For better visualization, the line scan does not show the scan of the entire length, but only a section from 8 µm to 22 µm. A slight decrease in silicon and a simultaneous increase in the remaining atoms, especially Ca can be seen at a distance of approximately 14 µm. Like the line scan of quartz from the fourth experiment, shown in Figure 5.12, this indicates an initiation of layer formation.

After no clearly catalytic activity could be detected on the micro-scale test-rig after the fourth day, it was decided to stop the sixth experiment.

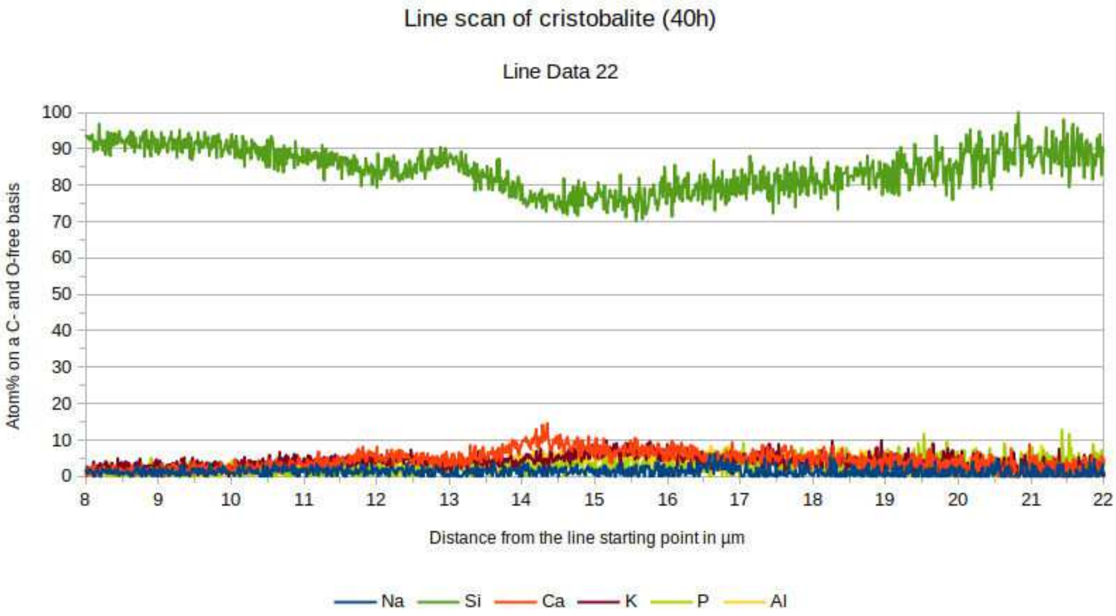

Figure 5.22: *Line scan in atomic percentage on a carbon-free and oxygen-free basis depending on the starting point of Line Data 22, for cristobalite after* 40 h *of fuel supply.*

5.1.7 Summary of the knowledge gained from the individual experiments

This section is intended to provide a brief summary of the findings observed and obtained during the experiments regarding the operational management of the fluidized bed system.

- **Design limitation of the system:**
  - During long-term experiments, condensate can build up in the filter, since the pipe for the extraction of the flue gas is not sufficiently thermally insulated.
  - The bypass for flue gas measurement should be installed behind the cyclone. In the current state of the testing plant this leads to increased ash deposits and clogging of the filter.
- **Fuel:**
  - The gear ratios of the two screw conveyor gears are not optimally geared to each other. It is not possible to achieve a delivery rate in the range between approximately 13 g/min and approximately 15 g/min with the existing configuration.
  - A high fuel supply tends to lead to higher combustion temperatures, a low fuel supply tends to result in lower combustion temperatures.
  - According to the observations and personal assessment, the volume flow of the fluidization medium has a far greater influence than the amount of fuel supply on the combustion temperatures.
- **Bed material:**
  - Emptying the bed material after each experiment have shown, that due to the current design and the current dimensions of the testing plant, a lot of the bed material is not involved in the interaction with the fuel.

  - With the current design and the current dimensions of the reactor, it turned out, that the testing plant can be operated with a quantity of approximately 5.5 kg of bed material under very constant operating parameters.
  - When using less bed material, it has been shown that constant operation of the system in the current configuration is very difficult.
  - A lot of bed material, leads to a relatively *sluggish* reacting system. Changes in the amount of fuel supply lead to a change in the operational management only after a significant delay. The system tends to overshoot.

- **Fluidization:**
  - The temperature of the preheating of the fluidization medium has hardly any influence on the combustion in the fluidized bed.
  - The experiments have shown that the achievable combustion temperatures are mainly dependent on the volume flow of the fluidization.
  - With very high volume flows of fluidization, a lot of heat is removed from the reactor and complete combustion takes place.
  - If the fluidization rates are too high, particularly when using quartz as bed material, small particles are pneumatically transported. However, these can be separated in the cyclone, together with the ash.
  - Low fluidization rates lead to less heat dissipation. If the fluidization is too low incomplete combustion can occur, which leads to increased concentrations of CO, CH_4 and above all, significantly higher soot formation.
  - Low fluidization rates lead to increased soot formation, which can quickly clog the flue gas measurement filter.

A large number of observations and experiences about the controlled operation of the testing plant could be collected by carrying out the experiments. In the following a personal recommendation, based on these observations and experiences of the experiments, should be given. Some of these recommendations are based on experiences and modifications, which are going to explained in more detail in Section 5.2. These recommendations are of course dependent on the fuel and are therefore primarily valid for bark pellets.

Recommended operating parameters

These recommendations refer to the condition of the testing plant in which the experiments were carried out. Modifications to the bench scale fluidized bed pilot plant may require changed operating parameters.

- **Miscellaneous:**
  - The duration of the experiment should be as long as possible so that the bed material can interact with the ash of the fuel for a sufficiently long time. A fuel supply of more than 50 h should be aimed for.
  - If possible, the measurement of the flue gas should only be started after the operating temperature for burning the fuel has been reached. This can prevent premature clogging of the filter and the measuring line.

  - The separated ash from the cyclone should be emptied after each day.
  - The filter of the measuring line should be cleaned after every day and the glass wool should be changed after every day of fuel supply.
  - After every experiment the measurement line should get cleaned by using acetone or other volatile substances.
  - The two screw conveyors should be cleaned at regular intervals to prevent the screw conveyors from getting stuck.
  - The inspection glass should be cleaned after each experiment.
  - In order to prevent condensation on the measuring lines, these should be heated.

- **Fuel:**
  - With regard to the cooling of the electric motor, it is better to run the screw conveyor of the small fuel tank at full load than to operate the screw conveyor of the big fuel tank at low speeds.
  - The small fuel tank should be completely filled before each day to ensure that enough pellets are available for the full load operation of the screw conveyor for more than 10 h hours of fuel supply.

- **Bed material:**
  - In order to keep operations as constant as possible, a quantity of approximately 5.5 kg of bed material should be used.
  - Cristobalite or quartz should be used, since these two bed materials showed a higher tendency to layer formation in the investigations at the SEM by line scans compared to Na-feldspar.

- **Fluidization:**
  - The fluidization rate should be kept as low as possible during operation. As a result, less heat is removed from the reactor and it is possible to supply fuel via the small screw conveyor.
  - A fluidization rate of approximately 65 l/min to 90 l/min should be set. These values refer to standard conditions, i.e. at a temperature of 273.15 K and a pressure of 1.013 25 bar.
  - This fluidization rate should also be observed during heat-up phase.
  - In order to keep the abrasion as low as possible, the fluidization rate should be set to 40 l/min during cool-down phase. These values refer to standard conditions, i.e. at a temperature of 273.15 K and a pressure of 1.013 25 bar.
  - With this fluidization rate and the above-mentioned fuel delivery rate, combustion temperatures of approximately 770 °C should be reachable.

5.2 Modifications of the bench scale fluidized bed pilot plant

As already mentioned in the description of the individual experiments, there were some complications that restricted the continuous operation of the testing plant. Some modifications to the testing plant were already carried out during the experiments. The following section describes these modifications and is intended to provide suggestions for detailed improvements so that smooth operation of the bench scale fluidized bed pilot plant can be guaranteed.

5.2.1 Screw conveyor

The screw conveyors have to transport the pellets under controlled frequencies from the fuel tanks to the combustion chamber.
As mentioned in 5.1.5 the screw conveyor of the small fuel tank stopped working on the fifth day of the first long-term experiment after about 45 h of continuously conveying pellets. After disassemble the whole small fuel tank and deconstruct the screw conveyor the reason could be identified. Obvious the raised pellets compacting as strong as the friction between the screw conveyor and the pipe wall was getting too strong. Possibly because of the two installed transmissions located behind the electric motor, there was enough torque available to block the screw conveyor irreparably. There was no chance to unlock the screw conveyor and get them perform again. As shown in Figure 5.23a, removal of the blocked screw conveyor out of the pipe was only possible by using a hydraulic press. Figure 5.23b shows the pellets, which were pressed into the spiral blade of the partially removed screw conveyor. Figure 5.23b and Figure 5.24b also show that the distances between the individual whorls of the spiral blade, coiled around the shaft of the screw conveyor, are smaller inside the fuel tank and increased inside the pipe. This should prevent the fuel from compacting. The compressed pellets from the spiral blade of the screw conveyor can be seen in Figure 5.23c.
After successfully detachment of the screw conveyor, the design of fuel supply was changed. The most important improvement is the new design of the delivery pipe of the small fuel tank. A new inspection glass was installed on top of the delivery pipe, which is fixed by screws on the sliced pipe. If the fuel supply where to be blocked again it would now be possible to remove the inspection glass to be able to clean the screw conveyor. It should not be necessary any more to detach the ball bearing, the gearbox and the electric motor and remove the whole screw conveyor. This is a huge advantage over the old construction. Luckily it was possible to repair the originally screw conveyor, so it could get installed again and no sophisticated modifications at the gearbox or the ball bearing had to be done. The new design is shown in Figure 5.24a and should prevent the screw conveyor from getting stuck again.
As shown in Figure 5.24b, now there is some free space between the screw conveyor and the inspection glass. It could be observed, that if the friction is getting to big, the pellets fall over the spiral of the screw conveyor instead of being crushed. This also prevents wedging of the pellets. The old design of the downpipe and the screw conveyor is shown in Figure 5.23d. Another big advantage of the new design is the possibility to refill either the big fuel tank or the small fuel tank during a running experiment. This is possible, because of two new ball valves installed at the fuel pipes. By closing one of the valves, the gas from the combustion chamber is not able to reach the fuel tank. However, if a fuel tank is refilled during operation, the purging with N_2 of the fuel tank that is to be refilled must be interrupted for safety reasons. If the ball valve is opened to refill the fuel tank when the fuel tank is under pressure, it can happen that fine fuel particles suddenly escape through the filler neck of the fuel tank.

(a) *Hydraulic press to remove the blocked screw conveyor.*

(b) *Pellets, pressed into the spiral blade of the screw conveyor.*

(c) *Pressed pellets, removed from the screw conveyor.*

(d) *Old design of the downpipe and the screw conveyor.*

Figure 5.23: *Disassemble of the screw conveyor of the small fuel tank, that got stuck due to compressed pellets, during the first long-term experiment.*

5.2.2 Heating shells

Since there is no combustion in the fluidized bed at low temperatures, the reactor must be brought up to operating temperature, before fuel delivery can begin. Therefore heating shells were used to heat up the combustion chamber and the bed material, without the need of using fuel. Only after the desired temperature has been reached, it is possible to start with the fuel supply. During heating up the reactor, it is important that the reactor is not getting heated up too quickly to prevent thermal stress and material fatigue. Heating shells are also intended to compensate the heat losses of the reactor and to ensure a constant temperature during the combustion.

During the experiments, a target temperature of at least 600 °C should be reached before

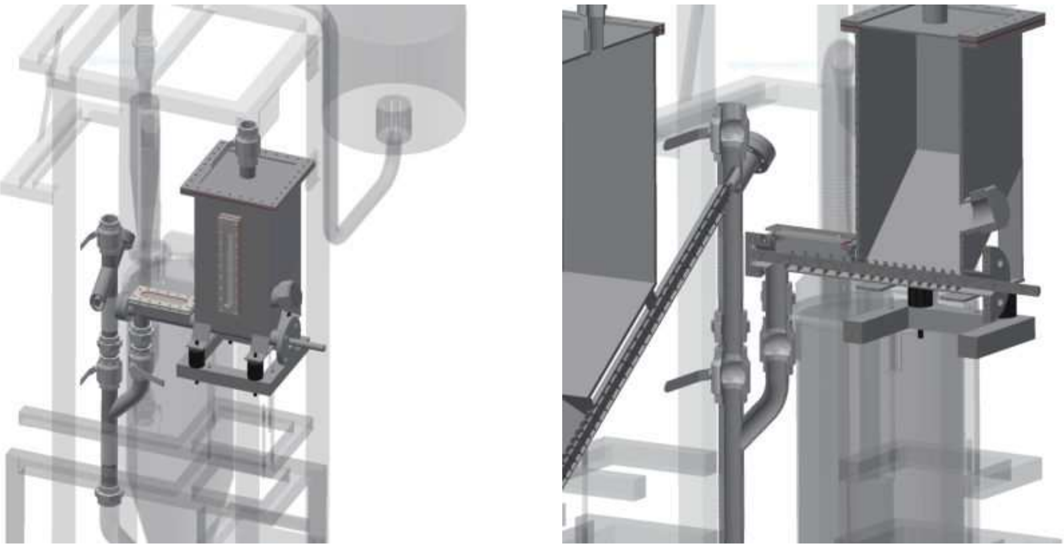

(a) *New design of the downpipes and the screw conveyor.*

(b) *Detailed, three quarter section of the new construction.*

Figure 5.24: *Improved implementation of the downpipes and the screw conveyor of the small fuel tank.*

starting the fuel feed. The heating rate was set at 30 °C per 10 min. It turned out, that it was not possible to use only the heating shells to reach a required temperature of at least 600 °C for the combustion chamber and the bed material. Although the reactor could be heated up at a constant heating rate during the experiments, the required temperature of at least 600 °C could not be reached. However the heating shells are designed for much higher temperatures and should easily reach this temperature. At a temperature of about 470 °C, it could be observed that the ground fault interrupter of the heating shells triggered reproducibly. Higher temperatures could not be reached with the heating shells.

The heating shells have their own electrical fuses and therefore they are protected by the rest of the system. However the fuse of the heating shells was not triggered always, but the ground fault interrupter of the entire system. As a result, the entire system was without electricity and therefore no fuel could be delivered by the screw conveyors.

Therefore from this point on, the heating shells for the reactor were switched off and fuel was used to further heat up the bench scale fluidized bed pilot plant. Due the use of fuel for heating up, there are some unwanted side effects and problems with the inspection glass, the measurement line and the filter, which are described in more detail in Subsection 5.2.6 and in Subsection 5.2.7.

The problems with the heating shells could only be solved after all the experiments had been carried out on the system. A possible defect could only be found after dismantling the thermal insulation of the cylindrical reactor and removing the heating shells. However, the exact origin of the problem could not be clearly identified. Maybe there was a short circuit between the thermal insulation of the system and the electrical power connections of the heating shells. The system is insulated with glass wool. The glass wool is held in shape by a thin aluminium foil, which also protects against external damage. The heating of the system led to a slight expansion of the components, which perhaps caused the short circuit between the aluminium foil of the thermal insulation and the electrical power connectors. The entire system is sufficiently grounded, which would explain the triggering of the ground

fault interrupter.
Another problem could have occurred directly on one of the two lower heating shells, which are arranged around the combustion chamber. Due to the arrangement of the measuring elements, which protrude through the thermal insulation into the combustion chamber of the testing plant, the heating shells had to be cut. This could also result in a short circuit between the wire mesh inside of the heating shell and the reactor wall or a measuring element. After no damage was visible by visual inspection, the heating shells and the area between the heating shells and the reactor were better insulated. Since the heating shells were insulated and installed again, it was possible to use the heating shells as originally intended. From now on, it is possible to achieve the required heating temperatures in the heating phase and during operation.

5.2.3 Electric motors, gearboxes and frequency converters

The two screw conveyors are each driven by an electric motor. One or more gearboxes for reduction can be attached between the electric motor and the screw conveyor. With regard to the variety of fuels, this ensures that higher or lower fuel masses can be conveyed into the combustion chamber from the fuel tanks. As explained in more detail in Subsection 4.3.1, the coordination of the two gear ratios, which were used for the experiments carried out in this master thesis is not optimally resolved. At a maximum delivery frequency of 50 Hz, the screw conveyor of the small fuel tank did not reach the minimum delivery rate of the screw conveyor of the big fuel tank at a frequency of 10 Hz.
The speed of the two electric motors can be set using frequency converters. The maximum frequency is 50 Hz and is determined by the mains frequency of the electricity in European electricity networks. Theoretically, the minimum frequency is not limited by the frequency converter. However, the experiments have shown that the electric motors overheat at low frequencies. The reason for this is the type of the installed electric motors. Cooling fins are attached to the outer housing of the electric motor, which emit the heat generated by the air flow from a fan, to the environment. The fan, which provides the air flow, is rigidly connected to the shaft of the electric motor. This has the disadvantage that the lower the speed of the electric motor, the lower the speed of the fan and the lower the cooling effect due to the air flow passing through the cooling fins.
During the experiments it could be observed, that at frequencies below 10 Hz the electric motors become very hot due to the reduced cooling. For this reason, the frequency inverters have been reprogrammed so that frequencies below 10 Hz cannot be set. The measure turned out to be useful because it effectively prevented overheating of the electric motors.

5.2.4 Ball bearing

In order to keep the friction losses as low as possible, the two screw conveyors are supported by ball bearings.
Because of the horizontal assembly position of the screw conveyor, there are some problems with the ball bearings. As shown in Figure 5.25a, some small particles of the fuel and some bed material could get into the ball bearing. Before performing the individual experiments, the different bed materials have to get into the combustion chamber. These were filled into the bench scale fluidized bed pilot plant via the ball valve at the upper end of the downpipe, located at the top of the feed pipe of the big fuel tank. As it turned out after the disassembling of the small fuel tank and the screw conveyor, bed material could get into the ball bearing

in this way.
This issue only affects the ball bearing, which is located at the end of the screw conveyor located at the conveying direction. Also only the ball bearing of the small fuel tank is affected by the issue, because the screw conveyor of the big fuel tank is not installed horizontally. The fuel delivery pipe of the big fuel tank is inclined at an angle of about 45°. So the fuel pellets and the small particles fall down into the fuel supply pipe of the reactor, before they could reach the ball bearing.

(a) *Due to the arrangement of the screw conveyor, bed material and fuel entered the cage of the ball bearing.*

(b) *Illustration of the amount of bed material and fuel that has accumulated in the flange of the ball bearing.*

Figure 5.25: *Problems caused by bed material and fuel, which gets into the cage of the ball bearing.*

Unfortunately this issue still partially exists, even with the new design of the small screw conveyor, shown in Figure 5.24a. Because of the new designed fuel supply pipes and the use of a Y-branch pipe, added bed material will not pass the small screw conveyor any more. Grind pellets are the only particles which can reach the ball bearing. In order to prevent fuel particles of the pellets from getting into the ball bearing, the screw conveyor would have to be arranged at a steeper angle, as with the big fuel tank. However, this would have required major and more extensive modifications to the bench scale fluidized bed pilot plant.

5.2.5 Connecting pieces for emptying the fuel tanks

Figure 5.24 shows another small detail improvement on the fuel tanks. In order to disassemble the small fuel tank, the pellets still contained inside the tank had to be removed. This was done with a vacuum cleaner by vacuuming the pellets through the top ball valve of the fuel tank. Not all pellets could be extracted in this way. The remaining pellets could only be removed by complex disassembling of the entire cover panel of the fuel tank.
Because of this, in the course of the modifications on the testing plant, a new connecting piece for emtying the fuel was welded onto each of the two fuel tanks. These connecting pieces are located in the lower area of the fuel tanks. Each of the two sockets is provided with a thread, which means that they can be sealed airtight by a bolted joint. This makes it possible to extract fuel quickly and easily from the fuel tanks.

5.2.6 Inspection glass

The inspection glass at the top of the reactor is not necessary for a smooth operation of the testing plant. However, sometimes it is very useful for visual control to see what is going on inside of the reactor.

Because of the combustion under high temperatures and the resulting fine ash particles, the ash and also some small particles of bed material settle down on the inspection glass. Gasification of the fuel can occur during the heat-up phase. The resulting tars also settle down on the inspection glass. Although there is a flushing with N_2 to prevent the inspection glass of getting dirty, it is not possible to fully hold back the particles. Especially during heating up phase with fuel, where there is no complete combustion, the glass is getting dirty very fast. So there is no possibility to see what happen inside the combustion chamber. The main problem with the existing flushing is the pressure drop of the existing feed line. There is only one N_2 feed line, which had to supply the inspection glass flushing and also had to supply both of the fuel tanks. The whole feed line is supported by a pressure of 2 bar. First of all, the float-type flow meter of the small fuel tank and the float-type flow meter of the inspection glass flushing were swapped, because the maximum flow rate of the float-type float meter of the small fuel tank was higher than the maximum flow rate of the float-type float meter of the inspection glass flushing. Also it it is not necessary for the small fuel tank to get high flow rates. The current used solution is shown in Figure 5.26.

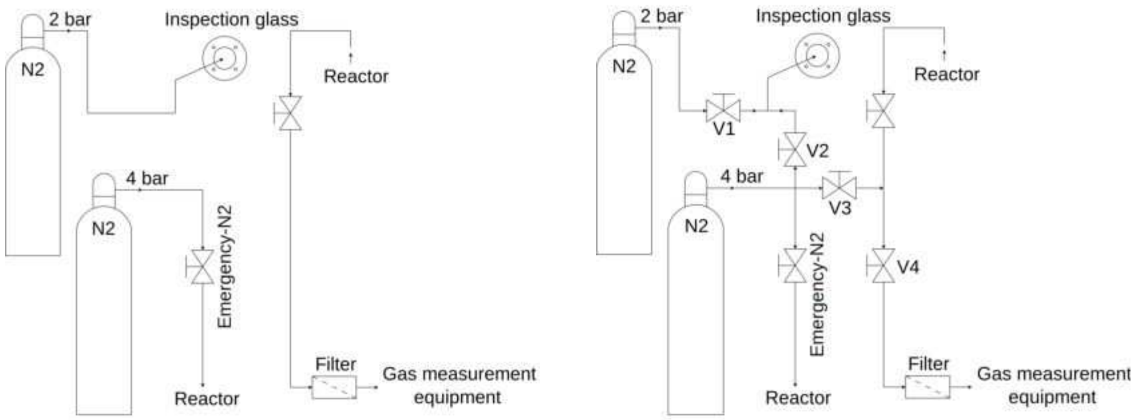

(a) *Original flow diagram of the original nitrogen pipes.*

(b) *Flow diagram of the modified nitrogen pipes.*

Figure 5.26: *Flow diagram of the nitrogen pipes, as the current solution to prevent the inspection glass of getting dirty.*

The N_2 feed line for the emergency stop was used to keep the inspection glass clean during heating up phase. As shown in the flow diagram 5.26a the N_2 feed line for the emergency stop is supported by a pressure of 4 bar. By mounting some new valves, now it is possible to switch the N_2 supply and use the higher pressure of 4 bar for the flushing of the inspection glass. These modifications can be seen in Figure 5.26b. After the desired temperature for combustion is reached and a constant combustion adjusts, usually the amount of tar reduces and it is possible to switch to lower pressure of 2 bar for flushing the inspection glass. The function of the emergency stop is not affected by this modification. As mention, this is just a temporary solution. Because of the new valves and new mounted feed lines, the pressure drop is still too high. After every finished experiment it is necessary to clean the inspection glass by using acetone for example.

The design of the existing inspection glass flushing corresponds to a pipe directed towards the inspection glass and is constructional acceptable designed. Only the pressure or the strength of the flushing is not sufficient to prevent the inspection glass from becoming dirty. A better solution would be to add a ball valve between the inspection glass and the reactor. The additional ball valve will only opened, when there is a visual inspection of the fluidized bed. The ball valve remains closed during operation and thus prevents the inspection glass from getting dirty.

5.2.7 Gas measurement

Flue gas measurement line

In order to be able to measure the composition of the flue gas, the gas measurement equipment explained in Subsection 4.4.1 was used. The measurement is carried out via a bypass through a measuring line, which branches off a partial volume flow of the flue gas, located at the upper end of the testing plant near the cyclone.

Due to the problems with the heating shells, which have already been described in Subsection 5.2.2, it was necessary to switch to fuel supply during heating up, before the testing plant has reached operating temperature. By using fuel during heating up phase, the combustion is not steady. Incomplete combustion leads to increased ash particles and tar. Because of continuous measurement of the flue gas, also during heating up phase, unburned particles will get into the measurement line. As a result, the ash, the tar and unburned particles will get stuck inside the measurement line and the free flow diameter for suck out is getting smaller. It was necessary to clean the measurement line after every experiment.

As shown in Figure 5.26b, due to the new arrangement of the pipes, it is possible to clean the measurement line by using N_2. By opening the valve *V3* and closing the valve *V4* the ash particles and possibly some fine particles of bed material are getting blown back into the reactor.

Another problem that could be observed on the measuring line is condensation. The measuring line runs along the steel frame of the testing plant. Since the measuring line is not insulated, condensation occurred. The condensate collected in the filter, which is located between the measuring line and the gas measuring device. The measuring line between the filter and the gas measuring device was equipped with a heating hose, whereby no condensate could form at least after the filter.

A better solution would be to install the bypass for flue gas measurement behind the cyclone. In the current arrangement, this results in increased ash deposits and a faster clogging of the filter. Attaching the bypass behind the cyclone would not give any falsified measurements of the flue gas composition, but would prevent ash accumulation in the filter.

It should be mentioned, that after every experiment the measurement line should also get cleaned by using acetone or other volatile substances.

Flue gas filter

Before the extracted flue gas reaches the gas measuring device, it is passed through a filter to prevent ash particles from getting into the gas measuring device. During the experiments, the filter was located between the measurement line of the testing plant and the heating hose leading to the gas measuring device.

The filter consists of a cylindrical, screwable casing in which there is a fine-meshed wire mesh. In front of the wire mesh, the filter is filled with glass wool. The glass wool is permeable to the extracted flue gas, but ash particles cannot pass through the glass wool and therefore

remain in the filter.
The experiments have shown, that the premature fuel supply during the heat-up phase leads to increase the ash and tar formation. This led in particular to an increased ash load on the filter. For this reason, after each day of an experiment, the filter was cleaned and the glass wool was replaced with new one. Figure 5.27 shows the load on the filter after one day (10 h) of fuel supply.

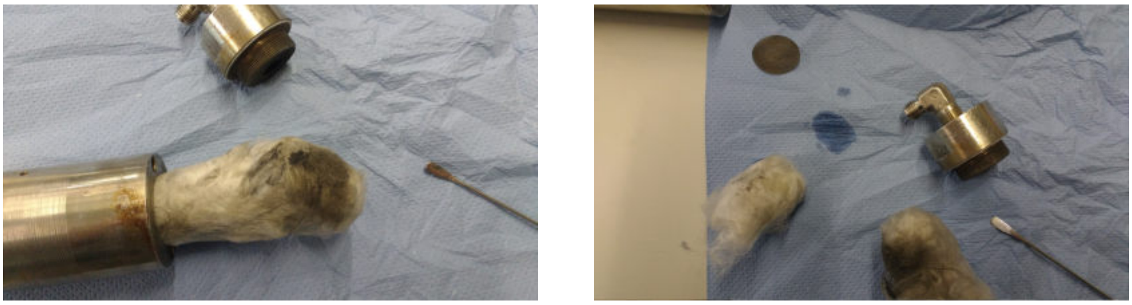

(a) *Glass wool enriched with ash particles.*

(b) *Disassembled filter with wire mesh and glass wool.*

Figure 5.27: *Problems caused by ash particles from incomplete combustion and condensation in the filter.*

During every experiments the filter works reliable and ash particles were not able to pass the glass wool, however it could be observed that also condensation settles down inside the filter. It was observed that the condensate remained mainly in the foremost part of the fine filter wool and did not reach the fine wire mesh at the rear end of the filter. Figure 5.27b shows a wet spot on the cloth underneath the disassembled filter, which comes from condensation from the filter. As a temporary solution, the filter was wrapped with a flexible heating tape so that it could be heated from the outside. This successfully prevents condensate in the filter.

5.2.8 Bottom of the reactor

The problem of the large amount of bed material has already been discussed in the previous sections. The flange which is screwed to the lower end of the reactor has already been explained in Section 4.3. Figure 4.5a shows a 3D rendering of the bottom of the reactor as it was used during the experiments. By performing the experiments, some disadvantages of the flange were recognized, which will be explained in more detail in this subsection.

Thermal insulation

At the beginning of the experiments, the entire reactor was encased in a coherent thermal insulation. It was assumed, that the flange at the lower end of the reactor did not have to be removed. Not even between the individual experiments. However, already the first experiment showed that the bed material could not be completely emptied via the ball valve at the lower end of the flange.
For checking, the bed material was weighed before each experiment was performed and after each experiment was completed. As it turned out, bed material got into the space between the reactor wall and the funnel. This bed material does not participate in the interaction with the fuel. There is no way to empty it through the ball valve at the lower end of the

flange. In order to be able to remove the remaining bed material, the thermal insulation had to be cut open. As a result, the thermal insulation had to be attached to the testing plant again before each experiment could be performed.
Figure 5.28a shows the cut thermal insulation at the lower end of the testing plant. The flange is already loose and is just being removed. The unused bed material which has accumulated in the interstices and has not participated in the interaction with the fuel is clearly visible.

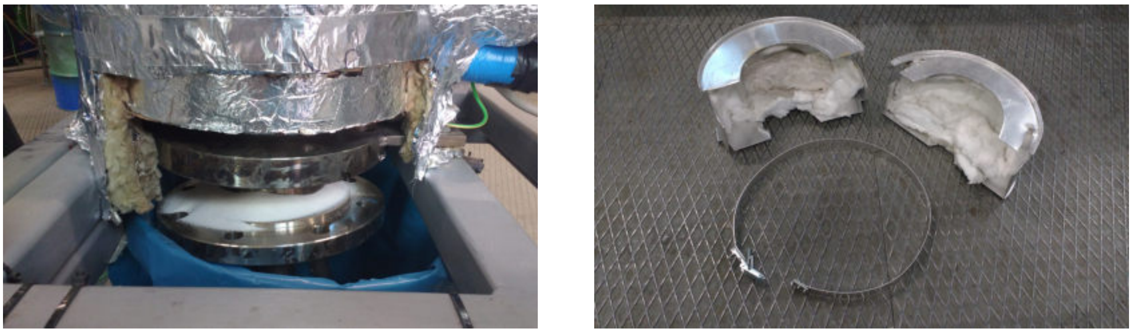

(a) *Cut thermal insulation at the lower end of the testing plant.*

(b) *Removable thermal insulation to make it easier to remove the flange.*

Figure 5.28: *Newly made and removable thermal insulation to simplify the dismantling of the flange.*

As cutting the thermal insulation was not a suitable method, a removable thermal insulation was made. This was made of aluminum sheet and essentially consists of two half-shells that enclose the lower flange. Inside, the two half-shells are lined with insulating material, to keep thermal losses as low as possible during operation. The two shells are held together in the assembled state by a riveted clamping device. Figure 5.28b shows the detachable thermal insulation in a dismantled state.
The bottom of the reactor is designed, so that a pipe is welded to the underside of the funnel. However, this pipe is not welded to the base of the column. For this reason, bed material not only gets between the reactor wall and the welded pipe under the funnel, but also into the cavity behind this pipe. In Figure 5.29a the maximum volume that can be taken up by the bed material is highlighted in yellow.

Dead volume of the flange

The design of the flange as well as the type and the design of the fluidization, which is carried out via two pipes protruding into the reactor, means that a lot of bed material has to be used to operate the system. The experiments have shown, that more than 5 kg of bed material is required for constant operation. As explained in more detail in Subsections 5.1.1 to 5.1.6, this amount was determined empirically and was also based in particular on the geometrical arrangement of the sensors for measuring the temperatures of the bed material.
After all experiments were carried out, the exact dimensions of the reactor and the flange could be taken. This allowed the volume, occupied by the bed material, to be calculated. Figure 5.29a shows the essential volumes that were used for the calculation.
The typical dead volume, meaning the volume of the bed material that did not take part in the interaction, was calculated with a total volume of 1.39 dm^3. In Figure 5.29a this corresponds to the area highlighted in red and blue. The volume up to the inlet of the second

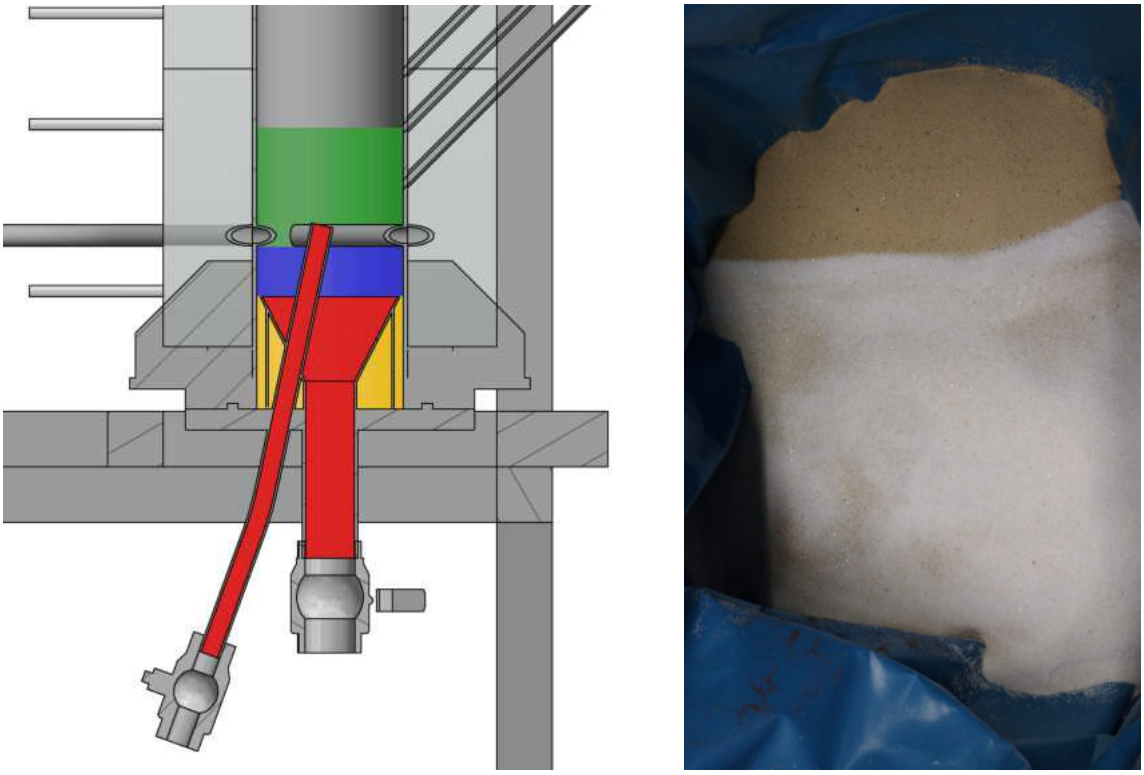

(a) *Dead volumes of the funnel and sampling (red), below the fluidization (blue) and below the funnel (yellow). Remaining filling volume of quartz, used in the fourth experiment (green).*

(b) *Color difference of the interacting, darker bed material and the much lighter bed material from the dead volume.*

Figure 5.29: *Implementation of the bottom of the reactor and the resulting high amount of bed material, which does not participate in the interaction with the fuel.*

temperature measuring line was calculated with 1.46 dm^3. In Figure 5.29a this corresponds to the area highlighted in green. The sum of both volumes results in a calculated total volume of 2.85 dm^3. This corresponds to the amount of 4.5 kg of quartz that was used in the fourth experiment and described in more detail in Subsection 5.1.4.

A check by multiplying the total volume of 2.85 dm^3 by the bulk density of quartz, the amount of bed material is calculated to be 4.56 kg. A back-calculation of the bulk density and the weighed quantity of 4.5 kg in the fourth experiment, resulted in a bulk volume of 2.81 dm^3. This volume coincides with the total volume of the bed material used in the fourth experiment, calculated from the dimensions of the testing plant. A value of 1600 $\mathrm{kg/m}^3$ [49] was used for the bulk density of the quartz. This density corresponds to the average bulk density of quartz with an average grain size distribution, such as used in the fourth experiment.

Based on this bulk density, it can be concluded that by multiplying by the calculated dead volume, approximately 2.23 kg bed material does not participate in the interaction. This value only refers to quartz as bed material.

The previously mentioned volume below the funnel, which is shown in yellow in Figure 5.29a, was not taken into account in the calculation. This volume represents the maximum possible volume under the funnel, which can theoretically be taken up by the bed material. It was not

possible to weigh the bed material that had accumulated there during the entire operation. Figure 5.29b shows the removed bed material after the second experiment, after 7 h of fuel supply. The illustration shows the color difference between the bed material that participated in the interaction with the fuel and the bed material that did not participate in the interaction with the fuel. Christobalite, which was in interaction with the fuel, is significantly darker than christobalite, which did not participate in the interaction.
However, the comparative analysis shows that the calculated volume corresponds very well to the weighed-in weight of the bed material. This is also confirmed by a visual inspection through the inspection glass at the top of the bench scale fluidized bed pilot plant.

New design of the flange

Figure 5.30a shows the bottom of the column as it was used during the experiments. Figure 5.30b shows a newly constructed bottom bottom of the column.

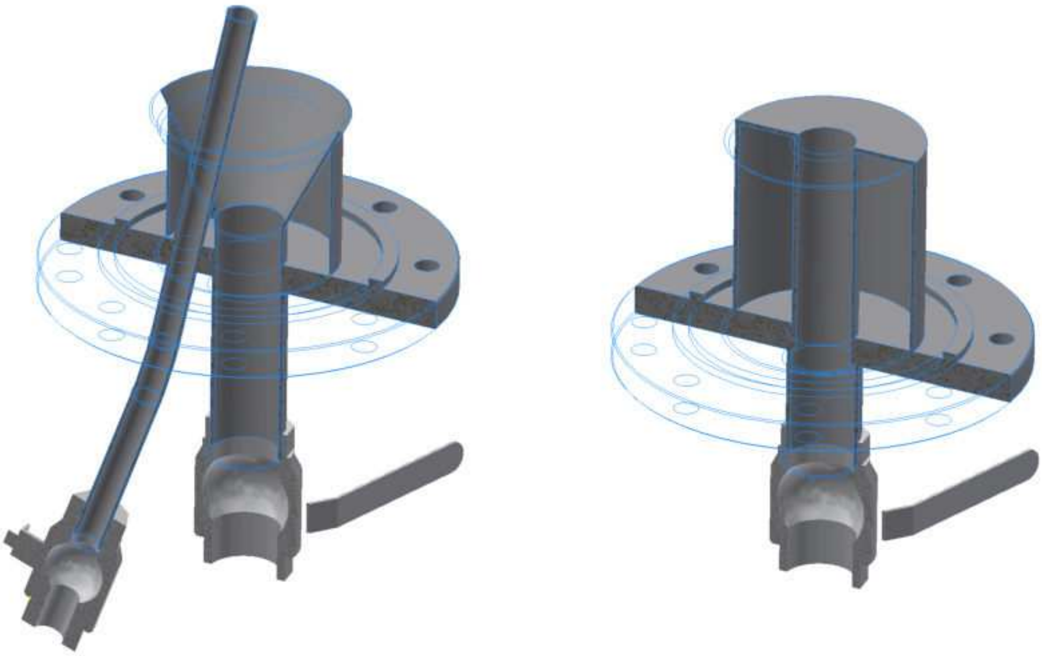

(a) *Half section through a 3D rendering of the flange used in the experiments.*

(b) *Half section through a 3D rendering of the newly designed flange.*

Figure 5.30: *Comparison of the bottom of the reactor used in the experiments and the newly designed bottom of the column.*

Special care was taken to keep the volume between the tubes for fluidization and the bottom of the column as small as possible. Since the experiments have shown that the current solution for taking bed material samples via ball valves is not sufficiently solved, a separate pipe for taking samples was not used for the new design of the flange. The length of the pipe for draining the entire bed material has also been significantly reduced. These measures are intended to keep the dead volume and thus the amount of bed material, that is not involved in the interaction with the fuel, as low as possible. Figure 5.31 shows a comparison in the installed state of the old and the new flange. The dead volume, which is shown in red, could be significantly reduced.

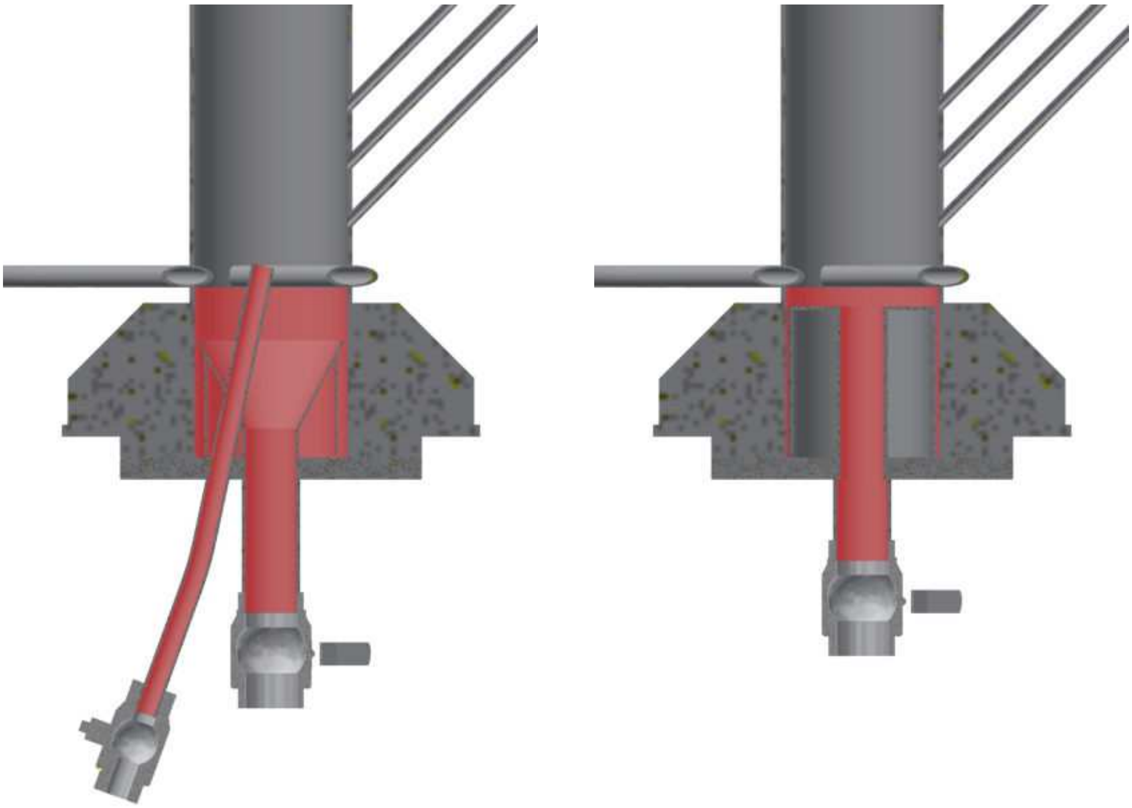

(a) *Dead volume of the bottom of the column used during the experiments.*

(b) *Dead volume of the newly designed bottom of the column.*

Figure 5.31: *3D rendering of different bottoms of the column and comparison of the dead volumes, highlighted in red.*

As shown in Figure 5.31, the dead volume cannot be completely prevented due to the design of the bottom of the column. A calculation of the dead volume with the new flange has shown that there is 0.89 dm^3 less dead volume compared to the previous construction. Multiplied by the previously mentioned bulk density of quartz, this corresponds to a weight of 1.42 kg. The new dead volume is thus calculated to be 0.50 dm^3, which corresponds to a weight of approximately 0.80 kg quartz. To achieve the same level of quartz as with the old design, about 3.14 kg bed material is required. That is about a third (31.3%) less than with the old design. In addition, the dead volume shown in yellow in Figure 5.29a can be completely avoided with the new design of the flange. Therefore, care should be taken that both the outer tube and the inner tube are welded to the bottom of the column. This prevents bed material from getting into the cavity between the outer and inner walls of the bottom of the column. In order to completely prevent the dead volume, the reactor would have to be equipped with a perforated bottom, for example. This would require extensive modification of the existing testing plant. However, a simple sampling of the bed material would no longer be possible and would have to be realized in a much more complex way than in the current construction.

The individual volumes would have to be calculated by geometrically dividing the components into individual, rotationally symmetrical objects. Some volumes can only be determined by integral calculations. The 3D modeling of the individual components of the testing plant considerably simplify the calculation of the individual volumes. With the help of the CAD program, physical quantities such as the volume can be determined very quickly and very precisely. This is one of the great advantages that 3D modeling offers.

5.3 Calculation of characteristic parameters

This section gives an overview of the characteristic parameters of the testing plant.
Section 4.2 has already explained the calculation of the SMD d_{sv} in more detail.
The superficial velocity u_s is independent of the bed material and is calculated according to equation 2.17. Since the superficial velocity u_s is dependent on the volume flow $\dot{Q}$ of the fluidization rate, the superficial velocity u_s was calculated for different volume flows of the fluidization medium. During the experiments, *typical volume flows* $\dot{Q}_{typical}$ of approximately 90 l/min were used for fluidization. As shown in Table 5.1 of the overview of the experiments, the corresponding values for the *minimum fluidization rate* $\dot{Q}_{min}$ of 65 l/min and the *maximum fluidization rate* $\dot{Q}_{max}$ of 180 l/min are also given as a representative. These values refer to standard conditions, i.e. at a temperature of 273.15 K and a pressure of 1.013 25 bar.
The Archimedes number Ar is required to calculate the minimum fluidization velocity u_{mf}. This dimensionless quantity is determined according to equation 2.23 and depends on the dynamic viscosity μ of the fluidization medium. Since the dynamic viscosity μ changes depending on the temperature, all calculations for a temperature of 25 °C and a temperature of 800 °C are given. The temperature of 25 °C is chosen to represent the ambient temperature, i.e. the temperature when the system is not heated. As the temperatures fluctuated between experiments during operation, a value of 800 °C is given to represent the operating temperature. The minimum fluidization velocity u_{mf} is therefore also given for different temperatures. Since equation 2.22 for calculating the minimum fluidization velocity u_{mf} is only valid for Reynolds numbers in the range from 0.001 to 4,000, the Reynolds number Re must be checked according to equation 2.20. Since the Reynolds number Re also depends on the dynamic viscosity μ of the fluidization medium, the Reynolds number Re is also given for the two temperatures of 25 °C and 800 °C. However, since the Reynolds number Re is also a function of the superficial velocity u_s, the previously mentioned fluidization rates $\dot{Q}_{typical}$, $\dot{Q}_{min}$ and $\dot{Q}_{max}$ must also be taken into account.
The terminal velocity u_t is calculated according to equation 2.29. Depending on the area in which the Reynolds number Re is located, different calculation methods must be used to determine the terminal velocity u_t. These areas have already been explained in more detail in Subsection 2.6.3. Depending on the area, the calculation of the drag coefficient c_w also changes. The Reynolds number Re is calculated according to equation 2.30 and is given for the two temperatures of 25 °C and 800 °C. After the Reynolds numbers are in the transition area ($0.2 < Re < 1{,}000$), equation 2.35 was used to calculate the drag coefficient c_w. As explained in more detail in Subsection 2.6.3, the determination of the terminal velocity u_t is not explicitly possible. Iteration methods for approximation were used to calculate the terminal velocity u_t.
All calculated characteristic parameters of the fluidized bed are summarized in Table 5.3.
Based on the calculated values, it is possible to see the areas in which the testing plant was operated during the experiments. For better comparability, Table 5.2 shows the flow rates calculated from the characteristic velocities.

Table 5.2: *Minimum and maximum flow rates at the characteristic temperatures, calculated from the characteristic velocities in Table 5.3.*

Flow rate *	**Temp.**	**Bed material**		
		Quartz	**Na-feldspar**	**Cristobalite**
$\dot{Q}_{mf}$ in l/min	25 °C	120	30	37
	800 °C	52	12	15
$\dot{Q}_t$ in l/min	25 °C	2762	1321	1569
	800 °C	2752	932	1189

* Refer to standard conditions: 273.15 K and 1.013 25 bar

According to equation 2.17, it is possible to calculate the fluidization rate $\dot{Q}$ if the cross sectional area of the reactor A and the superficial velocity u_s are known.

$\dot{Q}_{mf}$ corresponds to the flow rate which is necessary to leave the area of the fixed bed operation and to reach the area of a fluidized bed. $\dot{Q}_t$ denotes the flow rate, which characterizes the upper end of the fluidized bed. If $\dot{Q}_t$ is exceeded, the particles are emptied of the fluidized bed. All calculated flow rates are given for the three different bed materials as well as for the two previously mentioned temperatures of 25 °C and 800 °C.

Based on the calculated flow rates, it can be confirmed that the testing plant was operated in a fluidized bed state at all times. This confirms the visual controls that were carried out during the experiments using the inspection glass.

During the fourth experiment, in which quartz was used as bed material, the system was operated sometimes at flow rates of less than 120 l/min. The calculations show that this flow rate at a temperature of 25 °C would have been too low to leave the area of the fixed bed operation. However, since these low flow rates only occured in the heated bed material at operating temperatures of more than 25 °C, the fuel was always burned in the area of the fluidized bed.

As explained in more detail in Subsection 2.8.2, stationary fluidized beds are operated with fluidization rates of approximately 5 to 15 times the minimum fluidization velocity u_{mf}. This also corresponds to the fluidization rates achieved in the experiments for cristobalite and for Na-feldspar, as shown in Table 5.1 in Section 5.1. However, the fluidization rates of the fourth experiment, in which quartz was used as bed material, should have been chosen higher. As explained in more detail in Subsection 5.1.4, higher fluidization rates would lead to a significantly higher discharge of heat and a hiher discharge of the fine particles of the bed material, which is why the testing plant was not operated at these high fluidization rates.

The values for $\dot{Q}_{mf}$ given in Table 5.2 are therefore to be regarded as recommendations, which should not be undercut in order not to operate the testing plant in the area of fixed bed operation. The calculated maximum fluidization rates $\dot{Q}_t$, at which the entire bed material would be discharged, cannot be achieved with the bench scale fluidized bed pilot plant and the type of fluidization used here through inlet nozzles.

Table 5.3: *Summary of the calculated characteristic parameters of the bench scale fluidized bed pilot plant.*

Calculated parameter	$\dot{Q}$ *	Temp.	Bed material Quartz	 Na-feldspar	 Cristobalite	Annotation
Particle characteristic						
d_{sv} in µm	-	-	434	215	249	-
Superficial velocity						
u_s in m/s	65 l/min	-	0.32	0.32	0.32	Independent of the temperature and the bed material
	90 l/min	-	0.44	0.44	0.44	
	180 l/min	-	0.89	0.89	0.89	
Minimum fluidization velocity						
Archimedes number Ar	-	25 °C	7358.19	877.69	1232.24	Independent of the flow rate
	-	800 °C	337.98	40.31	56.60	
Reynolds number Re	65 l/min	25 °C	8.91	4.41	5.11	$0.001 < Re < 4{,}000$
		800 °C	2.48	1.23	1.42	
	90 l/min	25 °C	12.34	6.11	7.08	
		800 °C	1.39	0.69	0.80	
	180 l/min	25 °C	27.68	12.22	14.16	
		800 °C	2.79	1.38	1.60	
u_{mf} in m/s	-	25 °C	0.15	0.04	0.05	Independent of the flow rate
	-	800 °C	0.06	0.02	0.02	
Terminal velocity						
Reynolds number Re	-	25 °C	96.38	22.82	31.40	$0.2 < Re < 1{,}000$
	-	800 °C	10.85	1.82	2.69	
Drag coefficient c_w	-	25 °C	1.06	2.29	1.88	Valid for the transition area
	-	800 °C	3.83	16.55	11.76	
u_t in m/s	-	25 °C	3.47	1.66	1.97	Calculation by iteration
	-	800 °C	3.46	1.17	1.49	

[*] Refer to standard conditions: 273.15 K and 1.013 25 bar

Chapter 6

Conclusion and Outlook

The experiments have shown that the new bench scale fluidized bed pilot plant is very well suited for burning biogenic solid fuels in the form of bark pellets. After initial difficulties, the fuel was burned very homogeneously and under controlled conditions, in the most constant possible operation. The flue gas measurements have confirmed that stoichiometric complete combustion occurred during operation. The flue gas measurement showed that, among the measured gases, the fuel was mainly oxidized to CO_2. Under constant operating conditions, other emissions such as CO, CH_4 or H_2 are hardly present in the exhaust gas. This confirms the fact, that the fluidized bed technology enables a very homogeneous and complete thermochemical conversion of the biogenic fuel. The experiments have shown, that the testing plant is also very well suited to be operated with different bed materials.

However, the experiments have also shown, that the full potential of the bench scale fluidized bed pilot plant has not yet been fully exploited. A lot of experience could be gained through the experiments. The wealth of knowledge has primarily led to many detailed improvements to the testing plant. The knowledge gained is very helpful in preventing problems and possible faulty design when setting up further bench scale fluidized bed pilot plants.

Due to the geometric dimensions, a relatively large amount of bed material is required to operate the testing plant under constant conditions. In particular, the type of the bottom of the column and the structural design of the lower flange are not optimally selected in order to achieve rapid enrichment and layer formation on the surface of the particles of the bed material. The investigations of the bed material on the micro-scale test-rig have shown that during the experiments no sufficient layer formation on the surface of the particles occurred on any of the different bed materials. Further investigations at the SEM and investigations of the line scans also confirmed these findings.

In order to achieve meaningful results, the duration of the fuel supply would have to be increased significantly, so that there is a much longer interaction of the fuel with the bed material. However, this would have clearly exceeded the time frame of this master thesis. On the other hand, much less bed material would have to be used, as was done in other experiments with similar scope conditions [29].

The 3D modeling of the bench scale fluidized bed pilot plant is important so that the structural changes can be documented sufficiently well. Based on this 3D modeling, further modifications can be set up without having to model construction changes or retrofits from scratch. 3D modeling also significantly simplifies the calculations of the individual volumes and dead volumes. Lengthy, numerical solution processes are therefore no longer necessary.

The following suggestions for improvement can be made for future layer formation studies on this testing plant, which can be carried out with relatively little effort and with relatively few modifications:

- With regard to future experiments, a new column bottom as described in Subsection 5.2.8 should be used. This allows the dead volume to be significantly reduced, which means that the experiments can be carried out with significantly reduced amount of bed material.
- The gears of the two screw conveyors should be better coordinated. This eliminates the limitations encountered in these experiments and it is possible to convey any required fuel mass flow.
- In terms of the experiments, it seems sensible that instead of testing many bed materials interacting with fuel for a few hours, fewer bed materials should be tested, but for a longer period of time.

Nomenclature

Symbol	Description	SI base units
A	Cross sectional area	m^2
A_d	Ash content	$\%$
A_p	Surface area of a spherical particle	m^2
Ar	Archimedes number	$-$
c_w	Drag coefficient of a single sphere	$-$
d_k	Diameter of a sphere	m
d_p	Sieve diameter	m
d_{sv}, d_{32}	Surface/volume-related diameter (Sauter mean diameter)	m
d_s	Surface-related diameter	m
d_v	Volume-related diameter	m
E_i	Activation energy i	$\frac{J}{mol}$
F_A	Buoyancy force	N
F_G	Weight force	N
F_W	Resistance force	N
g	Gravitational force equivalent (g-force)	$\frac{m}{s^2}$
H	Height of the fixed bed	m
k_i	Reaction rate constant i (n$^{\text{th}}$ order)	$\frac{1}{s} \cdot (\frac{l}{mol})^{n-1}$
m_1	Mass of the empty bowl	kg
m_2	Mass of the bowl including the moist fuel	kg
m_3	Mass of the bowl including the dried fuel	kg
m_4	Amount after ashing the fuel	kg
m_{AIR-av}	Actual air available	mol
m_{AIR-st}	Stoichiometrically required air	mol
m_b	Mass of the total biomass	kg
m_w	Mass of the water	kg
M	Mass of the solid in the bed material	kg

Symbol	Description	SI base units
M_p	Mass of the particle	kg
$\dot{Q}$	Gas volume flow	$\frac{m^3}{s}$
$\dot{Q}_{mf}$	Minimum flow rate for fluidized bed operation area	$\frac{m^3}{min}$
$\dot{Q}_t$	Maximum flow rate for fluidized bed operation area	$\frac{m^3}{min}$
$\dot{Q}_{min}$	Minimum gas volume flow	$\frac{m^3}{s}$
$\dot{Q}_{max}$	Maximum gas volume flow	$\frac{m^3}{s}$
$\dot{Q}_{typical}$	Typical gas volume flow	$\frac{m^3}{s}$
Re	Reynolds number	$-$
u	Fuel moisture	$\%$
u_{mf}	Minimum fluidization velocity	$\frac{m}{s}$
u_s	Superficial velocity	$\frac{m}{s}$
u_t	Terminal velocity	$\frac{m}{s}$
$u_{t,Newton}$	Terminal velocity for Newton's area	$\frac{m}{s}$
$u_{t,Stokes}$	Terminal velocity for Stokes' area	$\frac{m}{s}$
V_b	Volume of the bed material	m^3
V_p	Volume of a spherical particle (including its pores)	m^3
V_{pore}	Volume of the pores	m^3
w	Water content	$\%$
ε	Fixed bed porosity	$-$
λ	Air–fuel equivalence ratio	$-$
μ	Dynamic viscosity of the fluidization medium	$\frac{kg}{m \cdot s}$
π	Mathematical constant (Archimedes' constant)	$-$
ρ_b	Bulk density (volumetric density)	$\frac{kg}{m^3}$
ρ_g	Gas density	$\frac{kg}{m^3}$
ρ_p	Particle density	$\frac{kg}{m^3}$
$\rho_{p,abs}$	Absolute material density	$\frac{kg}{m^3}$
ϕ	Particle form factor	$-$
ψ	Sphericity	$-$
Δp	Pressure drop	Pa

Abbreviations

Abbreviation	Full name
ATP	Adenosine triphosphate
BASF	Badische Anilin- & Soda-Fabrik
CAD	Computer-aided design
CFB	Circulating fluidized bed
DFB	Dual fluidized bed
DT	Deformation temperature
EDS	Energy dispersive X-ray spectroscopy
FCC	Fluid catalytic cracking
FT	Flow temperature
GHG	Greenhouse gas
HHV	Higher heating value H_s
HT	Hemisphere temperature
IEA	International Energy Agency
IGCC	Integrated Gasification Combined Cycle
IPCC	Intergovernmental Panel on Climate Change
LHV	Lower heating value H_i
LHV_{waf}	Water and ash free lower heating value H_i
MFC	Mass flow controller
SEM	Scanning electron microscope
SFB	Stationary fluidized bed
SMD	Sauter mean diameter
SST	Shrinkage starting temperature
WGSR	Water-gas shift reaction

Bibliography

[1] Hermann Hofbauer. *Brennstoff- und Energietechnologie, Kapitel 1 Energie in Österreich, Europa und weltweit, Teil 2*. 2019.

[2] BP p.l.c. *Statistical Review of World Energy 2020, 69th edition*. 2020.

[3] Renewed Projects Team, ed. *Global overview of energy sector*. 2017. URL: `https://renewedprojects.co.za/wp-content/uploads/2017/02/Global-energy-usuage-snce-1850-1024x715.png` (visited on 06/21/2019).

[4] Der Standard, ed. *Tausende Schüler streikten in ganz Österreich für das Klima*. Mar. 16, 2019. URL: `https://www.derstandard.at/story/2000099638685/zehntausende-schueler-streiken-fuer-das-klima-sie-wollen-ihre-zukunft` (visited on 06/24/2019).

[5] Die Presse, ed. *Mehr als 10.000 Schüler demonstrieren in Wien für Klimaschutz*. Mar. 15, 2019. URL: `https://diepresse.com/home/panorama/wien/5596117/Mehr-als-10000-Schueler-demonstrieren-in-Wien-fuer-Klimaschutz` (visited on 06/24/2019).

[6] Österreichischer Biomasse-Verband. *Energie aus Biomasse*. 2019.

[7] IEA Bioenergy. *Bioenergy – a sustainable and reliable energy source. A review of status and prospects*. 2009.

[8] Wikimedia Commons, ed. *World energy consumption by fuel*. 2018. URL: `https://commons.wikimedia.org/wiki/File:World_energy_consumption_by_fuel.svg` (visited on 06/21/2019).

[9] Hartmut Schumacher. *Dezentrale Energieerzeugung - Viele Kleine statt ein Großes*. 2017. URL: `https://www.energieratgeber-info.de/viele-kleine-statt-ein-grosses` (visited on 02/14/2020).

[10] E-Control. *Dezentrale Erzeugung in Österreich*. 2012.

[11] Matthias Kuba and Stefan Müller. *Thermische Biomassenutzung*. 2019.

[12] Richard Zahoransky and Hans-Josef Allelein. *Energietechnik: Systeme zur Energieumwandlung; Kompaktwissen für Studium und Beruf*. 5. überarb. und erw. Aufl. Wiesbaden: Vieweg + Teubner, 2010. ISBN: 978-3-8348-1207-0.

[13] Martin Kaltschmitt, Hans Hartmann, and Hermann Hofbauer. *Energie aus Biomasse: Grundlagen, Techniken und Verfahren.* 3., aktualisierte und erweiterte Auflage. Berlin Heidelberg: Springer Vieweg, 2016. ISBN: 978-3-662-47438-9, 978-3-662-47437-2.

[14] Austrian Standards Institute / Österreichisches Normungsinstitut. *ÖNORM M 7101: Begriffe der Energiewirtschaft - Allgemeine Begriffe.* Nov. 1, 2013.

[15] Austrian Standards Institute / Österreichisches Normungsinstitut. *ÖNORM EN ISO 18125: Biogene Festbrennstoffe - Bestimmung des Heizwertes (ISO 18125:2017).* Aug. 1, 2017.

[16] Matthias Kuba. *Biomasse für die energetische Nutzung, Kapitel 3.* 2019.

[17] Austrian Standards Institute / Österreichisches Normungsinstitut. *ÖNORM CEN/TS 15370-1: Feste Biobrennstoffe - Verfahren zur Bestimmung des Schmelzverhaltens der Asche - Teil 1: Verfahren zur Bestimmung charakteristischer Temperaturen.* Dec. 1, 2006.

[18] Austrian Standards Institute / Österreichisches Normungsinstitut. *ÖNORM EN ISO 18123: Biogene Festbrennstoffe - Bestimmung des Gehaltes an flüchtigen Bestandteilen (ISO 18123:2015).* Feb. 15, 2016.

[19] Zhongxin Tan and Anders Lagerkvist. "Phosphorus recovery from the biomass ash: A review". In: *Renewable and Sustainable Energy Reviews* 15.8 (Oct. 1, 2011), pp. 3588–3602.

[20] Hermann Hofbauer. *Wirbelschichttechnik - Anwendungen.* 2019.

[21] CHEMIE TECHNIK, ed. *Folgeentwicklungen der Ammoniaksynthese.* Nov. 13, 2013. URL: `https://www.chemietechnik.de/folgeentwicklungen-der-ammoniaksynthese/` (visited on 08/08/2019).

[22] Wikimedia Commons, ed. *Winkler-Generator.* Feb. 6, 2010. URL: `https://commons.wikimedia.org/wiki/File:Winkler-Generator.svg` (visited on 08/08/2019).

[23] Hermann Hofbauer. *Wirbelschichttechnik - Grundlagen.* 2019.

[24] The Guardian, ed. *Derek Geldart obituary.* Mar. 11, 2013. URL: `https://www.theguardian.com/education/2013/mar/11/derek-geldart-obituary` (visited on 08/08/2019).

[25] D. Geldart. "Types of gas fluidization". In: *Powder Technology* 7.5 (May 1, 1973), pp. 285–292.

[26] Gerd Mauschitz. *Mechanische Verfahrenstechnik - Grundlagen der Partikelmesstechnik.* 2018.

[27] Fabrizio Scala. *Fluidized Bed Technologies for Near-Zero Emission Combustion and Gasification.* 1st Edition. Cambridge: Elsevier Science, 2013. ISBN: 978-0-85709-880-1.

[28] Hakon Wadell. "Volume, Shape, and Roundness of Quartz Particles". In: *The Journal of Geology* 43.3 (Apr. 1, 1935), pp. 250–280.

[29] Hanbing He, Dan Boström, and Marcus Öhman. “Time Dependence of Bed Particle Layer Formation in Fluidized Quartz Bed Combustion of Wood-Derived Fuels”. In: *Energy & Fuels* 28.6 (June 19, 2014), pp. 3841–3848.

[30] Marcus Öhman, Linda Pommer, and Anders Nordin. “Bed Agglomeration Characteristics and Mechanisms during Gasification and Combustion of Biomass Fuels”. In: *Energy & Fuels* 19.4 (July 2005), pp. 1742–1748.

[31] Friedrich Kirnbauer and Hermann Hofbauer. “The mechanism of bed material coating in dual fluidized bed biomass steam gasification plants and its impact on plant optimization”. In: *Powder Technology* 245 (Sept. 1, 2013), pp. 94–104.

[32] H. Visser. *The influence of fuel composition on agglomeration behaviour in fluidized bed combustion.* Jan. 1, 2004.

[33] Hornbach Baumarkt AG, ed. *Pinienrinde FloraSelf fein, 60 L; Art. 8707092.* 2019. URL: `https://www.hornbach.at/shop/Pinienrinde-FloraSelf-fein-60-L/8707092/artikel.html` (visited on 06/21/2019).

[34] Cissonius GmbH, ed. *CF-420C Hammer Mühle mit Zyklon (Staubabscheider).* 2019. URL: `http://shop-cissonius.de/de/hammer-m%C3%BChlen/28-cf-420c-4260355210189.html` (visited on 11/27/2019).

[35] Cissonius GmbH, ed. *PP200 Pelletpresse.* 2019. URL: `http://shop-cissonius.de/de/pellet-pressen-e-motor/27-pp200-4260355210103.html` (visited on 11/27/2019).

[36] Austrian Standards Institute / Österreichisches Normungsinstitut. *ÖNORM EN ISO 18122: Biogene Festbrennstoffe - Bestimmung des Aschegehaltes (ISO 18122:2015)).* Feb. 15, 2016.

[37] Emerson Process Management, ed. *Rosemount NGA 2000.* 2001. URL: `https://www.emerson.com/documents/automation/manual-nga-2000-platform-sw-3-6-rev-a-rosemount-en-70116.pdf` (visited on 12/16/2019).

[38] NI - National Instruments, ed. *LabVIEW Systementwicklungssoftware.* 2019. URL: `https://www.ni.com/de-at/shop/labview.html` (visited on 12/15/2019).

[39] Andrea Ambrosi and Scott E. Denmark. “Die Wassergas-Shift-Reaktion in der organischen Synthese”. In: *Angewandte Chemie* 128.40 (Mar. 18, 2016), pp. 12348–12374.

[40] Mehmet Sankir and Nurdan Demirci Sankir. *Hydrogen Production Technologies.* 1st Edition. Beverly, MA Hoboken, NJ: Scrivener Publishing John Wiley & Sons, 2017. ISBN: 978-1-119-28366-9.

[41] Dr Rüdiger Paschotta, ed. *Dampfreformierung.* May 19, 2013. URL: `https://www.energie-lexikon.info/dampfreformierung.html` (visited on 03/06/2020).

[42] Matthias Kuba. “Interactions between bed material and biomass ash in dual fluid bed gasification”. PhD thesis. Vienna University of Technology, 2016.

[43] Christoph Hammerl.
"Time-dependent catalytic activity of used K-feldspar for biomass gasification".
MA thesis. Vienna University of Technology, 2019.

[44] Miloslav Nič et al. *Compendium of Chemical Terminology*. 2.1.0.
Research Triagle Park, NC: International Union of Pure and Applied Chemistry, 2009.
ISBN: 978-0-9678550-9-7.

[45] Autodesk, ed.
Inventor - Professional-grade 3D CAD software for product design and engineering.
2019.
URL: `https://www.autodesk.com/products/inventor` (visited on 12/16/2019).

[46] Elisabet Brus, Marcus Öhman, and Anders Nordin. "Mechanisms of Bed Agglomeration during Fluidized-Bed Combustion of Biomass Fuels".
In: *Energy & Fuels* 19.3 (May 2005).

[47] Thomas Karl Hannl et al. "Layer Formation on Feldspar Bed Particles during Indirect Gasification of Wood. 2. Na-Feldspar".
In: *Energy & Fuels* 33.8 (Aug. 15, 2019), pp. 7333–7346.

[48] Juraj Priscak. "Development of a New Method for Determination of Ash Behavior in Fluidized Bed Conversion Processes".
MA thesis. Vienna University of Technology, 2020.

[49] Tebbe-Neuenhaus, ed. *Quarzsand und Quarzkies - trocken*. 2019.
URL: `https://www.tebbe-neuenhaus.de/quarzsand/` (visited on 03/04/2020).

List of Figures

List of Tables